Aus der Klinik und Poliklinik für Hals-, Nasen- und Ohrenheilkunde

Klinikums der Ludwig-Maximilians-Universität München

Direktor: Prof. Dr. med. Martin Canis

Molecular characterization of EGF-mediated invasion in a 3D cellular model

Dissertation

zum Erwerb des Doktorgrades der Medizin

an der Medizinischen Fakultät der

Ludwig-Maximilians-Universität München

vorgelegt von

Jiefu Zhou

aus

Hunan, China

Jahr

2023

Mit Genehmigung der Medizinischen Fakultät der

Ludwig-Maximilians-Universität zu München

Erster Gutachter:	Prof Dr.Frank Haubner
Zweiter Gutachter:	Priv. Doz. Dr. Ursula Zimber-Strobl
Dritter Gutachter:	Prof. Dr. Dominik Paquet
ggf. weitere Gutachter:	_____
	_____
Mitbetreuung durch den promovierten Mitarbeiter:	Prof Dr.Olivier Gires
Dekan:	Prof. Dr. med. Thomas Gudermann
Tag der mündlichen Prüfung:	11.01.2023

Table of content

ZUSAMMENFASSUNG

Karzinome des Kopf-Halsbereichs (Head and neck squamous cell carcinoma: HNSCC) sind häufige Malignome, die in Epithelien des oberen Aerodigestivtrakts auftreten. Eine Überexpression und/oder Mutationen im Epidermalen Wachstumsfaktorrezeptor EGFR konnte in 80-90% aller HNSCC festgestellt werden und korrelierte mit vermindertem Gesamt- und krankheitsfreiem Überleben. Die Behandlung stark fortgeschrittener HNSCC Patienten beinhaltet die Adresierung des EGFR Signalweges unter Verwendung monoklonalen therapeutischer Antikörper oder spezifischer Tyrosinkinase Inhibitoren in Kombination mit einer Radiotherapie. Leider bleibt die Effizienz der EGFR-spezifischen Therapie mit dem monoklonalen Antikörper Cetuximab, welcher zur Behandlung von HNSCC durch die EMA und FDA freigegeben ist, limitiert. Dies beruht unter anderem auf dem Auftreten resistenzvermittelnder EGFR Mutationen und durch Mutationen, welche aufgrund der Therapie selektiert werden. Trotz einer Vielfalt EGFR-basierter Studien sind die Signalwege und Gene, welche essenzielle Rollen bei der EGF-vermittelten Invasion von Tumorzellen bislang nur unzureichend bekannt. Daher könnte ein verbessertes Wissen zu den molekularen Mechanismen der EGF-vermittelten Invasion hilfreich sein, neue therapeutische Zielmoleküle mit verbesserter Effektivität bei geringeren Nebeneffekten zu identifizieren.

Das Ziel dieser Studie war es ein 3D Modell zur Untersuchung der EGFR-abhängigen Signalwege und Zielmoleküle, welche in der EGF-vermittelten Invasion funktionell sind, zu etablieren. Zu diesem Zweck sollte das photokonvertierbare, fluoreszente Protein Dendra2 verwendet werden, um invasive Zellen in einer extracellulären Matrix selektiv zu markieren und isolieren. Anschließend sollten angereicherte, invasive Zellen mittels Next-eneration RNA Sequenzierung analysiert werden.

Das etablierte 3D Modell simulierte eine EGF-vermittelte lokale Invasion von HNSCC Zellen in ECM, welche vornehmlich vom MAPK/ERK Signalweg abbhängig war. Durch eine Photoconversion von Dendra2 von einer grünen zu einer roten Fluoreszenz in invasiven Zellen konnten diese von nicht-invasiven Zellen selektiv getrennt und angereichtert werden. Durch eine RNA-Sequenzierung invasiver, nicht-invasiver, unbehandelter und Inhibbitor-behandelter Zellen konnten transkriptomische Unterschiede mittels bioinformatischer Ansätze bestimmt werden. 449 Gene, welche am Stärksten zur signifikanten An- oder Abreicherung zentraler zellulärer Prozesse beitrugen, wurden mittels GSEA identifiziert. Aus dieser Genliste wurden 46 Gene identifiziert, welche DEGs (log2 FC >1, p-value < 0.05) und durch Cetuximab und/oder MEK Inhibitor gegenreguliert waren. Diese 46 Gene wurden mit Modulen ko-regulierter Gene, die in scRNA Datensätzen maligner HNSCC

Zellen am stärksten mit einer EMT und EGFR und MAPK Aktivität korrelierten, cross-referenziert. Diese Vorgehensweise führte zu Identifikation von 16 Genen mit starker Verbindung zu Zellinvasion and Gewebsremodellierung. Die Sphingosin Kinase 1 (SPHK1), eines der identifizierten 16 Genen, wurde als potenzielle Zielstruktur für die Hemmung der EGF-vermittelten Invasion validiert. Eine Hemmung von SPHK1 zeigte initiale Wirksamkeit bei der Inhibition der Invasion und bei der Unterstützung von Cetuximab Effekten.

Zusammenfassend wurden in der vorliegende Arbeit transkriptomische Unterschiede zwischen invasiven und nicht-invasiven HNSCC Zellen nach EGF-Behandlung definiert. Eine Gensignatur invasiver Zellen, welche in vitro mit EGF-vermittelter Invasion und in Tumor-Einzelzellen mit EMT, EGFR und MAPK Aktivität am stärksten korrelierte, wurde extrahiert. Präliminäre Daten konnten eines der 16 identifizierten Gene, SPHK1, als vielversprechendes Kandidatgen für die Hemmung der EGF-vermittelten lokalen Invasion definieren.

ABSTRACT

Head and neck squamous cell carcinoma (HNSCC) commonly occur in the mucosa of the sinuses, oropharynx, hypopharynx, and larynx. Overexpression or mutation of epidermal growth factor receptor (EGFR) is widespread in 80%-90% of HNSCC patients and correlates with reduced overall and progression-free survival. Treatment for highy advanced HNSCC patients includes anti-EGFR monoclonal antibodies or kinase inhibitors and concurrent radiotherapy. However, the efficacy of the EGFR-targeting monoclonal antibody Cetuximab is currently limited, partly due to pre-existing genetic alterations in *EGFR* that make them resistant to EGFR inhibition and to the ability to acquire secondary mutations under therapeutic pressure, contributing to treatment avoidance. Despite numerous EGFR-based studies, the pathways or genes that play essential roles in EGF-mediated invasion of tumor cells are still not fully understood when using EGFR inhibitors in HNSCC. Hence, a deeper understanding of the molecular mechanisms of EGF-mediated invasion may help to find therapeutic targets with greater effectiveness, lower dosage, and fewer side effects.

The aim of this thesis was to construct a 3D cellular model to study the downstream pathway(s) of EGFR mainly contributing to EGF-mediated invasion and to use the Dendra-2 photoconvertible protein to locate and isolate

invasive cells in EGF-mediated 3D invasion. Eventually, next-generation gene sequencing should be used to obtain transcriptome information of invasive cells and on Cetuximab inhibition, to dissect mechanisms of EGF-mediated invasion in HNSCC and find potential therapeutic targets.

The established 3D invasion assay demonstrated EGF induced local invasion of HNSCC cells into type I collagen matrix and that the MAPK/ERK signaling pathway downstream of EGFR dominates EGF-mediated invasion. Upon photoconversion of the green protein Dendra2 in locally invaded cells into a red fluorescence, invasive and non-invasive cells were separated by FACs. Bulk RNA-sequencing of invasive, non-invasive, control cells, Cetuximab and MEK inhibitor-treated cells was performed and transcriptomic differences were analyzed using bioinformatic approaches. Differences between invasive and untreated cells were addressed by gene set enrichment analysis (GSEA) and 449 genes leading edge genes with the highest contribution to biological hallmarks significantly enriched or suppressed in invasive cells were extracted. From these 449 genes, 46 genes were significantly up- or down-regulated (log2 FC >1, p-value < 0.05) and counter-regulated by Cetuximab and/or MEK inhibition. These extracted 46 genes were cross-referenced to gene modules obtained by weighted gene co-expression network analysis in single cell RNA-seq data from HNSCC patients, which showed the highest correlation with EMT,

EGFR and MAPK pathway activities. A total of 16 genes resulted from this analysis. Finally, sphingosine kinase 1 (SPHK1), as a member of these 16 genes, was targeted for inhibition in the 3D invasion assay, demonstrating preliminarily efficacy in blocking invasion and in supporting Cetuximab effects on invasive cells.

In summary, the present work defined transcriptomic differences in invasive HNSCC cells following EGF treatment and extracted a gene set correlated to EGF-mediated invasion in vitro and to EMT, EGFR and MAPK pathway acitivity in single malignant cells of HNSCC patients. Preliminary data further identified SPHK1 as a promising target for the inhibition of EGF-mediated local invasion.

ABBREVIATIONS

AREG, amphiregulin;

BTC, betacellulin;

CAFs, cancer-associated fibroblasts;

CTCs, circulating tumor cells;

CRT, chemoradiation therapy;

CSCs, cancer stem cells;

CSM, collagen and serum-free medium mixture;

DEGs, differential expressed genes;

DTCs, disseminated tumor cells;

ECM, extracellular matrix;

EGF, epidermal growth factor;

EGFR, epidermal growth factor receptor;

EMT, epithelial-mesenchymal transition;

EMT-TFs, EMT-activating transcription factors;

ERK1/2, extracellular signal–regulated kinase 1/2;

EPGN, low-affinity ligands epigen;

EREG, epiregulin;

EpCAM, epithelial cell adhesion molecule;

EpEx, extracellular domain of EpCAM;

FACS, fluorescence-activated cell sorting;

FGF, Fibroblast growth factors;

FDR, false discovery rates;

GSEA, Gene set enrichment analysis;

GFP-A, green fluorescent protein-area;

HPV, human papillomavirus;

HNSCC, head and neck squamous cell carcinoma;

HB-EGF, heparin-binding EGF-like growth factor;

IHC, immunohistochemistry;

ITH, inter-tumoral heterogeneity;

JAK, Janus kinase;

LMU, Ludwig-Maximilians-University;

MEK, MAPK–ERK kinase;

MET, mesenchymal-to-epithelial transition;

MATH, Mutant-allele tumor heterogeneity;

mTOR, mammalian target of rapamycin;

NPC, nasopharyngeal carcinoma;

NES, normalized enrichment scores;

OS, overall survival;

pEMT, partial EMT;

pERK, phosphorylated extracellular signal–regulated kinase;

PCA, principal component analysis;

PI3, phosphoinositide-3;

PLC, phospholipase C;

PD1, Programmed death-1;

PD-L1, Programmed Cell Death Ligand 1;

Raf, rapidly accelerated fibrosarcoma kinase;

Ras, rat sarcoma gene;

RTKs, receptor tyrosine kinases;

scRNA-seq, single cell RNA-sequencing;

SPHK1, Sphingosine Kinase 1;

STAT3, Signal transducer and activator of transcription 3;

TCGA, The Cancer Genome Atlas;

TFs, transcription factors;

TGF-α, transforming growth factor-α;

TME, tumor microenvironment;

TKIs, tyrosine kinase inhibitors;

VEGF, Vascular endothelial growth factor;

WGCNA, weighted gene co-expression network analysis;

1 INTRODUCTION

1.1 Head and Neck Squamous Cell Carcinoma

With more than 600,000 new cases worldwide each year, Head and Neck Squamous Cell Carcinoma (HNSCC) is the world's sixth most prevalent malignancy. According to the Global Cancer Observatory, the occurrence of HNSCC is rising and is expected to continue to climb (GLOBOCAN) (Bray et al., 2018; Ferlay et al., 2019).

The prevalence of HNSCC varies between nations and has often been linked to either excessive alcohol intake, cigarettes, or both. Human papillomavirus (HPV) carcinogenic strains, particularly HPV-16 and -18, are increasingly associated with oropharyngeal / pharynx malignancies, which are then termed HPV-associated HNSCC. The term HPV-negative HNSCC currently refers to HNSCCs of the oral cavity and larynx, which are still primarily linked to smoking. While Nasopharyngeal carcinoma's (NPC) causation is associated with more factors, such as eating habits, viral influences, and genetic (Rebbeck, 2008).

Genetic instability such as recurrent chromosomal deletion or acquisition and epigenetic modifications contribute to the tumorigenesis of HNSCC (Cancer Genome Atlas, 2015; Castilho, Squarize, & Almeida, 2017; Johnson et al., 2020). The tumor microenvironment (TME), in addition to genetic or epigenetic

modifications, is an important factor in cancer metastasis. Including endothelial cells, cancer-associated fibroblasts (CAFs), and immune cells, the TME in HNSCC is a complex and diverse combination of cells. Those cells have the capacity to degrade and remodel the extracellular matrix (ECM) or produce and trigger matrix-embedded growth factors (including EGFs, FGFs, VEGFs, and TGFs) that promote the growth of tumor cells, angiogenesis, and suppress the immune response (Eskiizmir, 2015; Johnson et al., 2020).

Despite the use of multifaceted treatment methods such surgery, chemoradiation therapy (CRT), and targeted therapy with anti-EGFR monoclonal antibodies and biologicals that target Programmed Death-1 (PD1)/ Programmed Cell Death Ligand 1 (PD-L1), patient survival rates are still low (Baumeister, Zhou, Canis, & Gires, 2021; Cramer, Burtness, Le, & Ferris, 2019; Johnson et al., 2020; Leemans, Braakhuis, & Brakenhoff, 2011; Leemans, Snijders, & Brakenhoff, 2018). Nowadays, multi-omic techniques, such as transcriptomics, proteomics, multi-dimensional flow, etc., are widely applied in studies to investigate potential reasons for the high resistance of HNSCCs to multi-modal treatment and get a deeper understanding of HNSCC development (Baumeister et al., 2021; C. Huang et al., 2021). Furthermore, DNA mutations, epigenetic modifications, and protein expression, including their activation level, and mechanisms of HNSCC metastasis, should be clarified (Stransky et al.,

2011). Therefore, combining multi-omic approaches to find novel prospective therapeutic targets and treatment strategies to overcome or lessen RCT resistance and to address metastatic progression is essential.

1.1.1 Heterogeneity and therapeutic approaches of HNSCC

The high heterogeneity of HNSCC has been revealed in recent years (Cancer Genome Atlas, 2015; Leemans et al., 2018; Puram et al., 2017). High intra- and inter-tumoral heterogeneity (ITH) creates a tremendous level of cellular variety, enabling the emergence of specific cellular subpopulations with unique transcriptomic signatures. Mutant-allele tumor heterogeneity (MATH), which is typically linked with shorter survival, is a criterion for the clinical outcome of patients based on the degree of genetic heterogeneity. A poor prognosis is associated with high mutational burden in gene coding regions. (Mroz, Tward, Hammon, Ren, & Rocco, 2015; Mroz et al., 2013). Treatment of malignant tumors is typically complicated by ITH, which poses significant challenges since standard therapies may omit to target tumor cell subpopulations, which can eventually be the origin of recurrences and/or metastatic spread (Baumeister et al., 2021; Puram et al., 2017).

In 2015, The Cancer Genome Atlas (TCGA) study provided a comprehensive view of somatic genetic changes by analyzing 279 HNSCCs (Cancer Genome Atlas, 2015). In HPV (-) HNSCCs, cell cycle, cell mortality, NF-κB signaling, and

other tumorigenic cascades are targeted by mutually exclusive classes of mutations including amplicons on chr. 11q with CCND1, FADD, BIRC2, and YAP1 or parallel mutations of CASP8 with HRAS. Regarding HPV (+) oropharyngeal tumors, gene mutations of PIK3CA, lack of TRAF3, and E2F1-amplification indicated an aberrant NF-kB activation, cell cycle and other oncogenic pathways as being crucial in the etiology and for the development of novel targeted therapeutics for these tumors. We may be able to accelerate the progress in prevention and therapy across tumor types if those common and distinctive heterogeneities can be further studied.

Intra-tumor heterogeneity refers to the fact that HNSCCs are formed of a heterogeneous collection of tumor cells exhibiting unique RNA transcript signatures, according to a single cell RNA-sequencing (scRNA-seq) study of oral cavity cancer patients by Puram *et al.* (Puram et al., 2017). These findings revealed that malignant cells in partial epithelial-to-mesenchymal transition (pEMT) were located near the edges of tumor areas. Another indication of the significance of this differentiation program in the metastatic cascade is the association between loco-regional lymph node metastases and tumors with a predominate p-EMT signature. And the gene signatures for partial pEMT differed between malignant cells within tumors (Bierie et al., 2017; Puram, Parikh, & Tirosh, 2018a; Puram et al., 2017; Schinke et al., 2022b). Numerous

phenotypic and functional traits, including motility, morphology, angiogenesis, proliferation, invasiveness, metabolism, and immunological resistance, are heterogeneous in HNSCC (Baumeister et al., 2021; Burrell, McGranahan, Bartek, & Swanton, 2013).

Nowadays, clinical criteria used to identify patients for participation in landmark trials of definitive therapy are usually applied to guide treatment decisions for HNSCC rather than stage categories (Bergers & Hanahan, 2008; M. A. Nieto, R. Y. Huang, R. A. Jackson, & J. P. Thiery, 2016a; Weinstein, Quon, O'Malley, Kim, & Cohen, 2010). The level of therapeutic effect, such as a monoclonal antibody, also depends on the subtype of tumor cells and their sensitivity to different treatments. One of the classic treatment combinations is EGFR monoclonal antibody cetuximab combined with radiotherapy to prevent chemotherapy toxicity in HPV-negative HNSCC patients. By using expression profiling, Chung et al. further discovered in 2004 that HNSCCs can be classified into multiple subtypes with varied prognoses, and even among EGFR-expressing tumors, they demonstrated various patterns of EGFR pathway activation. This indicates that the effectiveness of the treatment is closely related to the gene expression levels of the treatment-related pathways (Chung et al., 2004). Recent evidence suggests that the level of EGFR ligands, rather than EGFR itself, may be important for Cetuximab response (C. Huang et al.,

2021). Treatment advances in the past few years offer the possibility of limiting the toxicity of treatment and further improving outcome for patients with HNSCCs (Machtay et al., 2008; Nguyen-Tan et al., 2014; Vermorken et al., 2007). These improvements include minimally invasive transoral surgery, chemoradiotherapy, conventional fractionated radiotherapy, intensity-modulated radiotherapy, adaptive radiotherapy, proton beam therapy, cytotoxic chemotherapy, targeted therapies, immunotherapy, amongst others (Cramer et al., 2019; Johnson et al., 2020; Nieto et al., 2016a). However, despite these objective technical improvements in treatment, the survival of HNSCC patients remains unsatisfying. Together, these findings suggest that heterogeneity is a significant barrier to treating HNSCC effectively and that more patient-tailored approaches are in demand.

1.2 Epithelial-to-mesenchymal transition (EMT)

The epithelial-to-mesenchymal transition (EMT) is a cellular differentiation process during which epithelial cells downregulate their epithelial features, including a loss of cell polarity and cell-to-cell adhesion, and increased migratory or invasive capacity, to transdifferentiate into mesenchymal cells. *Hay et al.* first introduced EMT in 1968, and their research revealed early embryogenesis to be a program with clearly characterized cellular properties

(Hay, 1995; Sexén, 1970). It is commonly acknowledged that EMT occurs naturally throughout development, including early embryonic development, organogenesis development, wound healing, tissue regeneration and organ fibrosis, cancer progression and metastasis (Kalluri & Weinberg, 2009). Additionally, it is recognized that tissue fibrosis and cancer both can trigger EMT (Nieto et al., 2016a). The reverse process of EMT, known as mesenchymal-to-epithelial transition (MET), also occurs frequently during development. During the process of MET, cells usually adopt an apico-basal polarization and present junctional complexes including adherents and tight junctions, which are distinctive to epithelial cells, leading to the loss of migratory capacity (Nieto et al., 2016a).

However, the processes of EMT and MET are not binary shifts. The transition from an epithelial to a mesenchymal state is usually complete during embryogenesis. During normal development or in a pathological context, some cells may still reside in intermediate states with both epithelial and mesenchymal characteristics. Importantly, depending on the biological environment, these intermediate states might vary widely (Hay, 1995; Kalluri & Weinberg, 2009; Nieto et al., 2016a; Puram et al., 2018a; Schinke et al., 2022a; Thiery, Acloque, Huang, & Nieto, 2009; Yeung & Yang, 2017).

1.2.1 EMT in cancer

Changes in cell phenotypes known as EMT have been found to have a role in the tumorigenic process and might have been highjacked by tumor cells in analogy to cells undergoing EMT during gastrulation in the developing embryo. Indeed, the concept that EMT is a crucial factor in epithelial-derived tumor malignancies originated from the striking similarities between cell plasticity in embryonic development and cancer progression (Cano et al., 2000; Thiery, 2002). The process of tumorigenesis, cancer cell stemness, invasion, metastasis, and therapy resistance have all been linked to the EMT state. Specific transcription factors (TFs) described as canonical EMT-activating transcription factors are promoted by pleiotropic signaling factors (EMT-TFs). Canonical EMT-TFs SNAIL, SLUG, TWIST1/2, and ZEB1/2 (Figure 1), together with miRNAs, and epigenetic and post-translational regulators, contribute to the regulation of EMT (Brabletz, Kalluri, Nieto, & Weinberg, 2018; Lambert, Pattabiraman, & Weinberg, 2017; Nieto et al., 2016a). Eventually, EMT enables cancer cells to detach from primary carcinomas, to further migrate, and spread to locoregional or distant areas (Thiery, 2002).

In the cancer dissemination process, circulating tumor cells (CTCs), which are tumor cells that have detached from the primary tumor and have gained access to the blood and lymphatic circulation, play an essential role. Generally, CTCs

are considered the origin of locoregional and distant metastases, which has been demonstrated for metastatic breast cancer (Baccelli et al., 2013). The notion that CTCs express both epithelial and mesenchymal markers suggests an active EMT process, according to Yu et al. and Khoo et al. (Khoo et al., 2015; M. Yu et al., 2013). Furthermore, when breast cancer CTCs have transiently expanded, cells display a whole spectrum of EMT phenotypes, which are associated with different aspects of tumor progression. CTCs characterized by a restricted mesenchymal shift showed the highest metastatic potential, whereas CTCs in EMT were more resistant to chemotherapeutic treatment (Liu et al., 2019). Besides these differences in cellular phenotypes, there is proof that ECM components produced by CTCs may play a role in the successful colonization of distant organs (Khoo et al., 2015; Ting et al., 2014). According to Zheng et al. and Fischer et al.'s studies in breast cancer and pancreatic ductal adenoma-carcinoma, EMT might not be required for the progression of cancer into a metastatic state (K. R. Fischer et al., 2015; Zheng et al., 2015). Although these data are challenging, the role of EMT cannot be dismissed as a major factor in cancer progression, and many studies have demonstrated that EMT contributes to the progression of tumor metastasis in numerous cancer types (Beerling et al., 2016; K. R. Fischer et al., 2015; W. Y. Li & Kang, 2016; Maheswaran & Haber, 2015; Tang et al., 2014; Trimboli et al., 2008; Tsuji,

Ibaragi, & Hu, 2009; Ye et al., 2015).

Based on the strong connection between EMT and tumor heterogeneity, invasion, and metastasis reversing the EMT process might be a promising option for a re-differentiation therapy (Beug, 2009; Chua et al., 2011; R. Y. Huang, Guilford, & Thiery, 2012; Nieto, 2013; Thiery & Sleeman, 2006). For example, based on EMT models, Carmody et al. and Gupta et al. discovered lead drugs to target the HMLE_sh_ECad in cancer stem cells (CSCs) in breast cancers (Carmody et al., 2012; Gupta, Chaffer, & Weinberg, 2009; Gupta, Onder, et al., 2009). More compounds targeting different signaling pathways are proposed and developed in the context of EMT, for example regarding the TGFβR, EGFR, HGFR, phosphatidylinositol 3-kinase (PI3K)/Akt, ERK/MAPK, and PDGFR signaling pathways. These studies bring hope for clinical treatment and open potentially novel paths to therapy (Giannelli, Villa, & Lahn, 2014; Lamouille, Xu, & Derynck, 2014; Rodon et al., 2015). Promoting EMT reversal, however, occasionally carries the risk of making it more likely for disseminated tumor cells (DTCs) to enhance secondary metastases (Beerling et al., 2016; Brabletz, 2012; Nieto, 2013; Ocana et al., 2012; Tsai, Donaher, Murphy, Chau, & Yang, 2012). Therefore, it will be crucial to establish a suitable therapeutic window for administering an EMT-reversing drug and develop personalized treatment strategies for different patients and cancer types.

1.2.2 Dynamic process of EMT

According to the description by *Hay (1995)*, the classic definition of EMT is the transformation of epithelial cells into mesenchymal cells, which can give the impression that the process alternates between mesenchymal or epithelial phases. Recent research suggests that this dynamic transitional process is more flexible than previously assumed. Cells are believed to go through an intermediary stage rather than only fluctuating between the fully epithelial and mesenchymal states. Various studies have broadened the definition of EMT, especially the intermediary states called partial EMT or hybrid EMT (Figure 1). The partial EMT state has been noted in the correlation with cancer progression (Arnoux, Nassour, L'Helgoualc'h, Hipskind, & Savagner, 2008; Grigore, Jolly, Jia, Farach-Carson, & Levine, 2016; Kisoda et al., 2020; Parikh et al., 2019; Puram, Parikh, & Tirosh, 2018b). Co-expression of epithelial and mesenchymal markers from research in different cancer cell entities gives a clear indication for the existence of partial EMT states (Abell et al., 2011; Bierie et al., 2017; R. Y. Huang et al., 2012; R. Y. Huang et al., 2013; Jordan, Johnson, & Abell, 2011b). The word ‘‘metastable’’ was used to describe cells’ hybrid phenotype, and those metastable cells are suited for tissue local invasion (J. M. Lee, Dedhar, Kalluri, & Thompson, 2006; Tam & Weinberg, 2013). Furthermore, metastable states indicate dynamic phase transitions along energy gradients. This energy is

subsequently used to move the cell into the mesenchymal state, which corresponds to the intermediate EMT stage (Zadran, Arumugam, Herschman, Phelps, & Levine, 2014).

While *Shamir et al.* discovered that Twist1-induced invasion does not require a full-EMT and *Nieto et al*. had demonstrated that plasticity doesn't have to reach a fully differentiated epithelial state, cells may be more likely to exhibit CSC properties in an intermediate EMT state. (Nieto, 2013; Schmidt et al., 2015; Shamir et al., 2014). This is also the rationale for the hypothesis that "migratory CSCs" exist at the invasive edge of tumors (Jordan, Johnson, & Abell, 2011a; Prat et al., 2010). The high accumulation of partial-EMT at the border of the HNSCC tumor was also confirmed by single-cell sequencing and by imaging in HNSCCs (Baumeister et al., 2018; Puram et al., 2017).

In conclusion, the preferential localization of tumor cells in partial EMT at the leading edge of primary HNSCCs may enable collective migration of cell populations, increase invasive potential, and strongly predict lymph node metastasis, invasion, and extranodal extension.

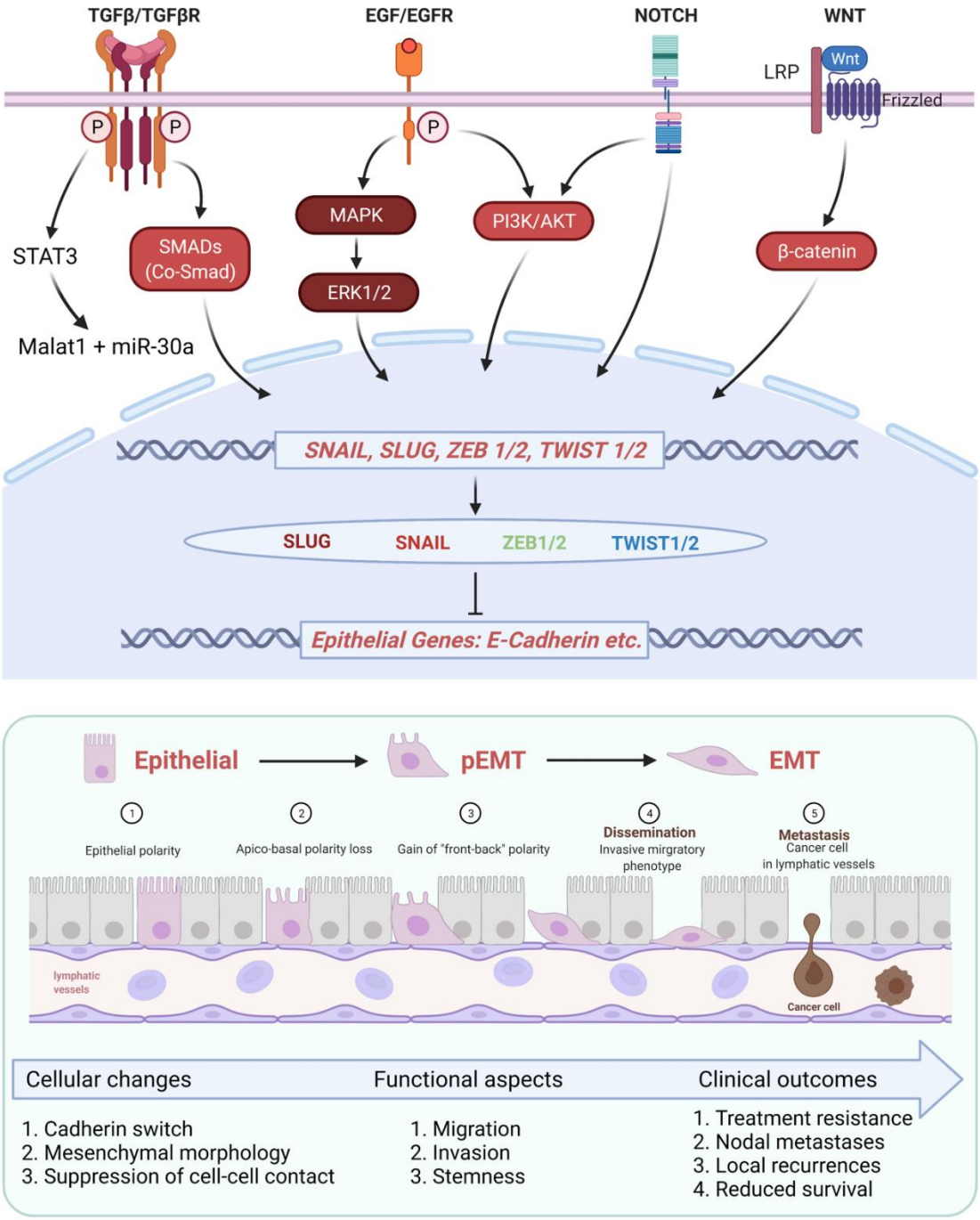

Figure 1 Central signaling pathways in HNSCC that induce (partial) EMT and Schematic diagram of the EMT process and its impact.

The central ligands, receptors, signaling parts, and transcription factors that contribute to full and partial EMT induction are shown. It has been noted that the EMT-TFs SNAIL, SLUG, ZEB1/2, and TWIST1/2 are expressed more when TGF-R, EGFR, NOTCH, and LRP/Frizzled are active. Enhanced migration,

invasion, and stem-like features that are linked with (p)EMT affect treatment resistance, metastasis development, and recurrences, which in turn affects the clinical outcome of HNSCC patients (Figure adapted from (Baumeister et al., 2021)).

1.3 Epidermal Growth Factor Receptor (EGFR)

1.3.1 EGFR

About 20 years after the discovery of Epidermal Growth Factor (EGF) in 1962, the epidermal growth factor receptor was discovered (Cohen, 1962; Cohen, Carpenter, & King, 1980; Cohen, Ushiro, Stoscheck, & Chinkers, 1982). EGFR is a 170-kDa transmembrane glycoprotein that has a C-terminal intracellular kinase domain, a transmembrane region, and an extracellular N-terminal ligand-binding domain (Herbst, 2004). EGFR is one of a family of four receptor tyrosine kinases (RTKs) known as ErbB / HER in humans (Figure 2), including the remaining members ErbB2/ HER2, ErbB3/HER3, and ErbB4/HER4 (Kalyankrishna & Grandis, 2006; Lemmon, Schlessinger, & Ferguson, 2014). The EGFR triggers signaling pathways that regulate cell proliferation, survival, and differentiation, when it becomes activated by the appropriate ligand.

1.3.2 EGFR in cancer

Normal epithelial cells do express EGFR, but this cell surface receptor is frequently overexpressed or mutated in many types of cancers. EGFR

dysregulation is commonly linked to a poor prognosis and lower overall survival. Additionally, EGFR activation helps tumor cells overcome chemotherapy and radiation treatment, causing chemoradiotherapy resistance (Avraham & Yarden, 2011; Blobel, 2005; Bossi et al., 2016; W. Han & Lo, 2012; Herbst, 2004; Kalyankrishna & Grandis, 2006).

The EGFR signaling pathway is a typical ligand-dependent pathway. EGFR activates downstream pathways primarily upon binding to seven known ligands, including high-affinity ligands: EGF, heparin-binding EGF-like growth factor (HB-EGF), transforming growth factor-α (TGFα), and betacellulin (BTC) and low-affinity ligands epigen (EPGN), epiregulin (EREG), and amphiregulin (AREG) (Harris, Chung, & Coffey, 2003; Herbst, 2004). Additionally, *Pan et al*. identified the soluble ectodomain of EpCAM (epithelial cell adhesion molecule) called EpEx as a novel ligand of EGFR in 2018 (Pan et al., 2018). Interestingly, different EGFR-dependent cellular responses to various ligands have been shown in several studies, and specific cell lines respond differently to individual EGFR ligands, which manifests in differentiation, cell proliferation, motility (Figure 2) (Freed et al., 2017; Nyati, Morgan, Feng, & Lawrence, 2006; Roepstorff et al., 2009; Wilson et al., 2012). Additionally, various EGFR ligands cause qualitatively and quantitatively distinct downstream signals and are associated with specific in vivo phenotypes. For example, in the extracellular

domain of EGFR, the ligands epiregulin (EREG) and epigen (EPGN) stabilize several dimeric conformations. As a result, partial agonists of EGFR dimerization such as EREG or EPGN cause less persistent EGFR dimerization than EGF. However, this reduced dimerization results in longer-lasting EGFR signaling, which in turn causes a response in breast cancer cells that is associated with differentiation as opposed to proliferation. (Freed et al., 2017; Ronan et al., 2016).

After ligand binding to EGFR, several main pathways downstream of EGFR become activated (Figure 2), including phospholipase C (PLC)γ/protein kinase C (PKC), Ras/Raf/Mitogen-activated protein kinase (MEK)/extracellular-signal-regulated kinase (ERK), phosphatidylinositol-3-kinase (PI3K)/Akt, mammalian target of rapamycin (mTOR), Janus kinase (JAK)2/signal transducer and activator of transcription STAT3 (Signal transducer and activator of transcription 3). Those pathways are important for tumor progression, growth, and survival (W. Han & Lo, 2012; Kalyankrishna & Grandis, 2006). Among those pathways, the RAS-RAF-MEK-ERK and the PI3K-AKT-mTOR signaling pathway, which regulate survival, differentiation, and cell proliferation, are the two main EGFR downstream signaling pathways (Ciardiello & Tortora, 2008).

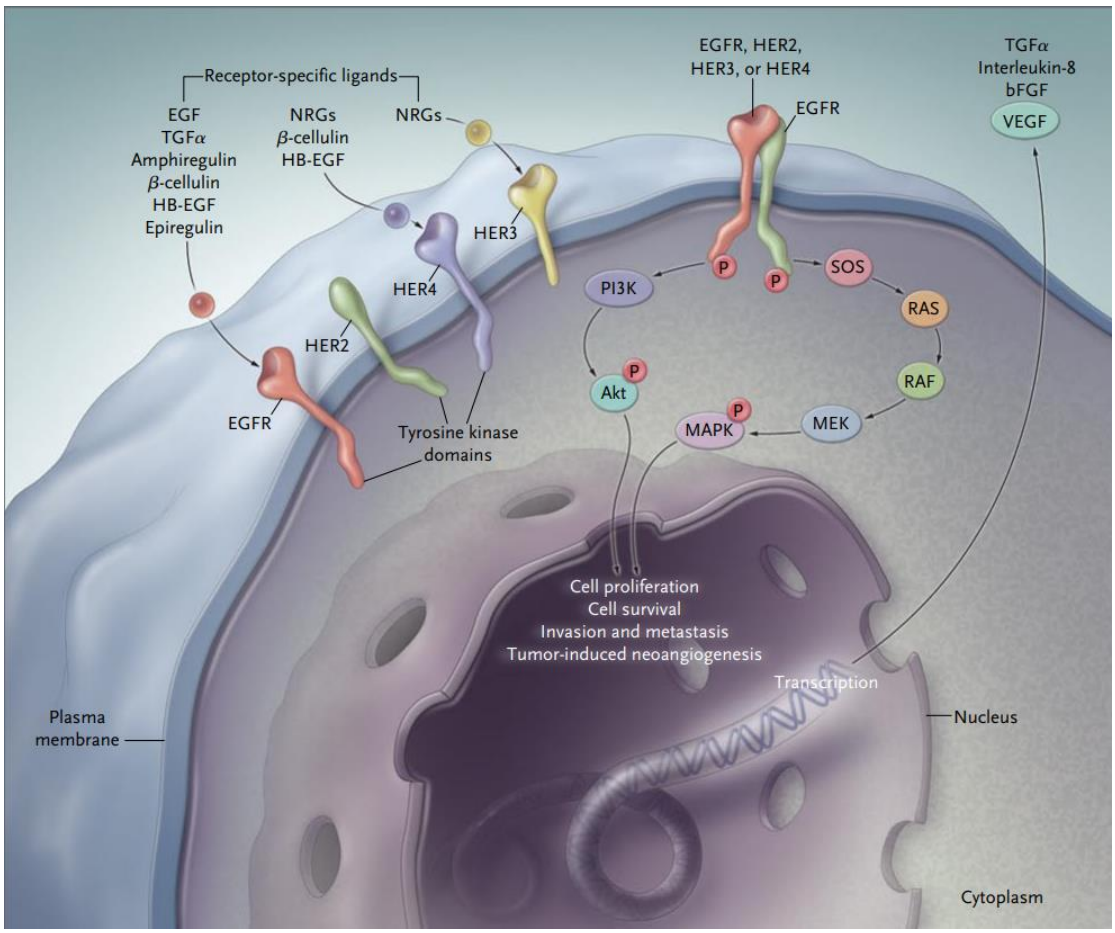

Figure 2 Downstream signaling pathways regulated by EGFR activation.

The diagram depicts the binding of a receptor-specific ligand to the extracellular region of an EGFR or EGFR-related receptor, followed by the formation of a functionally active EGFR-EGFR homodimer or heterodimer that results in the ATP-dependent phosphorylation of specific tyrosine residues in the intracellular domain of EGFR. A complicated program of intracellular signals to the cytoplasm and ultimately to the nucleus is triggered by phosphorylation. Two major pathways of EGFR downstream are shown: RAS-RAF-MEK-ERK and the PI3K-Akt pathways (Figure adapted from (Ciardiello & Tortora, 2008)).

1.3.3 EGFR biology in HNSCCs

EGFR plays a significant role in the pathophysiology of HNSCC and there is a high prevalence of EGFR overexpression in HNSCC (Hynes & Lane, 2005;

Kalyankrishna & Grandis, 2006). mRNA levels are increased by 92% and protein expression levels are likewise increased in HNSCC compared to normal mucosal (Bei et al., 2004; Grandis & Tweardy, 1993; Ongkeko, Altuna, Weisman, & Wang-Rodriguez, 2005). Furthermore, EGFR expression levels are higher in poorly differentiated and highly advanced tumor cells, and the field cancerization theory is supported by the overexpression of EGFR in normal epithelium next to the tumor (Grandis & Tweardy, 1993). Further evidence of significant EGFR overexpression was found during the transition from dysplasia to squamous cell cancer (Shin, Ro, Hong, & Hittelman, 1994). The level of EGFR expression at the different sublocalizations of head and neck cancers might vary. EGFR expression was less prominent in larynx tumors than it was in pharynx and oral cavity tumors (Takes et al., 1998).

In HNSCC, increased EGFR expression is correlated with a poor prognosis (Kalyankrishna & Grandis, 2006). In a study based on oropharyngeal carcinoma, EGFR was found in the nucleus in addition to the cytoplasm. And in patients with high EGFR expression, these patients with nuclear-localized EGFR expression are generally associated with higher local recurrence and lower disease-free survival (Psyrri et al., 2005). Numerous HNSCC-based studies have found that downstream effectors of EGFR, such as ERK1/-2, Akt, STAT3, and STAT5, are highly activated in tumor cells. According to the *Albanell et al.*

study, EGFR overexpression was associated with enhanced ERK activation in HNSCC. At the same time, elevated ERK activation strongly correlates with higher proliferation and advanced tumor stage (Albanell et al., 2001). Phosphorylated Akt was found to be 57% to 81% overexpressed in HNSCC tumors compared to healthy samples (Ongkeko et al., 2005).

In summary, HNSCC tumor development, metastasis, survival, EMT, etc., are influenced or promoted by high EGFR expression and/or its downstream effectors through several oncogenic signaling pathways.

1.3.4 Anti-EGFR treatment in HNSCC

Based on the essential role played in the biology of HSNCC, EGFR has been studied in a wide range of preclinical and clinical settings. Nowadays, two mainstream anti-EGFR treatment approaches have been identified (Figure 3). Targeting the extracellular domain of the receptor with monoclonal antibodies like Cetuximab and Panitumumab is one approach, and another approach aims at inhibiting the kinase domain of EGFR using low molecular weight tyrosine kinase inhibitors (TKIs) (*e.g.*, Erlotinib, Gefitinib, or Afatinib) (Fasano et al., 2014; Troiani et al., 2016).

Anti-EGFR antibodies, such as Cetuximab, Zalutumumab, Panitumumab, lead to degradation and internalization of antibody-receptor complexes by

competing with EGFR ligands, and also can lead to tumor cell death through NK-dependent antibody-mediated cytotoxicity (Lurje & Lenz, 2009; Markovic & Chung, 2012). TKIs can block the intracellular phosphorylation cascade to inhibit EGFR signaling (Figure 3). The first-generation TKIs gefitinib and erlotinib are anilinoquinazolines that bind reversibly through the K745 site in the ATP-binding pocket, and increase anti-tumor activity in vitro by inhibiting AKT and MAPK pathways (Cassell & Grandis, 2010; Pao et al., 2004; Stamos, Sliwkowski, & Eigenbrot, 2002). Compared with the first-generation TKI inhibitors, the second-generation EGFR-TKI (Afatinib) can irreversibly bind to EGFR1, HER2 and HER4 receptors, resulting in long-lasting receptor inhibition (Guo et al., 2019; Macha et al., 2017; Machiels et al., 2015; Solca et al., 2012).

Even though anti-EGFR therapy has potential, more work is needed to investigate the mechanisms of intrinsic and acquired resistance. New clinical trials are currently being conducted to determine the efficacy of Cetuximab in combination with other targeted agents, biomarkers, or immunotherapy to find potential novel therapeutic strategies for HNSCC patients.

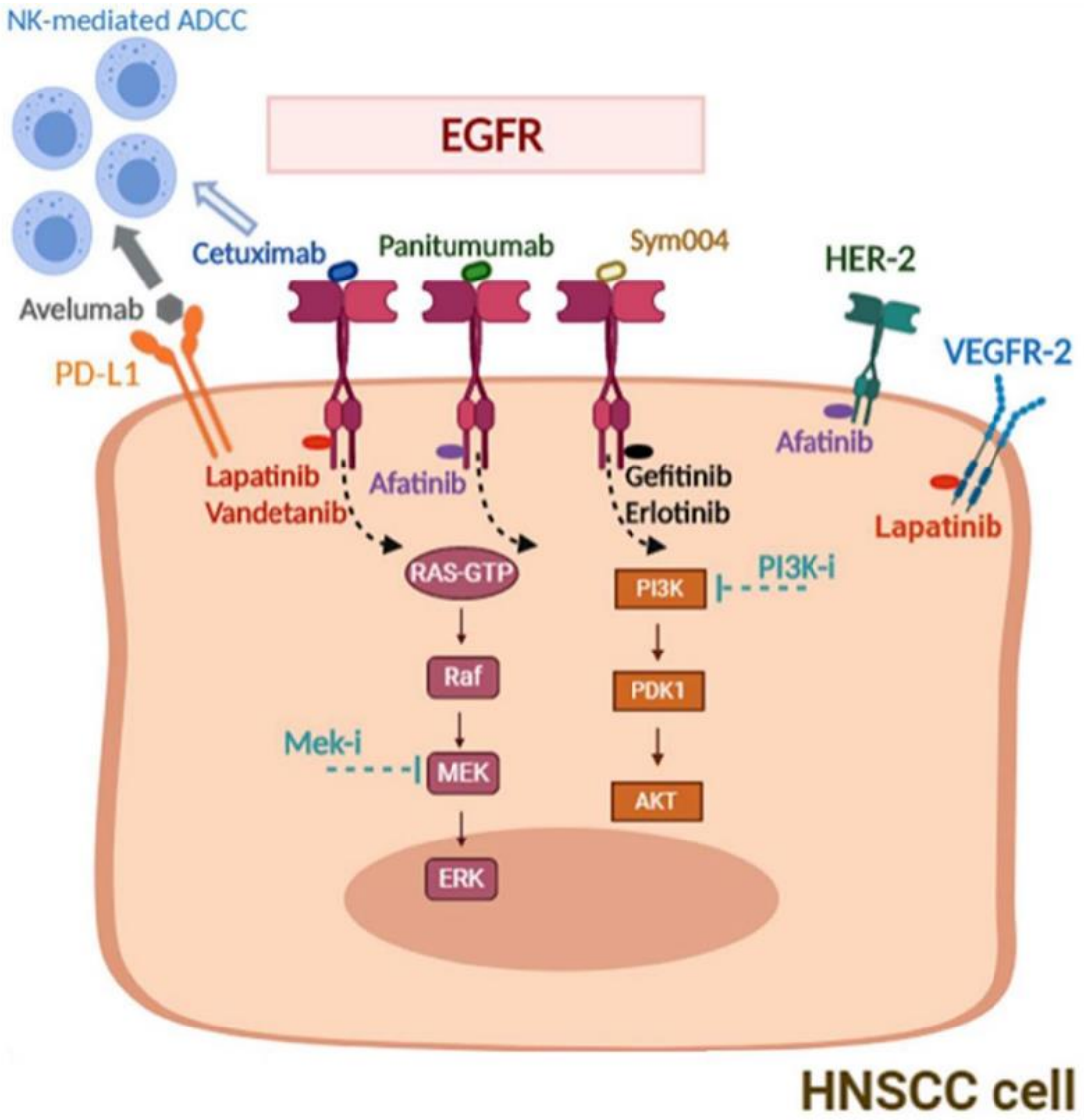

Figure 3 EGFR pathways and targets for HNSCC combination strategies (Figure adapted from (Fasano et al., 2021))*.*

1.4 Leader cells in collective cancer invasion

Cancer invasion is a fundamental feature of metastasis, the process by which cancer cells penetrate adjacent tissues, including mesenchymal single-cell invasion or amoeboid, collective invasion, etc. (Friedl, Locker, Sahai, & Segall, 2012).

According to the conventional view on the metastatic cascade, tumor cells undergoing EMT, changing their phenotype to acquire mesenchymal and migratory features, emerge in the bloodstream as single cells (CTCs) or locally invade the tissue around the primary tumor, most likely causing local recurrence.

As an alternative to this perception, collective cell migration is now receiving more attention. Numerous reports described that the primary mechanism in the metastatic cascade of collective cancer invasion is the involvement of a leader-follower organization (Casanova-Acebes et al., 2021; Kozyrska et al., 2022; Saenz-de-Santa-Maria, Celada, & Chiara, 2020; Vishwakarma, Spatz, & Das, 2020). Leader cells can sense the environment, create invasion tracks (Figure 4), and can coordinate with follower cells at the biochemical and biomechanical levels to support cancer invasion (Vilchez Mercedes et al., 2021). Recently, the collective invasion of cancer has been recognized as a key mechanism of solid tumor progression, so it is particularly important to further understand the collective invasion process and underlying molecular mechanisms.

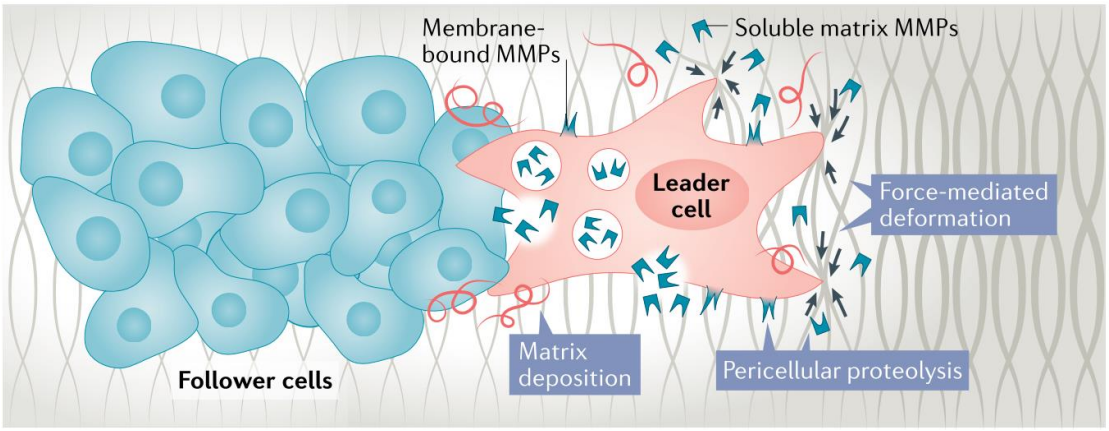

Figure 4 **Invasion track generation**

To provide a follower cell invasion route with low resistance, leader cells modify the extracellular matrix. Leader cells can facilitate the invasion of follower cells by depositing matrix proteins that serve as anchors to follower cells.

2 MATERIAL AND METHODS

2.1 Cell lines and treatments

Short tandem repeat (STR) analysis (Helmholtz Center Munich, Germany) was used to confirm FaDu and Kyse30 cell lines obtained from ATCC and DSMZ. DMEM or RPMI 1640 supplemented with 10% fetal calf serum (FCS) were used to cultivate FaDu and Kyse30 cells, respectively. FaDu and Kyse30 cell lines were cultivated using sterile tips and fluids under hygienic conditions. Cells were grown in an incubator at 37°C, with 5% CO2 and 95% humidity.

In 2D culture and the 3D model, the treatment with Epidermal Growth Factor (EGF, PromoCell PromoKine, Heidelberg, Germany), Epidermal Growth Factor Receptor (EGFR) inhibitor Cetuximab (Merk Serono, Darmstadt, Germany, 10µg/mL), MEK1/2 (MAPK–ERK kinase) inhibitor AZD6244 (Selleckchem, Munich, Germany; 100nM), and Akt signaling pathway inhibitor MK2206 (Selleckchem, 1uM) was conducted in serum-free culture medium.

2.2 Cultivation of cells

In order to cultivate the cells, FaDu and Kyse30 cells were seeded in T25/T75 flasks with DMEM/RPMI640 medium supplemented 10% fetal calf serum (FCS) and 1% penicillin/streptomycin. Cells were detached from the cell culture

surface by incubating in a 0.5% trypsin solution for 5-10 minutes at 37°C after being rinsed with phosphate-buffer saline solution (PBS) and reached a confluency of 75%. Cells were centrifuged at 400 g for five minutes to terminate the reaction, then they were resuspended in 2 mL of culture media and seeded into fresh cell culture flasks. Every 48 to 72 hours, FaDu and Kyse30 were passaged.

2.3 Cell counting

Cells were taken out after trypsin treatment in order to count the cells. Thereafter, 10 µL of the cell sample and 10 uL of a 0.4% trypan blue solution was thoroughly mixed and 10 µL of the sample mixture were loaded on an EVE™ Cell counting slide (NanoEntek, Korea). Then put the EVE™ Cell counting slide into the instrument's slide port with the sample side (side A) facing out. When the picture is adjusted for focus and the EVE™ Automated Cell Counter (NanoEntek, Korea) is used to count the cells, the Counter will display the concentration of living and dead cells as well as the viability of the cells..

2.4 EMT induction

The following procedures were used to induce the epithelial-to-mesenchymal

transition (EMT) in FaDu and Kyse30 cells: 200.000 cells/well were plated into 6-well plates, which were then cultivated in FCS-containing media for 24 hours before being withdrawn and being washed with PBS and cultured in serum-free medium for a further 24 hours. Then 9nM recombinant EGF (Abcam, Cambridge, UK, #ab50036) was given to cells for EMT induction, and cells were extracted 72 hours later for further processing. Using a Leica DMi8 microscope, morphologic changes were observed in images (Leica, Wetzlar, Germany).

2.5 Spheroid formation and embedding

Spheroids were formed in BIOFLOAT ultra-low attachment 96-well round-bottom plates (faCellitate, Mannheim, Germany). Different cell numbers were tested in the ultra-low attachment 96-well round-bottom plates to define the best cell seeding number. Seeding numbers of 3,000 per well were used for invasion experiment. To simulate the extracellular matrix (ECM) and provide the three-dimensional structure for cell invasion. Type I collagen (Corning, Oak Park, Bedford, MA, USA) was used to generate a type I collagen and serum-free medium mixture (CSM). Spheroids were embedded in CSM (concentration was adjusted to 1.7 mg/mL). To prevent the spheroids from attachment to the bottom, 40 uL of CSM was coated in the 35mm Glass Bottom u-Dishes (Ibidi, Matrinsried, Germany) and incubated for 15 minutes for solidification. Then,

160 uL CSM with embedded spheroids were added on the top of the first CSM coating layer, and the total volume of 200uL (coating layer and embedded spheroids) was put back to incubation for another 15 minutes. After the 200uL CSM has solidified, it can be used for subsequent experiments, including induction of invasion and inhibition of invasion.

2.6 Induction of spheroid invasion

To induce EGF-mediated invasion in spheroids, SF medium (DMEM for FaDu and RPMI 1640 for Kyse30) with 9 nM EGF was added on the top of 200uL solid spheroids embedded-CSM (as described in spheroid formation) and the spheroid in CSM was allowed to invade for up to 72h. All spheroids were cultivated in a 5% CO2 atmosphere at 37°C for the induction of invasion. Images were taken using a Leica DMi8 microscope 5x/10x under PH channel.

2.7 Inhibition of spheroid invasion

To inhibit EGF-mediated invasion in spheroids (as described in spheroid invasion induction), 10μg/mL Cetuximab, 100nM AZD6244, or 1uM MK2206 were used. A time period of 72hours was chosen for in both cell lines FaDu and Kyse30. All spheroids were cultivated in a 5% CO2 atmosphere at 37°C for the induction of invasion. Images were taken using a Leica DMi8 microscope

5x/10x under PH channel.

2.8 Quantification of invasion

The entire spheroid area (A1) around the outer perimeter and the core area (A2) were quantified by ImageJ, and the area of A1 minus A2 was used to evaluate the invasive area. To assess how far invasive cells migrated, the farthest cells from the center were selected (10 cells per spheroid), each distance from the center point measured and averaged. This distance was defined as invasive distance. Circularity (circularity = 4pi(area/perimeter^2)) was utilized as an indirect measure of the shape and was quantified by measuring the spheroid outer invasive perimeter. All three invasive parameters were quantified by ImageJ/Fuji.

2.9 Transfection of photoconvertible plasmid

FaDu and Kyse30 cell lines were stably transfected with an expression plasmid for the photoconvertible Dendra2-Farnesyl-5 protein (#57717, Addgene, Teddington, UK) using MATra reagent (IBA, Goettingen, Germany) following the manufacturer's recommendations. Stable cell clones were selected with 1150µg/mL neomycin in culture medium. Kyse30 cells were stably transfected with Dendra2-Farnesyl-5 plasmid (Dendra2) using Lipofectamine™ 2000

transfection reagent (Invitrogen™, Carlsbad CA, USA) and were selected with 1150µg/mL neomycin (G418).

2.10 Flow cytometry and fluorescence-activated cell sorting (FACS)

For flow cytometry and cell sorting, samples of transfected Dendra2 cell) and non-transfected control WT cells were trypsinized and adjusted to 1-5*10^6 cells per mL, filtered in a 50 µm falcon cell strainer, and kept in 15 mL tubes with ice-cold sample buffer (PBS supplemented with 1-2% FBS, EDTA 2mM, and HEPES 25mM). Cell sorting was conducted in the BD FACS Aria Fusion-4 laser cell sorter (Biomedical Center (BMC), Core Facility Flow Cytometry, Faculty of Medicine, LMU Munich) and based on the fluorescent characteristics of Dendra2 cells. Green fluorescence intensity of FaDu-Dendra2 and Kyse30-Dendra2 cells was detected in the Alexa Fluor 488-A channel and sorted by the BD FACS Aria Fusion-4 laser cell sorter. RNA-free tubes were used for sample collection in full medium or PBS for cell cultivation or RNA applications.

FaDu-Dendra2 and Kyse30-Dendra2 cells were sorted into high- and medium-intensity Dendra2-fluorescence subpopulations. The high-intensity fluorescence subpopulation of FaDu-Dendra2 and Kyse30-Dendra2 were expanded and cultivated for further experiments.

For bulk RNA sequencing sample collection, photoconverted (green to red)

FaDu-Dendra2 and Kyse30-Dendra2 samples were FACS sorted based on PE/ Alexa Fluor 488-A channel fluorescences. SYTOX™ Red Dead Cell Stain (Thermo Fischer-S34859) was used to monitor cell viability in flow cytometry. Results were analyzed by software BD FACSDiva version 8.0.1.

2.11 Photoconversion

Spheroids were generated with Dendra2-Farnesyl-5 plasmid transfected cells (FaDu and Kyse30) as described in the “Spheroids formation and embedding” section. Photoconversion of spheroids was conducted with a Leica DMi8 microscope system or a TCS-SP8 scanning system (Leica, Nussloch, Germany). The green fluorescent Dendra2-Farnesyl-5 protein can be photoconverted from to red fluorescence based on its structural and spectroscopic characterization (see *Table 1*). The wavelength of 405nm laser light irradiation or DAPI (violet) channel was used for the photoconversion of Dendra2 protein. Multiple target areas of spheroids were selected under the stage function M&F mode and X-Y-Z coordinates of the target areas were automatically recorded by Leica software (LAS X). All cells in the target area were exposed to DAPI channel or 405nm laser, with the microscope setting: FIM 100%, IL-Fld 2 round, time interval (2 secs), exposure (5 secs), cycle (4 times). Spheroids were ready for FACs preparation after photoconversion.

Images were adjusted by Fiji/ImageJ and LAX S.

Table 1 Attributes and transitions wavelength of the Dendra2 protein

Attributes			**Transitions**		
State	Ex λ	Em λ	From	To	Switch λ
Green	490nm	507nm	Green	Red	405nm
Red	553nm	573nm	Green	Red	480nm

2.12 Dual spheroid generation

Dual spheroids were generated with FaDu-WT cells and FaDu-Dendra2 cells to test the diffusivity of various treatments (EGF, Cetuximab). First, 2,000 FaDu-Dendra2 cells per well were seeded into 96 wells of ultra-low adherent plates to create a fluorescence core (Green) on day one. FaDu-Dendra2 (fluorescence) cells were allowed to form a stable fluorescence core for 24 hours, then 8,000 FaDu-WT (non-fluorescence) cells were added into the same well. After another 24 hours, FaDu-WT cells surrounded the core of FaDu-Dendra2 cells, generating a dual spheroid composed of a fluorescent inner core and a non-fluorescent outer area.

2.13 Time-lapse imaging and diffusivity test

An Ibidi stage top incubation system (Ibidi, Gräfelfing Germany) was used for cell incubation. Leica DMi8 microscope was equipped with the Ibidi heating and gas incubation systems. The temperature of the incubator chamber was adjusted to 37 °C (37 °C) and the 5% CO2 at a flow rate of 10 L/hour and 80% humidity was provided by Ibidi gas incubation system. All settings can be adjusted by the peripherals or through the IncuControl software Version 1.0.3 (Ibidi, Gräfelfing Germany).

Through time-lapse imaging, dual spheroids were used to test the diffusivity of EGF and Cetuximab. FaDu-Dendra2 dual spheroids were plated into Ibidi 35mm lass Bobttom u-dishes (Ibidi, Matrinsried, Germany) as described in the “Spheroid formation and embedding” section. Treatment with 9nm EGF or 9nm EGF plus 10 ug/mL Cetuximab was used for EGF-mediated invasion or EGF-mediated invasion inhibition. Then, Ibidi 35mm glass bottom u-dishes were put into the Ibidi incubator 35mm insert (#10934, Ibidi, Matrinsried, Germany) and fitted into the incubator chamber. Upon completion of spheroid detection, the focus (Z coordinate) was adjusted manually according to the FITC channel (green fluorescence). Then, all target spheroids and their positions, including X-Y-Z coordinate information, were marked and recorded in the Leica DMi8 microscope system and the LAS-X software. Microscope setting: FIM 100%,

IL-Fld 6 round, time interval (20 minutes), exposure (PH channel 10 ms; FITC channel 50 ms), cycle (217 times = 72hours), and PH channel and FITC channel were used for 72 hours observation. All images were adjusted by Fiji/ImageJ and LAS X.

2.14 IHC staining

For immunohistochemistry (IHC) staining, spheroid samples were collected, embedded in Tissue Tek gel (Sakura Finetek Europe, 2408 AV Alphen aan den Rijn, Netherlands), and quickly frozen in liquid nitrogen. Using a Cryostat model CM 1900 (Leica, Nussloch, Germany), cryo-preserved spheroid samples were sectioned into serial slices with a 4 m thickness and fished with glass slides. All of the samples were first fixed for 5 minutes at room temperature (RT) in acetone, then for 5 minutes at RT in the dark with 3.5 percent paraformaldehyde (PFA). Next, samples were rinsed three times in PBS (0.01 M) for 5 minutes at room temperature. Sections were incubated for 30 minutes at room temperature with a goat anti-human IgGFc peroxidase-conjugated antibody (1:500 in Tris), followed by two PBS washes (0.01 M). Samples were finally stained using amino-ethylcarbazole (AEC, A6926, Sigma, St.Louis, USA). Hematoxylin was used to counterstain (blue). Images were captured using an Olympus BX43F fluorescent microscope and CellEntry software after samples

were covered with Kaiser's glycerol gelatin (Merck) (Olympus, Tokyo, Japan).

Alternatively, spheroids were directly fixed within the collagen matrix for an *in situ* staining of antigens. Medium in the u-Dish was removed, and spheroids were washed once with PBS, and fixated with 2% PFA in PBS at pH 7.4 for 20 min at RT. Thereafter, samples were permeabilized with PBS containing 0.5% Triton X-100 for 10 min at 4°C and rinsed three times with PBS, 10-15 min per wash at RT. Then, primary block with PBS and 10% goat serum was performed for 1 hour followed by a secondary block with PBS and 10% goat serum for 30 min. Samples were then incubated with primary antibody (1:500, SPHK1 antibody (PA5-28584), Invitrogen) in the secondary block solution overnight at 4°C, washed three times (each 20 min), and then incubated with secondary antibody (goat anti-rabbit Alexa 488, 1:250) is supplemented with 10% goat serum for 40 minutes at RT. Washed three times (20 minutes per time). Nuclei were counterstained with DAPI for 15 min at RT. Samples were then washed once with FBS for 5 min at RT. Pictures were taken using a Leica DMi8 microscope system.

2.15 Samples collection for RNA sequencing (RNAseq)

On day one, 8,000 FaDu-Dendra2 cells or 10,000 Kyse30-Dendra2 cells were seeded to generate spheroids as described in the 2.5 Spheroid formation and

embedding section. Cells were grown in ultra-low adherent plates with complete medium for 48 hours. Thereafter, spheroids were collected and embedded in type I collagen as described in the “Spheroid formation and embedding” section with at least 12 spheroids per 35 mm glass dish. Samples were divided into different groups, including serum-free and high-dose EGF (EGF^h, 9 nM), Cetuximab group (9 nM EGF + 10 μg/mL Cetuximab), MEK inhibitor group (9 nM EGF + 100 nM AZD6244). Fadu-Dendra2 spheroids and Kyse30-Dendra2 spheroids were treated in different groups for 72 hours. Thereafter, invasive cells in Dendra2-expressing spheroids were photoconverted as described in the “Photoconversion” section. 10-12 invasive areas per spheroid and 40 spheroids in each group were photoconverted. After the photoconversion process, cells were isolated from the CSM. Firstly, the medium was removed from the dish and 0.1 mg/mL collagenase (C9722, Sigma, Missouri, USA) was used to degrade the collagen in the CSM for 15 minutes at 37°C. Secondly, dishes were checked under the microscope to ensure no collagen was left, spheroids were centrifuged at 400g for 4 minutes and collected into RNAse-free tubes (1.5 mL). At last, to obtain single cells for cell sorting, all spheroids were resuspended in Accutase for 10 minutes (#07922, STEMCELL Technologies, Cologne, Germany) and pipetted up down gently to prevent cell aggregation. After centrifuging and washing twice with PBS, the single-cell

suspension was prepared in ice-cold FACS buffer for sorting. Cells were sorted as described in the “Flow cytometry and Fluorescence-activated cell sorting (FACs)” section. At least over 1,000 cells per group were sorted into RNAse-free tubes for RNAseq. All treatment samples came from three or four biological replicates.

2.16 RNA-sequencing samples: Quality test and library preparation

For the 3'-RNA sequencing (RNASeq), RNA extraction was conducted by cooperation partners at the Helmholtz Zentrum München Deutsches Forschungszentrum für Gesundheit und Umwelt (GmbH). Qiagen RNeasy Micro Kit (Cat.74004, QIAGEN GmbH, Hilden, Germany) and DNAse I digest were used for RNA extraction and at the end the RNA was eluted in 14 uL water.

Extracted RNA was quantified with the Qubit-Fluorometer and reverse transcribed with QuantiTect reverse transcription kit (Qiagen). The quality of RNA was assessed using a Bioanalyzer 2100 System (Agilent Technologies Inc., SA) with the Agilent RNA6000Pico kit (#5067-1513, Agilent Technologies Inc., USA). RNA integrity was evaluated by calculating the percentage of fragments larger than 200 nucleotides (DV 200). In the case of low RNA concentration, samples were evaporated using a SpeedVac vacuum concentrator. For the library prep, the Lexogen QuantSeq 3′ mRNA-Seq Library

Prep Kit FWD for Illumina was used according to the manufacturer´s instructions using 50ng RNA (SKU:015.96, Lexogen GmbH, Austria) with additional Add-on PCR (SKU:020.96, Lexogen GmbH, Austria) for all samples. Depending on the result from this Add-on PCR, samples were split into two groups with either 17 or 19 amplification cycles. Thereafter, 16 µL of the library preparation was transferred to a new plate. Quant-iT™ PicoGreen™ dsDNA Assay Kit (P 7589, invitrogen, USA) and the Bio analyzer High Sensitivity DNA Analysis Kit (#5067-4626, Agilent Technologies, Inc., USA) were used to check the quality and concentration of the libraries. Then, 3-prime RNA-sequencing was performed on an Illumina NovaSeq platforms (Illumina, Inc. USA) by the Novogene company (Company Limited, UK). RNA-seq profile pre-processing was conducted in cooperation by Kristian Unger at the HMGU. Genes with a sum of count greater than 300 across all samples were kept for further analysis.

2.17 General data analysis and statistics

Data analysis was performed by R language (version 4.1.2 (2021-11-01) - "Bird Hippie"). The downstream bioinformatics analysis was completed in cooperation with Zhongyang Lin and Zhengquan Wu. Microarray derived RNA profiles of Cetuximab resistant/sensitive cell lines (1Cc8/SCC1) were retrieved from Gene Expression Omnibus (GEO) by GEOquery package (accession

number GSE21483).

2.18 Overview of samples

Count read data were variance-stabilizing transformation (VST) transferred, which is a combination of scaling and accounting for variability of low counts. The *dist* function was applied for calculating sample-to-sample distances and clustered samples were indicated in heatmaps. Further, principal components based on transferred gene expression were also computed by principal component analysis (PCA), and the first two components, which best explain differences between samples, were utilized for visualizing the distribution of samples.

2.19 Differential expression analysis

With count read data as input, the *DESeq2* package was used for differential gene expression analysis. Genes with adjusted P <0.05 and log2(foldchange) > 1 were defined as differential expressed genes (DEGs) in comparisons of treatments (*e.g.*, Out vs. SF). The results of DEGs were visualized by volcano plots implementing.

2.20 Gene set enrichment analysis (GSEA)

The *ClusterProfiler* package was applied for functional enrichment analysis and visualization. Genes were ranked by log2(foldchange) generated from individual differential expression comparisons. By using *bitr* function, gene symbols were transferred into ENTREZID. Hallmark gene sets (v7.5.1) were downloaded from Molecular signature database (MSigDB). GSEA was performed based on pre-ranked genes and pre-defined hallmark gene sets (n = 50 with n = 200 defining genes each). Hallmarks significantly activated or suppressed were selected based on a default p value of 0.05. Moreover, normalized enrichment scores (NES) and corresponding false discovery rates (FDR) were also computed for all hallmarks in order to adjust the significance level.

2.21 Co-expression module analysis

Co-expression modules associated to EMT and MAPK, PI3K, and EGF EGFR pathway activities were investigated using weighted gene co-expression network analysis (WGCNA, WGCNA package was used, and the threshold is $P<0.05$). In the single cell RNA-seq dataset GSE103322, the genes with the highest (top 25%) variance in expression levels across samples were imported to the WGCNA. Scale independence and mean connectivity analysis

with varying power levels were used to derive the soft threshold of module analysis. To describe the cluster amongst modules, a cluster dendrogram was created.

2.22 Module-trait analysis

To find important co-expression modules associated with the clinical features, information on the biological processes and pathways EMT, MAPK activity, PI3K activity, and EGFR activity were collected (as trait). The pathway activities and biological processes were inferred by ssGSEA (Hänzelmann, Castelo, & Guinney, 2013) according to gene sets (WP, KEGG, and Hallmarks) deposited on MSigDB. According to the correlation between modules and traits, Module-trait relationships were calculated; Modules that were substantially correlated with specific traits were then found (P value < 0.05, module size < 500); Significant modules' genes were exported for additional analysis.

2.23 Statistical analysis

Unless otherwise stated, results are shown as the mean value and standard error of the mean (SEM) of three separate experiments. Using Prism's Student's T-test, significant differences between the two groups were determined (GraphPad Software, San Diego, USA). The ANOVA test with

Bonferroni adjustments in Prism was used to assess significant differences between more than two groups. Significant levels were indicated by the symbols *p-value 0.05, **p-value 0.01, ***p-value 0.001, and ****p-value 0.0001.

3 RESULTS

Head and neck squamous cell carcinomas (HNSCCs) have a poor overall survival (OS) below 50% after five years. During metastasis formation, cell invasion and migration are essential factors. Among the many causes of tumor invasion, the process of epithelial to mesenchymal transition (EMT) is widely recognized as a critical step. Previous experiments from our lab determined that epidermal growth factor (EGF) can induce tumor cells to undergo EMT (Pan et al., 2018). However, the process of HNSCC invasion and its essential mechanisms is incompletely understood. Therefore, it is imperative to build models that mimic this invasion process and help verify whether EGF can induce tumor cell invasion in a 3D cell microenvironment and explore mechanisms of EGF-mediated invasion.

3.1 EGF induces morphological changes in HNSCC cell lines.

Research from our lab demonstrated that EGF could mediate EMT in HNSCC carcinoma cells through an EGFR-dependent pathway in two-dimensional cell culture (Pan et al., 2018; Schinke et al., 2022a). To confirm previous conclusions, FaDu and Kyse30 cell lines were treated with high-dose EGF concentrations (9 nM) for 72 hours. EGF^{high}-treated cells, especially Kyse30, had an elongated fibroblast-like shape and reduced cell-cell interaction after

treatment, indicative of EMT (Figure 5).

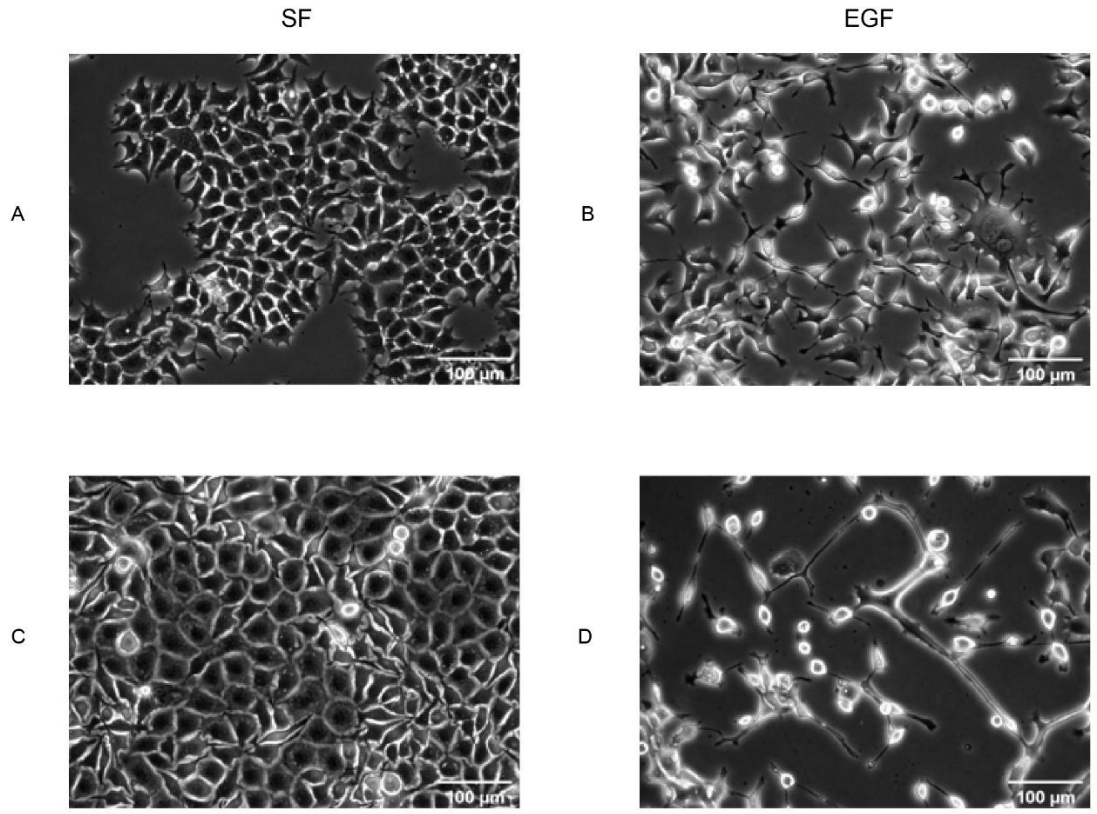

Figure 5 EGF-mediated morphology changes in FaDu and Kyse30.

FaDu and Kyse30 cells were serum-starved and treated with serum free medium or serum free medium with EGF^{high} (9 nM). After 72 hours, images were taken with the Leica DMi8 microscope at 10x in the PH channel. Scale bar: 100 um. Shown are representative pictures of four groups: (A) FaDu SF, (B) FaDu EGF^{high}, (C) Kyse30 SF, (D) Kyse30 EGF^{high}.

3.2 EGF-mediated invasion in 3D cellular model

3.2.1 3D cellular model establishment

To mimic the *in vivo* process of tumor invasion, a 3D tumor cell environment was recapitulated *in vitro*. Extracellular matrices (ECMs) are well-organized

networks of cells and non-cellular components found in all tissues and organs. ECMs not only act as physical scaffolding for cells but also govern a variety of biological activities such as cell proliferation, migration, or cancer invasion. ECMs comprises a wide range of matrix macromolecules with different compositions. Collagens, elastin, fibronectin (FN), and laminins are fiber-forming proteins that are highly acidic and hydrated molecules that make up ECMs. ECMs are mostly composed of collagen type I and cartilage collagen type II to a lesser extent (Theocharis, Skandalis, Gialeli, & Karamanos, 2016). Collagen type I is also widely used to construct a tumor 3D environment (Tevis, Colson, & Grinstaff, 2017). Therefore, collagen type I served to simulate the ECM structure for tumor cell invasion in our experiments.

Spheroids were generated with FaDu tumor cells in BIOFLOAT ultra-low attachment 96-well round-bottom plates. To provide a stable 3D environment and a suitable pore size for tumor cell invasion in the 3D environment (collagen-SF medium mixture (CSM)) different cell numbers (3,000 or 5,000) and concentrations of CSM were tested. The results showed that at a concentration of 1.7 mg/mL CSM, spheroids of 3,000 cells maintained the most stable structure compared to the other three conditions (Figure 6). According to other studies on collagen pore size, 1.5 mg/mL collagen matrices have a median pore size of 10.99 μm (T. Fischer, Hayn, & Mierke, 2019), which provides sufficient

space for cells to invade or migrate through pores. The concentration of 1.7 mg/mL served as CSM concentration for all following experiments. The results were consistent in both FaDu and Kyse30. To simplify the description, only the results of the FaDu cell line are shown unless specifically mentioned.

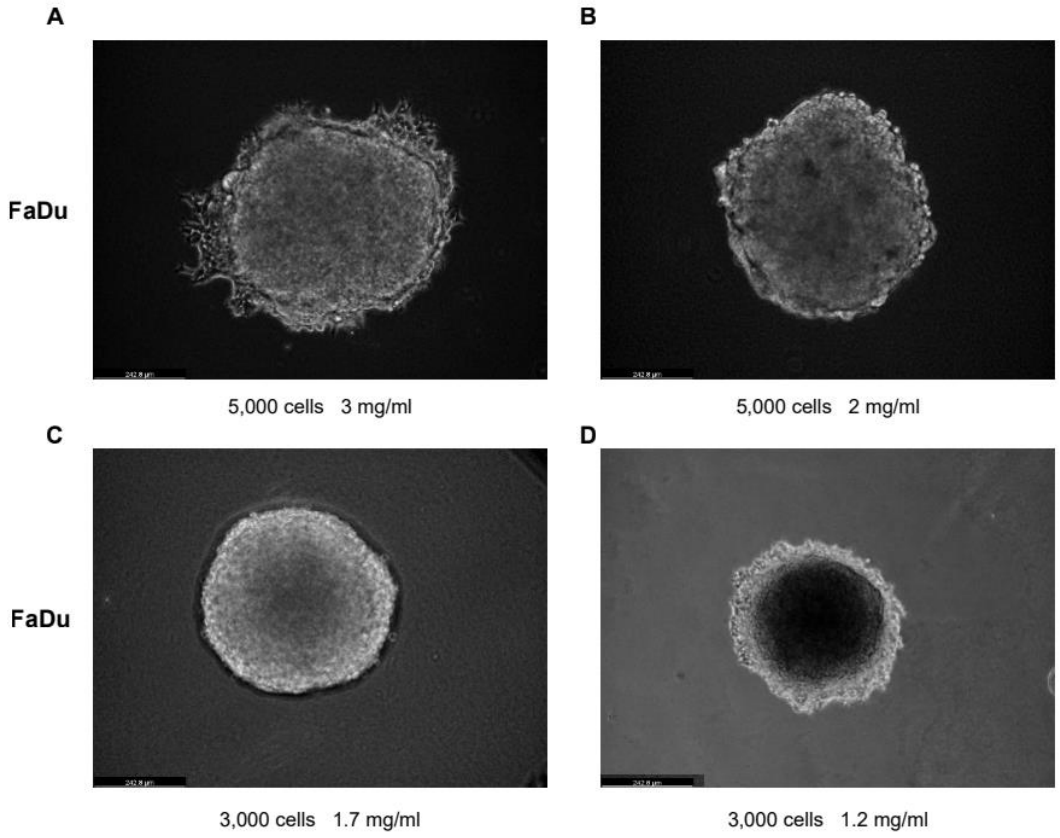

Figure 6 Collagen concentration test.

Tumor cell spheroids were generated in BIOFLOAT ultra-low attachment 96-well round-bottom plates. Spheroids were embedded in CSM as described in the Methods section. Morphology pictures were taken with a Leica DMi8 microscope in the PH channel. Shown are representative pictures of four different condition: (A) 5,000 cells, CSM concentration:3 mg/mL, (B) 5,000 cells, CSM concentration: 2 mg/mL, (C) 3,000 cells, CSM concentration: 1.7 mg/mL, (D) 3,000 cells, CSM concentration: 1.2 mg/mL.

3.2.2 EGF-mediated spheroid invasion in 3D cellular model

To further address whether EGF can induce invasion in an ECM environment, tumor spheroids were placed into 35mm glass dishes as depicted in Figure 7, and 40 µL CSM were precoated to prevent the spheroid from attaching directly to the bottom of the glass (Figure 7, 1). Then, EGF (9nM) with and without EGFR inhibitor Cetuximab (Figure 7,1 and Figure 8) were added into the medium to investigate whether EGF specifically induces 3D invasion.

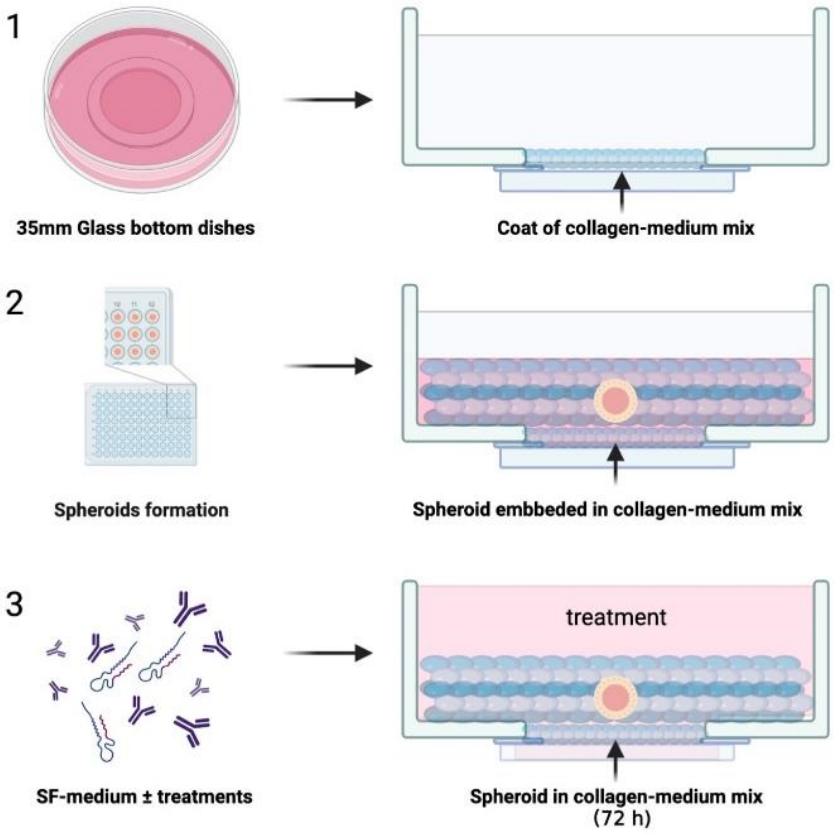

Figure 7 Spheroid embedding and treatment.

Schematic representation of the 3D tumor spheroid model embedded into type I collagen-SF medium mix. Treatments are: (1) 40 µL of collagen SF-medium

mix were coated at the bottom of 35mm glass dish. (2) Tumor spheroids were generated in BIOFLOAT ultra-low attachment 96-well round-bottom plates with 3,000 cells per well. Spheroids were embedded in CSM as described in the Methods section and were incubated for 10-15 minutes at 37°C, with 5% CO2 and 95% humidity. (3) Two mL of SF-medium with/without treatment were added on top of the collagen-SF medium mix for the different groups.

Time-lapse imaging was performed with FaDu spheroids over a time period of 48hours. Time-lapse imaging results demonstrated that no tumor cells invaded in the SF control group within 48 hours (Figure 8, left row). In contrast, in the EGF (9nM) treatment group, tumor cells gradually invaded from the spheroid to the surrounding CSM starting from 16h, and the tight spheroid structure became looser over time (Figure 8, middle row). In the group co-treated with EGF (9nM) and Cetuximab (10 μg/mL), the results showed that EGF-mediated tumor cell invasion was significantly inhibited by Cetuximab, with only a few tumor cells still invading the surrounding CSM, and the spheroid structure remained tighter compare to the EGF group (Figure 8, right row).

Hence, the time-lapse imaging results show that EGF can induce HNSCCs invasion in 3D structures in which collagen is the main component. Furthermore, Cetuximab, a specific inhibitor of EGFR, significantly inhibited this process, demonstrating that the 3D invasion was EGF/EGFR-specific.

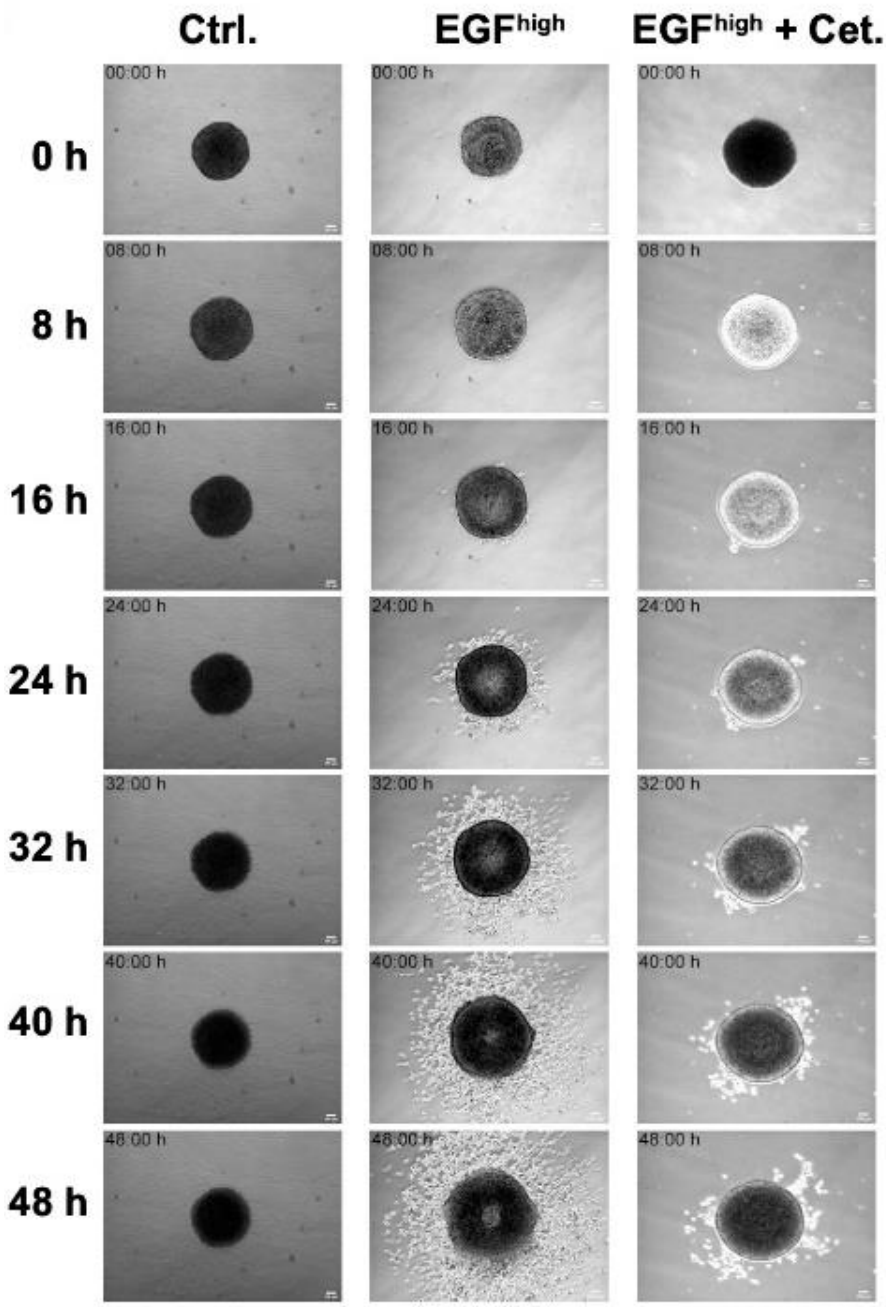

Figure 8 Time-lapse imaging for EGF-mediated invasion and inhibition

FaDu tumor cell spheroids were generated in ultra-low attachment plates and seeded in 35mm dishes as described in Figure 3. Representative pictures of SF, EGF (9 nM), and EGF (9 nM) plus Cetuximab (10 µg/mL) treatment groups at a total of 7-time points over 48 hours are shown (8-hour intervals between

pictures in each group). To simplify the description, only the results of the FaDu cell line are shown.

3.2.3 Molecular diffusion in 3D tumor spheroid model

Although we deduced from the previous results that EGF causes HNSCC cells to invade three-dimensional formations, it is still unknown how well EGF and Cetuximab disperse and penetrate the whole spheroid formation. To address this open question, Spheroids treated for 24 and 48 hours with EGF plus Cetuximab encapsulated in CSM as described in Figure 8 were cryo-preserved and processed into sections . Spheroid sections were stained with a goat anti-human IgGFc peroxidase-conjugated secondary antibody to assess the localization of Cetuximab within the spheroid.

At 24 and 48 hours, immunohistochemistry staining revealed no positive staining in the control staining without secondary antibody (negative) (Figure 9, Upper panels). On the other hand, sections incubated with secondary antibody displayed red positive staining of Cetuximab equally dispersed across the center and external areas of the spheroid (Figure 9, Bottom line). Hence, the presented staining revealed that Cetuximab permeated the whole spheroid with a diameter of approx. one millimeter.

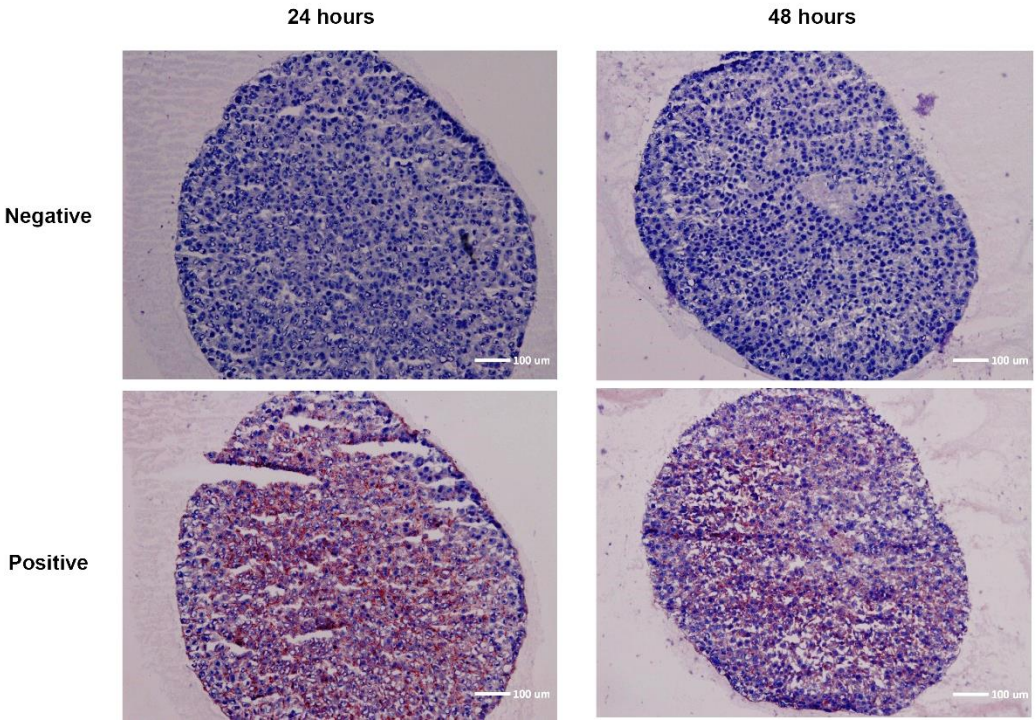

Figure 9 Immunohistochemistry staining of Cetuximab in FaDu.

FaDu cell spheroids were generated in BIOFLOAT ultra-low attachment 96-well round-bottom plates by seeding 8,000 cells. Spheroids were treated with 9 nM EGF and 10 µg/mL Cetuximab for 24 hours and 48 hours as described in Figure 7. Spheroids were cryo-preserved, sectioned, and stained with a goat anti-human IgGFc peroxidase secondary antibody at 24 and 48 hours, respectively. Shown are representative pictures of four different groups: Negative control 24 hours (without secondary antibody; Top left), Negative control 48 hours (Top right), Positive control 24 hours (with secondary antibody; Bottom left), Positive control 48 hours (Bottom right).

3.2.4 Invasive cells originate from all layers of spheroids

Next, an experiment was designed to explore the origin of invading cells within spheroids, *i.e.* outer leaflets or from any location in spheroids. Wild-type FaDu cells (FaDu-WT) were transfected with Dendra2-Farnesyl-5 plasmid (Green fluorescence) (3.3). Then, FaDu-Dendra2 cells were used to form a small spheroid representing a core, surrounded by FaDu-WT cells without

fluorescence, creating a dual spheroid structure (See further description in (2.12)). Such a dual spheroid was then applied to the constructed 3D invasion model (Figure 7).

We expected a concentration gradient of EGF and Cetuximab within spheroids (Figure 10, Top left) where the concentration gradually decreases from the outside to the inside (Hirschhaeuser et al., 2010; Peirsman et al., 2021; Tevis et al., 2017). Therefore, dual spheroids were treated with EGF concentrations inducing cell invasion and spheroids were analyzed by time-lapse fluorescence microscopy. Green fluorescent cells located at the core of the dual spheroids migrated, penetrated the whole spheroid, and eventually invaded the outer type I collagen (Figure 10, Bottom left). Co-treatment of dual spheroids with EGF and Cetuximab blocked the migration and invasion of fluorescent tumor cells from the core, demonstrating that Cetuximab efficiently blocks EGFR-mediated migration and invasion throughout the entire spheroid. Time-lapse fluorescence microscopy visualization of the dynamics of invasion showed that starting around 16 hours, green-fluorescent FaDu cells began to migrate and permeate the entire spheroid, invading the collagen surrounding the spheroid (Figure 10, EGF^{high} column). The invasive distance progressively increased over time (Figure 10, EGF^{high} column) and invasive cells entering the type I collagen ECM represented a mix of green-fluorescent cells from the spheroid core and non-fluorescent cells from the periphery, as shown in the merged picture on the right in EGF^{high} column (Figure 10). This result demonstrates that the invasive tumor cells originated from the entire spheroid.

In contrast to the strong induction of invasion in the EGF^{high} group, Cetuximab substantially inhibited EGF-mediated invasion upon co-treatment (Figure 10, Bottom left). Furthermore, time-lapse imaging revealed that Cetuximab

indiscriminately suppressed the EGF-mediated invasion of both FaDu-Dendra2 cells in the core and peripheral FaDu-WT cells (Figure 10, EGF^{high} plus Cet column). However, the inhibition was not complete and a small proportion of cells entered type I collagen starting at 16-hours. Hence, the EGF plus Cetuximab group's results show that Cetuximab effectively blocks EGF-mediated invasion throughout the spheroid.

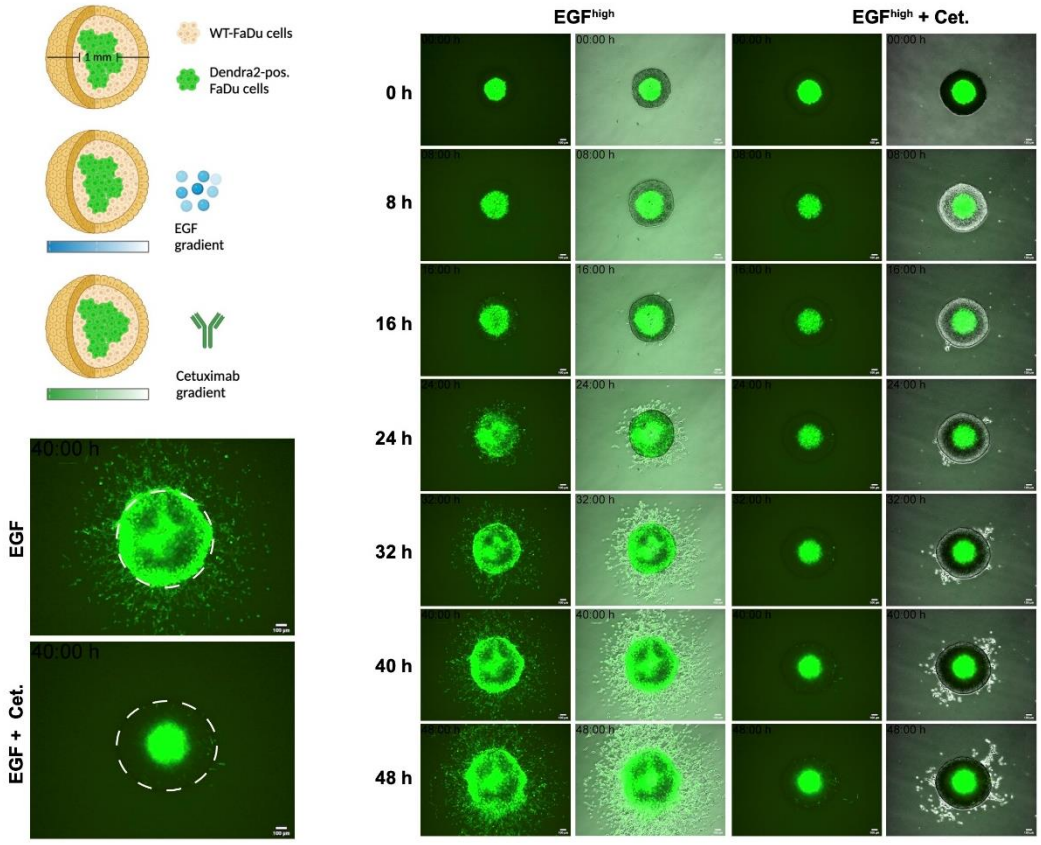

Figure 10 Origin of invasive cells and time-lapse imaging.

Dual spheroids were generated as described in the Dual spheroid generation section (2.12). The structure of dual spheroids is shown in the scheme on the top left: the internal green FaDu-Dendra2 cells and the external non-fluorescent FaDu-WT cells are included along with theoretical concentration gradients of

EGF and Cetuximab (Top left). Fluorescence picture of EGF (9nM) and EGF(9nM) plus Cetuximab (10 µg/mL) at 40h are shown (Bottom left). Time-lapse imaging pictures (0-48h) were taken with a Leica DMi8 microscope in the FITC (GFP) and PH (Phase contrast) channels and are shown on the right. Representative pictures of EGF^{high} (GFP, left; GFP and phase contrast Merged, right) and EGF^{high} plus Cetuximab treatments (GFP, left; GFP and phase contrast Merged, right) are shown.

3.2.5 Invasion inhibition by inhibitors of EGFR-associated pathways

Based on our previous research, it is known that among the two pathways downstream of the EGF-EGFR pathway, the MAPK/ERK signaling pathway plays a more important role than the PI3K/AKT signaling pathway in EGF-mediated EMT (Pan et al., 2018).

To explore which EGFR-associated pathway is most relevant in 3D invasion, tumor cell spheroids were either kept untreated under serum-free conditions (SF) or treated with EGF^{high}, EGF^{high} plus Cetuximab, EGF^{high} plus MEK inhibitor or EGF^{high} plus AKT inhibitor. FaDu and Kyse30 maintained the same pattern across all groups, according to the representative pictures. There was essentially little cell invasion in the SF group. EGF^{high} enhanced cell invasion greatly, whereas Cetuximab and MEKi decreased cell invasion significantly. The AKTi treatment partially blocked the invasion (Figure 11).

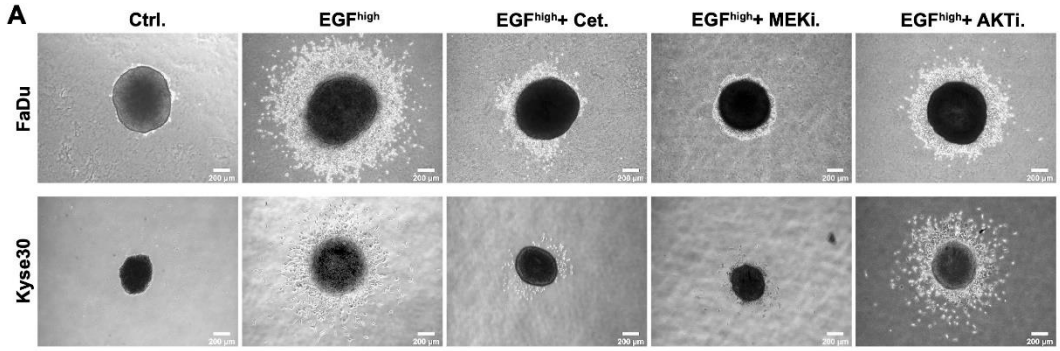

Figure 11 EGF-mediated invasion and inhibition.

Tumor cell spheroids were generated and embedded in CSM as described in the Method section. Pictures were taken with a Leica DMi8 microscope in the PH channel. Shown are representative pictures of five groups in FaDu (Upper line) and Kyse30 (Bottom line) cell lines. From the left to the right: Ctrl (SF), EGF^{high} (9 nM), EGF^{high} (9 nM) with Cetuximab (10 µg/mL), EGF^{high} (9nM) with AZD6244 (100nM, MEK inhibitor), EGF^{high} (9 nM) with MK2206 (1uM, AKT inhibitor). Scale bar: 200 µm.

3.2.6 Quantification of the invasion

To identify and assess differences between treatments, ImageJ software was used to quantify the invasion of five treatment groups: *Ctrl (Serum free), EGF^{high} (9 nM), EGF^{high} (9 nM) and Cetuximab (10 µg/mL), EGF^{high}(9nM) and MEK inhibitor (100 nM), EGF^{high} (9 nM) and AKT inhibitor (1 uM)*. Quantitative indicators refer to two parameters: Invasive area and invasive distance (Figure 12, upper). The invasive area represents the area covered by tumor cells outside of the boundaries of the initial spheroid. The invasive distance refers to the maximal distance covered by tumor cells measured from the spheroid center.

The results in FaDu cell line showed that the EGF^{high} group had the highest invasion area and invasion distance, which was statistically significant compared to all the remaining groups. The invasion was strongly inhibited in the CET and MEKi groups compared to the EGF^{high} group, and the degree of invasion was close to that of the SF group. The AKTi group was more invasive than the CET and MEKi treatment groups, but still statistically significant compared to the EGF^{high} group (Figure 12, bottom).

The result of the Kyse30 cell line was identical to that of the FaDu cell line in that EGF treatment remained the strongest inducer measured as invasion area and distance. The Cetuximab and MEKi (AZD6244) treatment groups greatly prevented cell invasion as compared to the EGF group, and their values were comparable to the SF group and statistically significant. The AKTi group had less invasion than the EGF group. However, the difference was only statistically significant in the invasion area measure (Figure 12, bottom).

Hence, these quantification results of inhibitor treatments demonstrated that Cetuximab and MEKi (AZD6244) strongly inhibit EGF-mediated 3D invasion, while AKTi (MK2206) only partially inhibits the process. This indicates that the RAS-RAF-MEK-ERK pathway plays a major role in the process of EGF-EGFR-mediated invasion in our 3D cellular model.

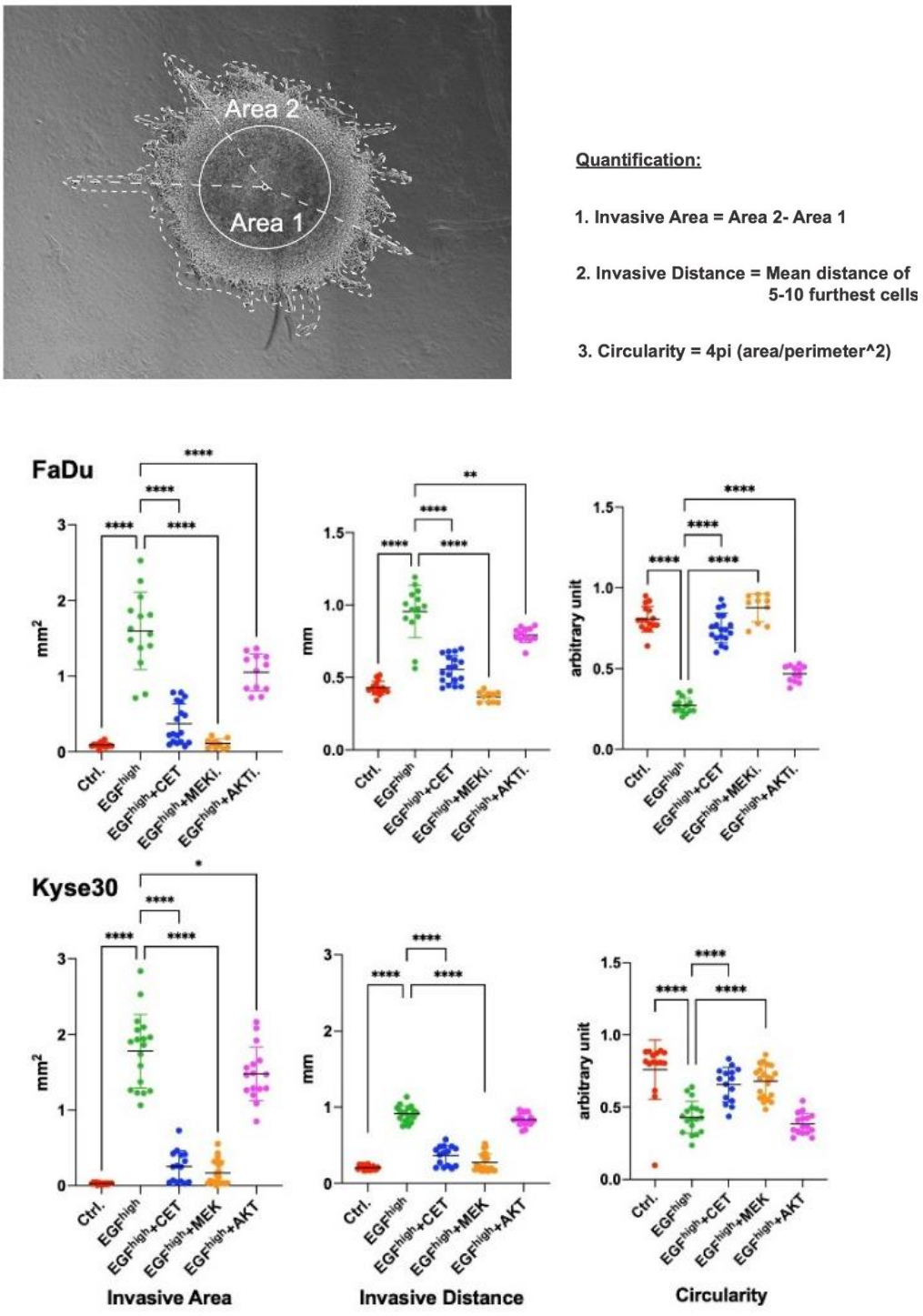

Figure 12 Quantification of invasion in the 3D tumor spheroid model.

Upper picture describes the quantification method of 3D invasion. Area 2 (Outer dashed line) includes the whole spheroid center plus the invasive part. Area 1 (Inner Circle) is the center part representing the initial spheroid. The invasion

*distance is the straight dotted line. 3D invasion quantified result (bottom) are shown for FaDu and Kyse30 cells, including Ctrl (Serum free), EGF^{high} (9 nM), EGF^{high} (9 nM) and Cetuximab (10 µg/mL), EGF^{high} (9 nM) and MEK inhibitor (100 nM), EGF^{high} (9 nM) and AKT inhibitor (1 µM) groups. Shown are means with standard deviations (SD) from at least n = 3 independent experiments performed in 3D invasion assay (72 hours) with several single spheroids depicted by individual filled circles. One-Way ANOVA with Šídák's multiple comparisons test, Brown-Forsythe test and Bartlett's test p-values * 0.05, ** 0.01; *** 0.001, **** 0.0001.*

3.3 Dendra2-Farnesyl-5 plasmid transfection and photoconversion

3.3.1 Dendra2-Farnesyl-5 plasmid (Dendra2) transfection

Locating, selectively enriching, and characterizing individual cell populations of interest in the 3D cell model is a prerequisite to understand the process of EGF-mediated invasion. Therefore, a Dendra2-Farnesyl-5 expression plasmid encoding the photoconvertible Dendra2 protein was transfected into FaDu and Kyse30 cell lines for stable expression. FaDu cells were transfected with photoconvertible Dendra2 plasmid using MATra reagent and selected with neomycin (G418). Kyse30 cells were transfected with Dendra2 plasmid using Lipofectamine™ 2000 Transfection Reagent and selected with neomycin (G418).

Four different antibiotic concentrations were examined to find the best antibiotic concentration: 100µg/mL, 450µg/mL, 800µg/mL, and 1150µg/mL. From the representative pictures, we deduced that 1150µg/mL was the more efficient

antibiotic concentration for selection, which was utilized to select the Dendra2-transfected cells (Figure 13).

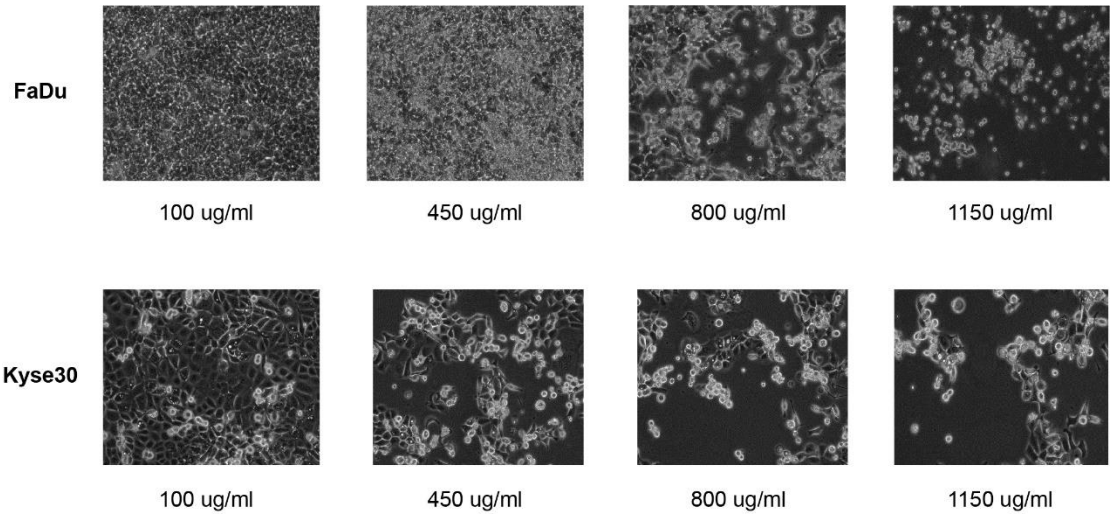

Figure 13 Antibiotic concentration test.

Representative pictures showing the FaDu or Kyse cell line were selected after 24 hours by adding four different concentrations of neomycin:100μg/mL, 450 μg/Ll, 800μg/mL, and 1150μg/mL.

3.3.2 Establishment of high expression Dendra2 cell clones

Transfected cells showed heterogeneous fluorescence expression after transfection and selection of the Dendra2 plasmid. To utilise Dendra2 cells for photoconversion in subsequent experiments, transfected cells with a high expression of Dendra2 were sorted by fluorescence-activated cell sorting (FACS). A step-by-step gating method was used to prepare single live cells (An & Chen, 2018). Forward scatter (FSC) and side scatter (SSC) parameters were used to gate and separate cells from debris, as illustrated in Figure 14A upper. Cells were gated to eliminate doublets or multiplets using FSC-width (FSC-W)

vs. FSC-height (FSC-H) and SSC-area (SSC-A) vs. FSC-area (FSC-A). After gating single live cells, green fluorescent protein-area (GFP-A) vs cyan fluorescent Protein-are (CFP-A) was used to define medium and high green fluorescent intensity area (Figure 14A, upper). To get the high-fluorescent intensity cells, a GFP fluorescence value range from $8.6x10^2$ to $3.3x10^3$ was gated as P3 and from $7.3x10^3$ to 10^5 as P4. P3 and P4 were defined as medium and high fluorescence intensities, respectively (Figure 14, A, bottom). Medium and high-fluorescent groups were sorted into 15 mL tubes for cell culture and further experiments. Eventually, we obtained 2% of FaDu highly fluorescent cells, and 1.6% of Kyse30 highly fluorescent cells, which were reseeded in T-25 flask after FACS, and representative images can be seen in Figure 14B. The FaDu-Dendra2 and Kyse30-Dendra2 cells are presented in phase contrast and FITC channels, and the sorted high-fluorescent cells have a distinct green fluorescence.

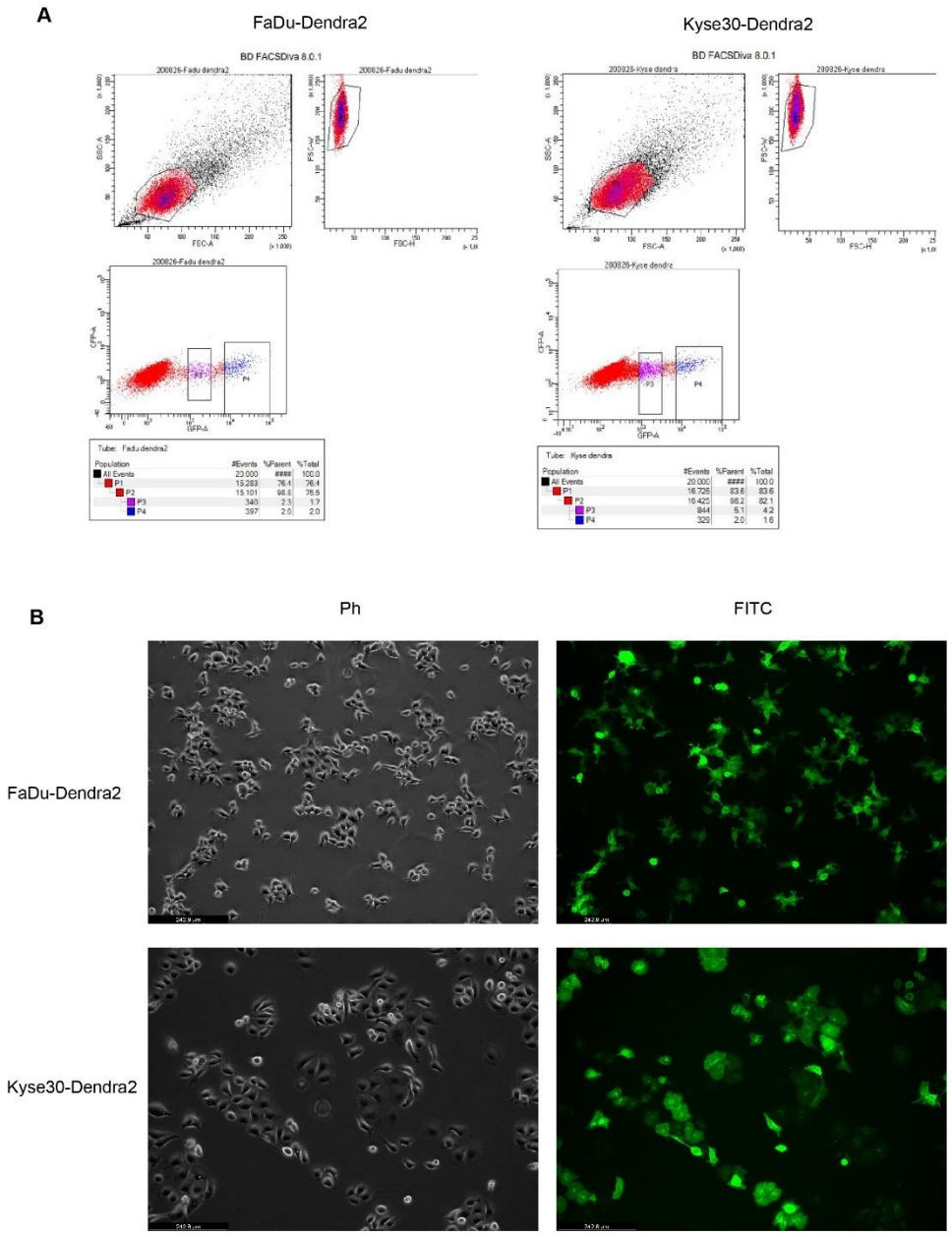

Figure 14 Sorting for high-fluorescence intensity population.

(A) Gating strategy for the enrichment of high-fluorescence Dendra2 expressing cells (FaDu and Kyse30) according to different GFP fluorescence intensity based on (FSC-W) vs. FSC-height (FSC-H) and SSC-area (SSC-A) vs. FSC-area (FSC-A). P3 is gated as a medium-fluorescent group, P4 is gated as a high-fluorescent group. (B): Representative pictures (in phase contrast and FITC channels) of sorted FaDu-Dendra2 and Kyse-Dendra2 with high fluorescence intensity.

3.3.3 Dendra2 protein carried by cells can be selectively photoconverted

After successfully transfecting and sorting FaDu-Dendra2 and Kyse30-Dendra2, the photoconversion process was examined to further exploit photoconversion options.

FaDu-Dendra2 spheroids were used for a photoconversion test in which invasive cells were selected within a target area for conversion. The entire spheroid including invasive cells was recorded in the PH and FITC (Dendra2) channels. The target cell area to be photoconverted is depicted by white frame (Figure 15, phase contrast and Dendra2).

The FITC (Dendra2-green) channel shows a green fluorescence signal in the target area before laser irradiation, whereas the TXRED (Dendra2-red) channel shows no cell fluorescence signal in the target area. After 20 seconds of laser irradiation at 405nm wavelength within the target area, cells in the TXRED (Dendra2-red) channel target area begin to convey red fluorescent signals (Figure 15,non-converted). The FITC (Dendra2-green) channel, on the other hand, continues to show a signal, indicating that the green Dendra2 protein in the cells in the area has not been entirely photoconverted. Hence, the presence of a red signal in the TXRED channel indicates that photoconversion of a part of the Dendra2 protein in the target area has been accomplished. With this technique, labeling and specific enrichment of invasive cells in situ in the

context of 3D invasion is feasible (Figure 15, photoconverted).

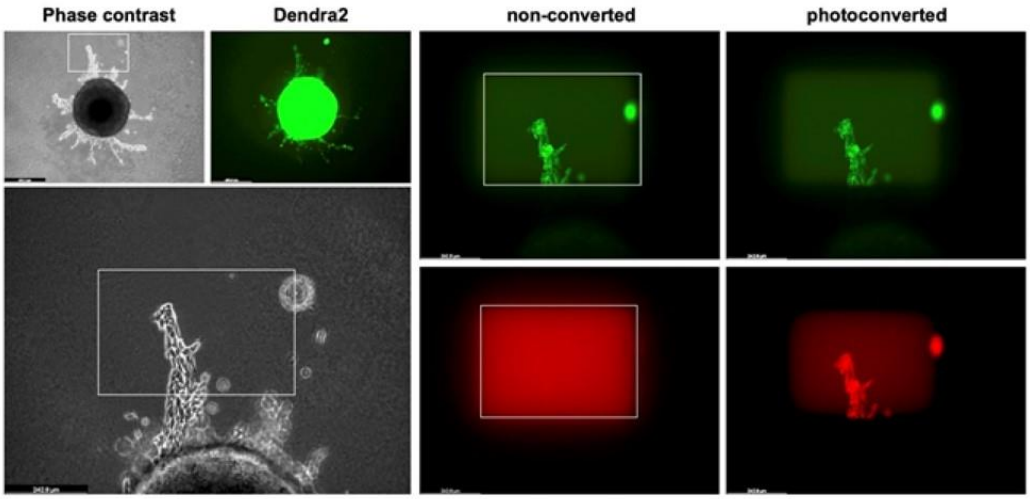

Figure 15 Photoconversion of Dendra2 protein in situ in invasive cells of a 3D tumor spheroid model.

FaDu-Dendra2 spheroids embedded in type 1 collagen were recorded in phase contrast and FITC channels (top left). The photoconversion target area is depicted as a white box with a magnified image (bottom left). The non-converted and photoconverted target areas are visualized in the FITC channel (Dendra2-green, upper right panels), and photoconverted Dendra2 in the TXRED channel (Dendra2-red, lower right panels). For photoconversion, all cells in the target area were exposed to DAPI channel with the microscope setting: FIM 100%, IL-Fld 2 round, time interval (2 secs), exposure (5 secs), cycle (4 times).

3.3.4 Flow cytometry-based enrichment of photoconverted tumor cells

Upon photoconversion, tumor cells have a dual red and green fluorescence, whereas non-converted cells only have green fluorescence. To verify whether photoconverted and non-converted cells can be distinguished by the intensity of red and green fluorescence, so as to achieve the purpose of sorting target

cells, flow cytometry was used to detect fluorescence profiles.

Using flow cytometry, the size and range of fluorescence of FaDu-WT cells were initially determined as controls (by SSC-A vs. FSC-A and PE-A vs. FITC-A) (Figure 16, top). Non-converted FaDu-Dendra2 cells were characterized by high green fluorescence (FITC-A) intensities compared to the FaDu-WT (Figure 16, Bottom left). However, cell suspensions composed entirely of photoconverted cells showed an upward shift, indicating that all cells with green fluorescence also exhibited red fluorescence (PE-A) following photoconversion (Figure 16, Bottom middle). To test for sensitivity, photoconverted and non-photoconverted cells were combined in a 1:4 ratio group. A proportion of 20 percent of photoconverted cells was well differentiated from the remaining non-converted cells in flow cytometry (Figure 16, Bottom right; “20% photoconversion”). Based on these findings, photoconverted and non-photoconverted cells can be detected and distinguished in flow cytometry.

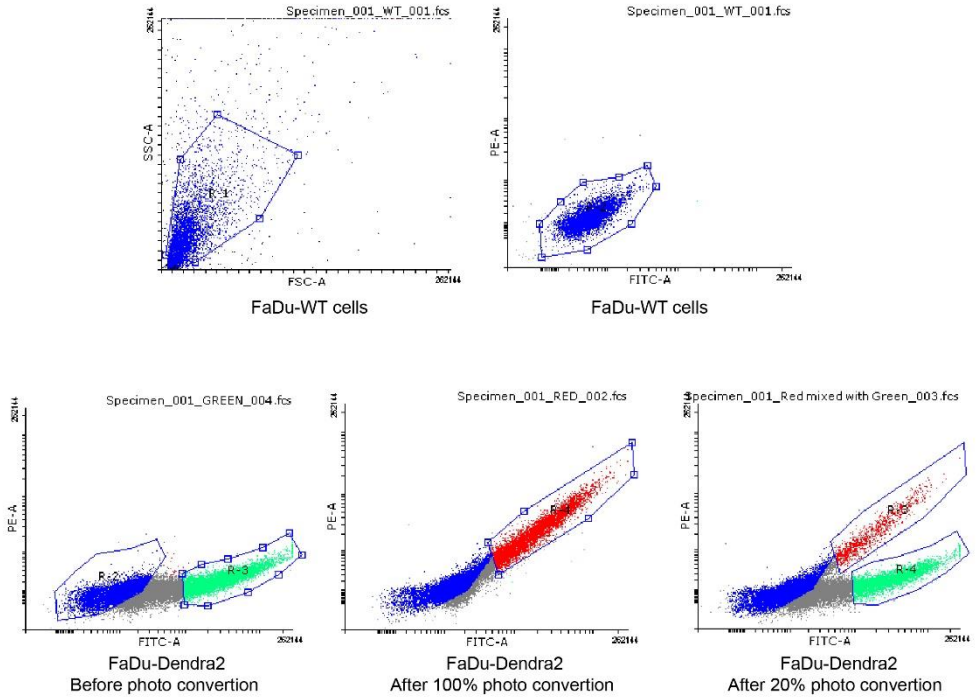

Figure 16 Specific detection of photoconverted tumor cells by flow cytometry

Shown is the gating strategy for the distinction of photoconverted FaDu-Dendra2 tumor cells. The size (Top left, R-1) and range of fluorescence (Top right, R-2) of FaDu-WT were gated by SSC-A vs. FSC-A and PE-A (Red) and FITC-A (Green). High fluorescence non-converted FaDu-Dendra2 cells were gated in R-3 (Bottom left), and 100% converted FaDu-Dendra2 cells were gated in R-4 (Bottom middle). Flow cytometry dot plot profiles of a mix of 20% photoconverted cells and 80% non-converted cells is shown in the 20% photo conversion group (Bottom right).

3.3.5 Reseed of sorted Fadu-Dendra2 cells

To test the state of cells and whether they can be cultured after FACS . After sorting, cells were reseeded to 6-wells plate for observation. The results showed that the cells were vital and started re-adhering to the culture dish after 4 and 8 hours of reseed. Cells appeared morphologically healthy (Figure 17,

left) and Dendra2 fluorescence was not affected by sorting (Figure 17, right).

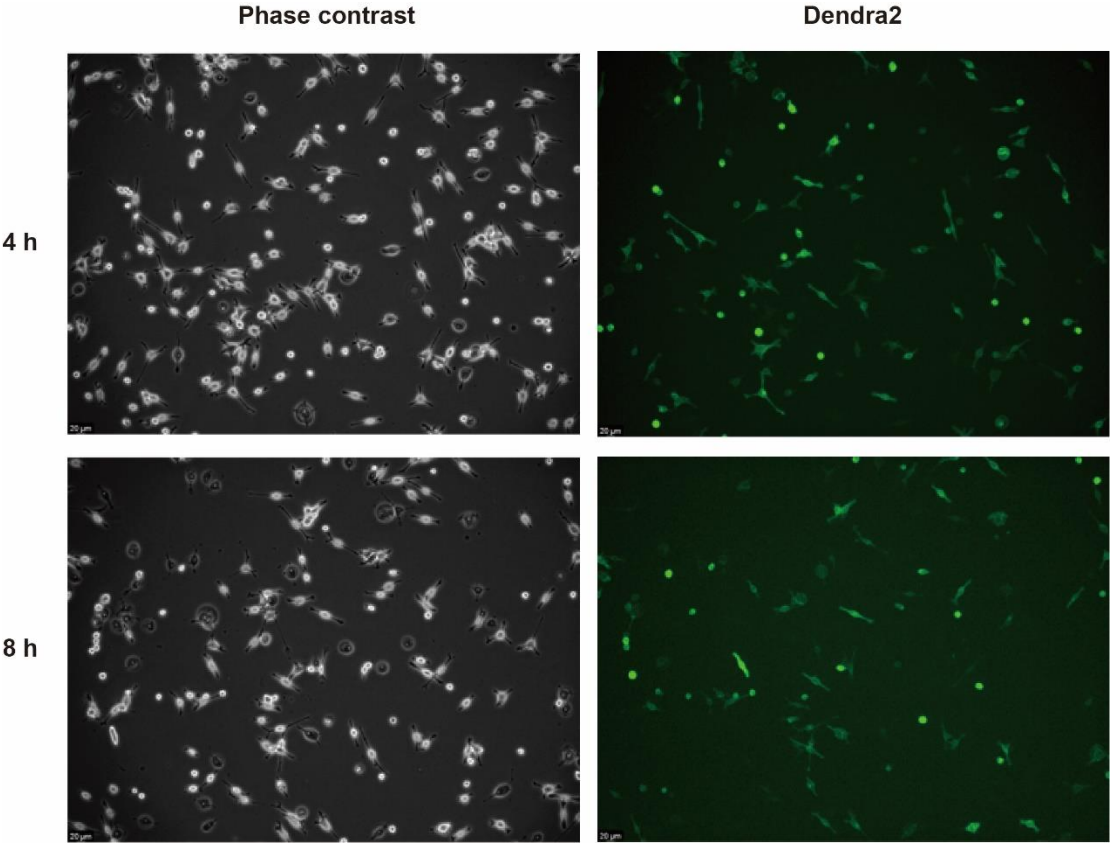

Figure 17 Reseed of sorted FaDu-Dendra2.

Shown are representative pictures of FaDu-Dendra2 after fluorescence-activated cell sorting. The pictures at the 4-hour time point (Top line) and the 8-hour time point (Bottom line) were taken in the phase contrast (Left column) and FITC (Dendra2) channels (Right column), respectively.

3.4 Sample collection for Bulk-RNA sequencing

3.4.1 Characterization of Dendra2-red/green in fluorescence-activated cell sorting for sample collection

We have previously demonstrated that photoconverted and non-

photoconverted cells can be detected and differentiated in flow cytometry based on pure photoconverted and pure non-photoconverted samples. However, in the process of collecting cell samples by formal flow sorting, because the red and green fluorescent cells will come from the same spheroid. During the photoconversion process, due to the scattering of the laser beam, the cells in the small surrounding area of laser irradiation also had been partially-photoconverted and had very low-intensity red fluorescence, leading to an intermediate state between the red and green samples. Therefore, in the actual sorting process, we adjusted the FACs-gating strategy in order to obtain high-intensity red or completely green samples as much as possible (that is, to eliminate red-green fluorescent intermediate cells), and when gating, we selected as far away as possible. The area of another color creates a clear buffer area, reducing the possibility of the two colors overlapping.

To sort the subpopulation of invasive cells by FACs, through FSC-A vs SSC-A and SSC-A vs SSC-H parameters, FaDu-WT was used to determine the size and granularity (Figure 18A, P1) and remove doublets or multiplets (Figure 18A, P2) using the FSC-A vs. SSC-A and SSC-A vs. SSC-H parameters. Non-converted-FaDu-Dendra2 and photoconverted-FaDu-Dendra2 were utilized to define green fluorescent expression regions (Figure 18B, green) and red fluorescent expression regions (Figure 18C, red), which were differentiated by

keeping a specified distance (buffer) between the two regions, using PE-A (red fluorescence) vs. FITC-A (green fluorescence) channels.

Next, FaDu-Dendra2 cells spheroid were embedded in collagen and treated with 10 μg/mL EGF. After 72 hours, cells in spheroids were partially photoconverted, and collagen-spheroids mixture were subjected to collagen digestion and single cell suspension were used for a test of cell sorting. Photoconverted red cells and non-photoconverted green cells were successfully clustered, as evidenced by results in Figure 18D, E. A total of 87,684 FaDu Dendra2 red cells (Figure 18D) and 34,795 FaDu Dendra2 green cells (Figure 18E) were sorted, accounting for 21.9% and 7.2% of the P2 of the original samples, respectively. FaDu cell line is shown as an example.

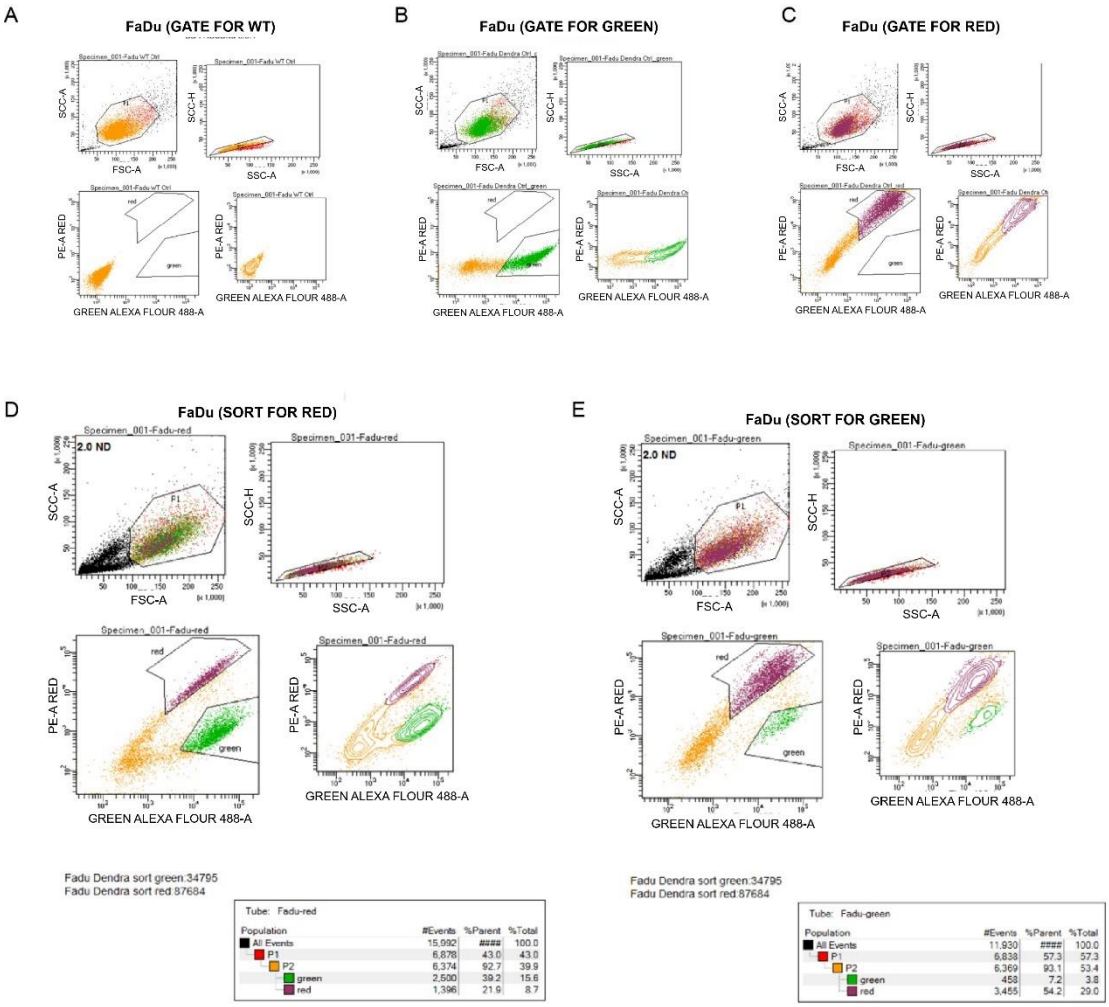

Figure 18 Clustering and fluorescence-activated cell sorting of Dendra2 photoconverted and non-converted cells

Flow cytometry dot plot for gating: (A) FaDu-WT cells, (B) non-converted FaDu-Dendra2 (green), (B) photoconverted FaDu-Dendra2 (red). Flow cytometry dot plot for sorting: (D) FaDu-Dendra2 (red) cells, (E) FaDu-Dendra2 (green) cells. Cells were sequentially gated in P1 and P2 (FSC-A vs SSC-A and SSC-A vs SSC-H). Gates used for Dendra2-red/Dendra2-green clustering are shown as red/green regions (PE-A vs. FITC-A) The proportion and number of sorted cells are shown in the sequential gating (Bottom).

3.4.2 Purity assessment for sorted cells

To assess the purity of sorted cells, green and red sorted cells (Figure 18D, E)

were re-analyzed by flow cytometry. The P1, P2, red, and green gates used for the purity assessment were identical to the FAC-sorting parameters (Figure 18).

Flow cytometry re-analysis indicated that all sorted Dendra2-green fall into the green-gate range, with green cells accounting for 99 percent and red cells accounting for 0% (Figure 19, left panel). Photoconverted Dendra2-red cells that have been sorted all fall into the red-gate range, with green cells accounting for 0% and red cells accounting for 100% (Figure 19, right panel). This demonstrated that the purity of the cell populations is ensured after sorting and that there is no contamination between red and green cells.

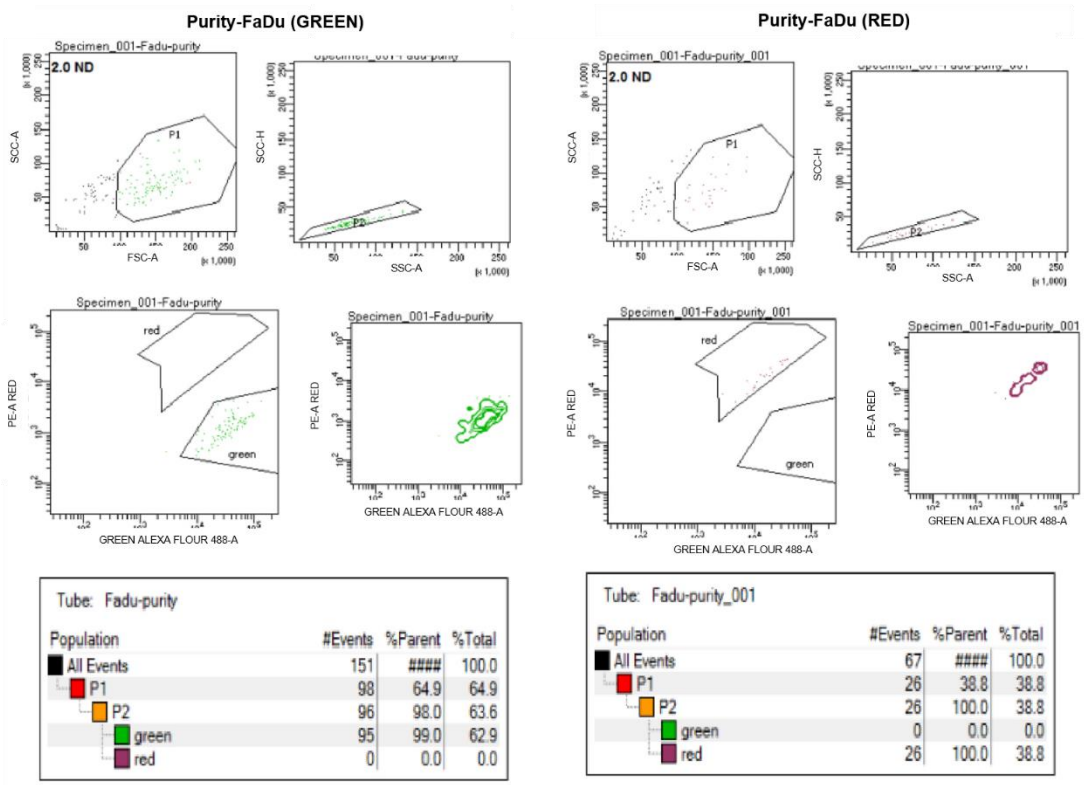

Figure 19 Purity assessment for sorted cell

Representative graphs depict sorted Dendra2-green/Dendra2-red cells that were sequentially gated in P1 and P2 (FSC-A vs SSC-A and SSC-A vs SSC-H). Gates used for Dendra2-green (left panel, upper and middle) / Dendra2-red (right panel, upper and middle) clustering are shown as red/green region (PE-A vs. FITC-A). Sequential gating was performed for the purity of red/green population.

3.4.3 Samples collection from tumor cell treatment groups

To further explore molecular mechanisms associated with EGF-mediated invasive cells in 3D cellular model, samples from five different treatment groups were investigated: 1. SF-control group 2, Invasive cells of the EGF treatment group (Out) 3, Migratory but non-invasive from cells EGF treatment group (Core), 4 non-invasive cells from the EGF/Cetuximab co-treatment group, and 5. non-invasive cells from the EGF/MEK inhibitor co-treatment group. All samples were collected as four independent biological replicates. The work-flow for sample collection is shown in Figure 20. Out and Core cells were sorted according to red and green fluorescence, while all viable cells from spheroids in in the SF, Cetuximab, and MEKi groups were sorted without photoconversion based on the lack of obvious invasive cells.

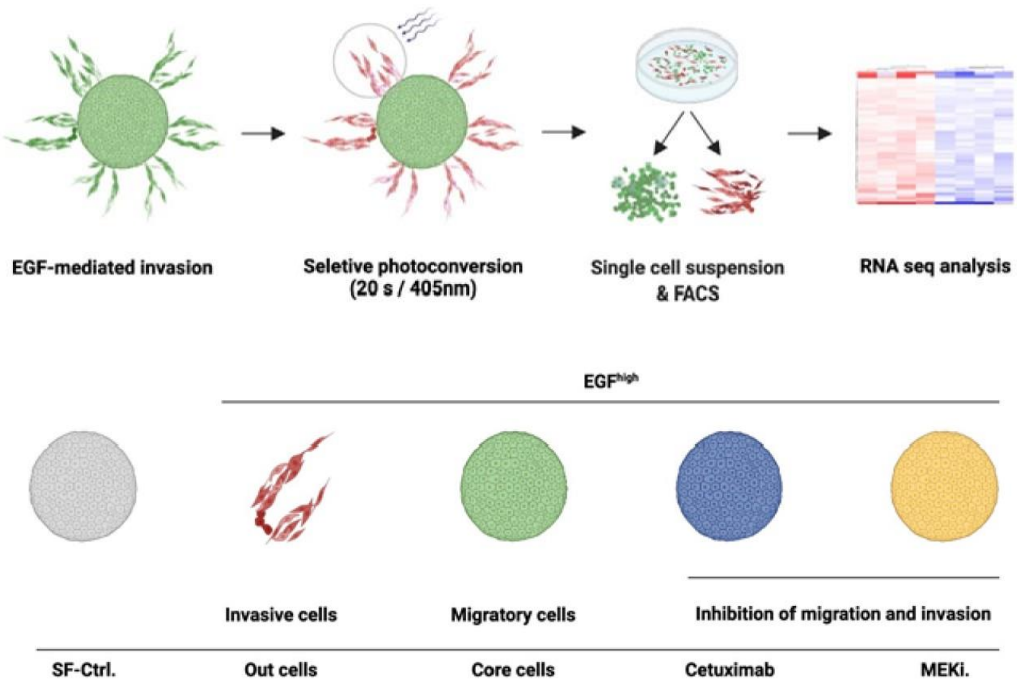

Figure 20 Schematic representation of sample collection

Schematic representation of sample collection for bulk RNA-seq. Invasive cells induced by EGF-treatment were selectively photoconverted by a 20s treatment with 405nm light. In parallel, migratory but non-invasive cells induced by EGF-treatment were selectively photoconverted by a 20s treatment with 405nm light, too. Cell bulks were sent for Bulk RNA-seq (Upper line). Five sample groups were collected: 1. SF-control group 2. Invasive cells of the EGF treatment group (Out) 3. Migratory but non-invasive from cells EGF treatment group (Core), 4. non-invasive cells from the EGF/Cetuximab co-treatment group, and 5. non-invasive cells from the EGF/MEK inhibitor co-treatment group (Bottom line, from left to right).

3.5 Data quality assessment by sample clustering and visualization

3.5.1 Heatmap of the sample-to-sample distances and Principal component (PCA)

RNAseq data was preprocessed in cooperation with Kristian Unger at the HMGU Munich. Reads(counts) were aligned to the GRCh38/hg38 human genome using STAR pipeline. Two samples (Kyse30 O-1, Co-1) were excluded due to low quality. Sample-to-sample distances were demonstrated by using *dist* function (Figure 21, upper in FaDu and Kyse30). The distance matrix heatmap gives us an intuitive inspection of how similar or differing samples are. The sample distances between the same groups are close and cluster well, as seen in the heatmap (Figure 21, upper panel).

To visualize experimental variables and batch effects affecting the overall impact, Zhongyang Lin used a principal component analysis (PCA). 12567 genes with total counts (across all rows) greater than 300 were selected and used for PCA and subsequent analysis. Principal component 1 explained 77% and a PC2 10% of variance in the transcriptional data across all treatments. The clustering inside each group is consistent with the very close sample-sample distance estimates. The “Out” group clustered closely together with the “Core” group on the far left in the PCA, while the SF group clustered on the far right of the PCA, hence showing the biggest differences in PC1. Cetux and

MEKi, the two inhibitor groups, showed an intermediate localization in the PCA, between Out/Core and SF clusters. Furthermore, the two inhibitor groups differed from the remaining samples with respect to PC2 (Figure 21, lower panel).

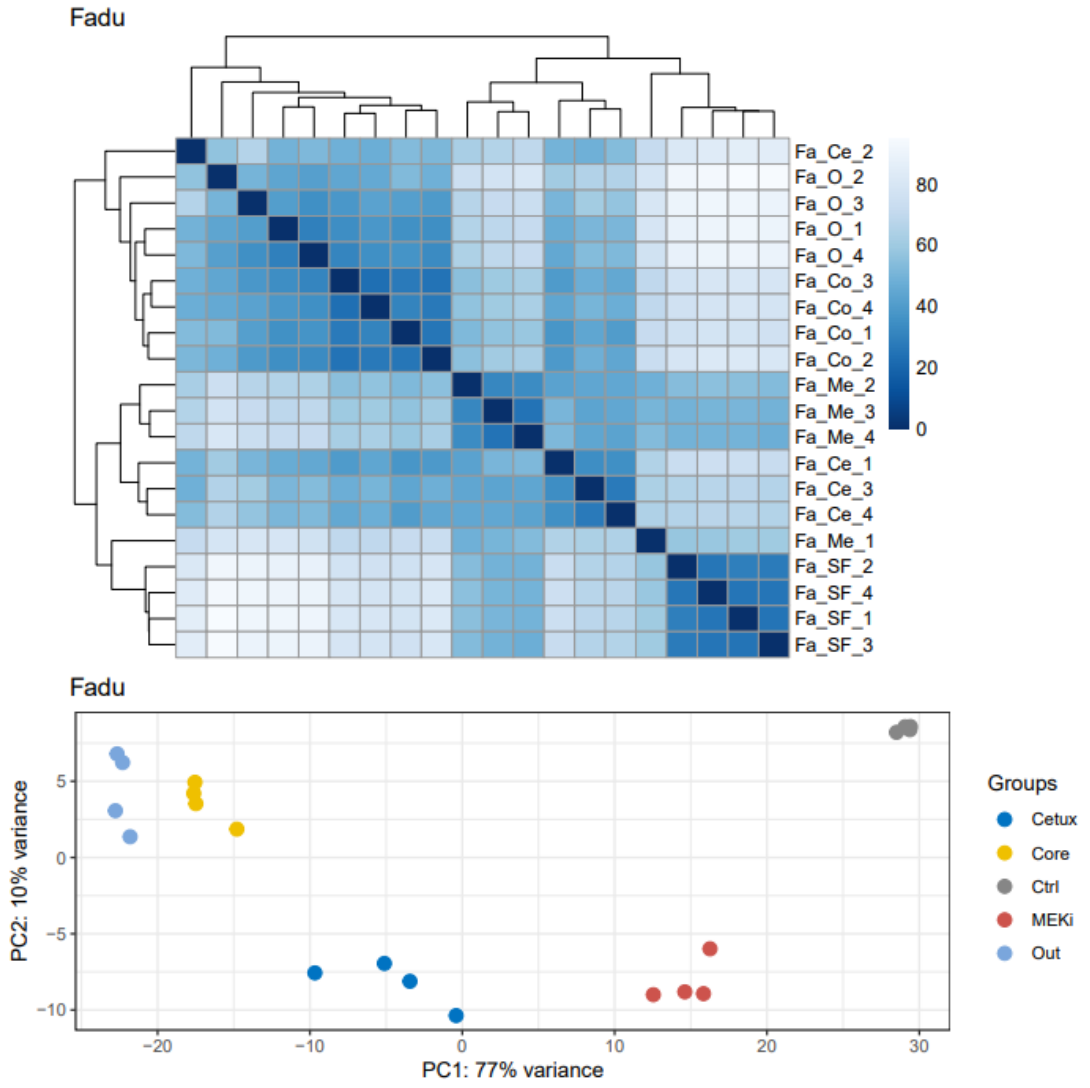

Figure 21 Heatmap of the sample-to-sample distances and principal component plot of the samples.

Sample-to-sample distances are presented as a heatmap, as well as the principal component analysis (PCA) of FaDu cells. In the study, all expressed

genes were considered. At least three separate experiments per treatment group were examined. PC1 and PC 2 are depicted with explained variance. Ctrl: Serum free, Out: Invasive cells (9 nM EGF), Core: Migratory cells (9 nM EGF), Cetux: Cetuximab group (9 nM EGF + 10 µg/mL Cetuximab), MEKi: MEK inhibitor group (9 nM EGF + 100 nM AZD6244).

3.6 Transcriptional regulation of EGF-mediated invasion in a 3D cellular model

3.6.1 Biological processes defined by Hallmarks of Molecular signature database (MSigDB) and leading-edge genes

To explore biological processes potentially involved in the regulation of EGF-mediated invasion and further study the contribution of genes in specific biological processes, the differential expression comparison of the Out vs. SF group was ranked by log2 (foldchange). A gene set enrichment analysis (GSEA) was performed according to the description in the method by using these ranked differential gene expression values,

50 Hallmark gene sets from MSigDB were utilized to summarize and depict distinct biological processes. Significantly activated and suppressed hallmarks were chosen with a preset p-value of 0.05. Furthermore, normalized enrichment scores (NES) and related false discovery rate (FDR) were computed for all hallmarks.

Through GESA, regulated hallmarks of Kyse30 (n=29) and FaDu (n=23) were

identified, respectively (Figure 22, middle and right bubble charts). After the intersection of the hallmarks of the two cell lines, 16 common hallmarks were extracted (Figure 22, left panel). We assumed that the gene set contributing to these 16 hallmarks comprises genes that contribute the most to EGF-mediated invasion in 3D cellular model (Figure 23, left box).

In line with induction of EMT upon EGF^{high} treatment, the MSigDB hallmarks “Epithelial-Mesenchymal Transition) was significantly activated in both cell lines (Figure 23). Next, leading-edge genes were extracted from all 16 intersected hallmarks to establish genes that contributed the most to the activation or suppression of all intersected hallmarks (Fleming & Miller, 2016) (Figure 23, right).

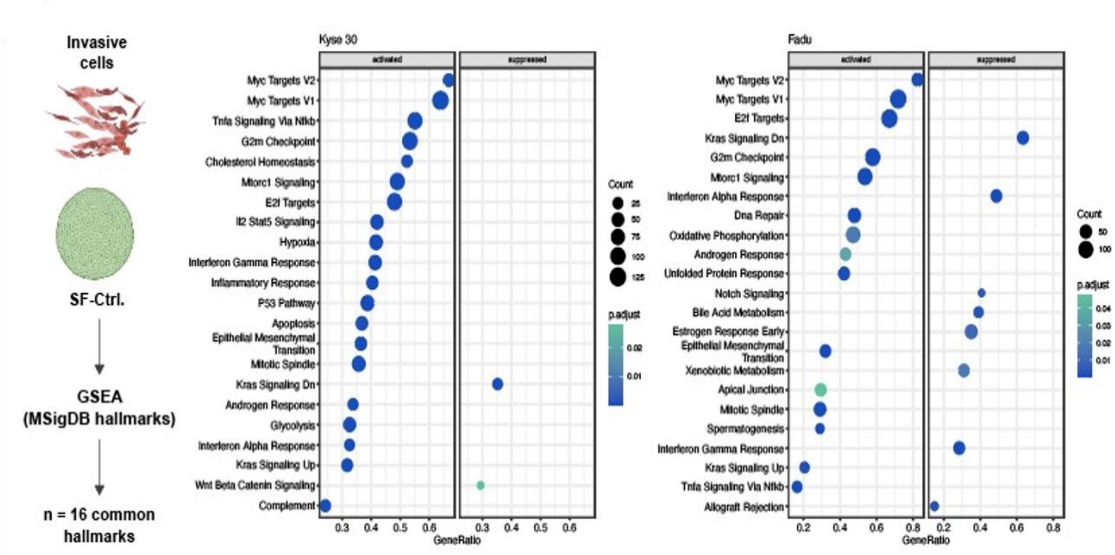

Figure 22 Common hallmarks from MSigDB-based GESA.

Shown is the schematic representation of the workflow resulting in the extraction of 16 common hallmarks from Kyse30 and FaDu cell lines (left).

MSigDB-based Gene set enrichment analysis of Kyse30 and FaDu and bubble charts showing top 22 and 23 hallmarks of Kyse30 and FaDu, respectively (middle and right).

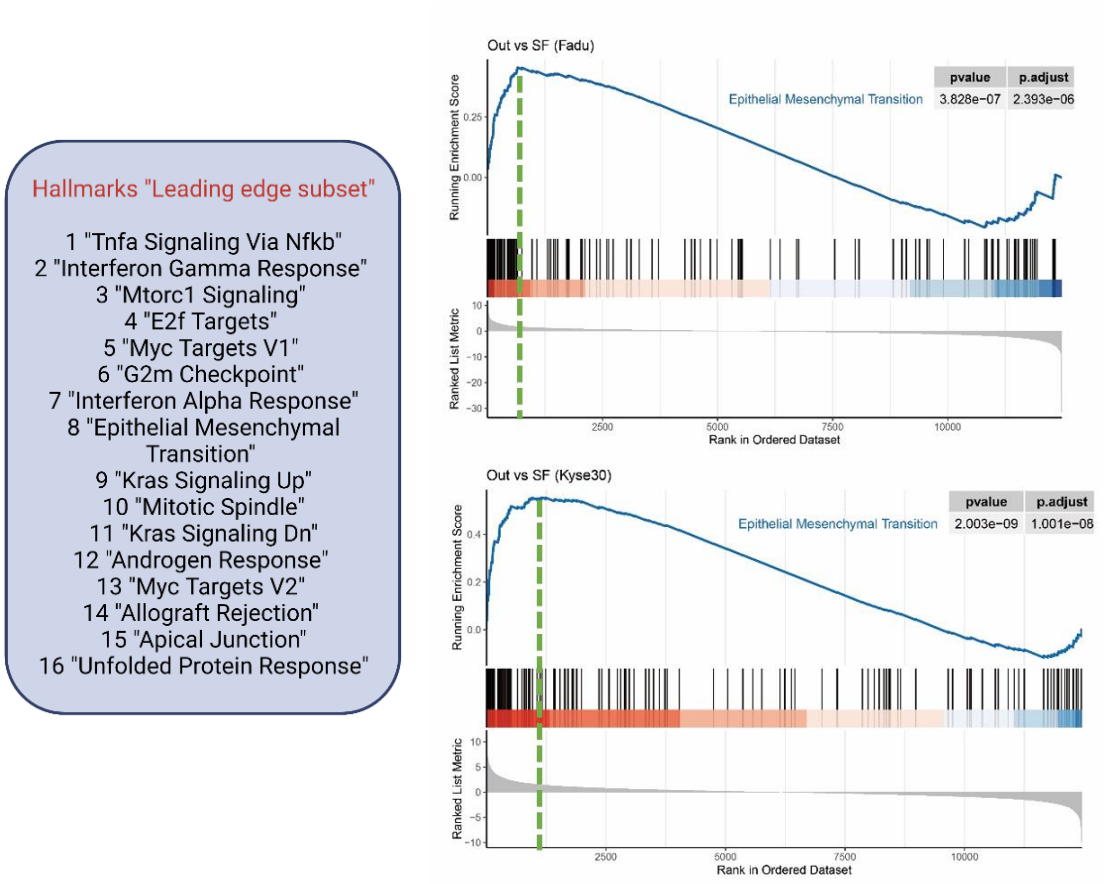

Figure 23 Extraction of leading-edge genes.

16 hallmarks commonly regulated in invasive cells are shown in the left box. As an example of the 16 hallmarks, the leading-edge subset of genes within the Epithelial-Mesenchymal Transition hallmark enrichment plot are shown (Kyse30, right upper; FaDu right Bottom). p-values for GSEA and q-values for FDR ($p < 0.05$, and FDR<0.1). Hits on the left of green dashed lines are regarded as a leading-edge subset, while red and blue gradient hues stand for positive and negative regulation, respectively. The plot's top right corner displays the p.value and p.adjust value in addition to the blue line representing cumulative enrichment score, black lines representing gene set ranking location, and gray lines representing ranking metric scores.

3.6.2 Counter-regulated leading-edge genes in invasion/inhibition comparisons.

In the next step, genes most closely associated with EGF-mediated invasion were identified upon comparison with inhibitor-treated samples. First, differentially expressed genes (DEGs) of OUT/SF, Cetux/OUT, and MEKi/OUT comparison were screened with a Log2FC>1 and an adjusted p-value＜0.05 as thresholds. Only DEGs from OUT/SF that were counter-regulated by Cetux and/or MEKi were further analyzed. The resulting 41 up-regulated and down-regulated genes represented a list of candidates mostly contributing to EGF-mediated invasion (Figure 24).

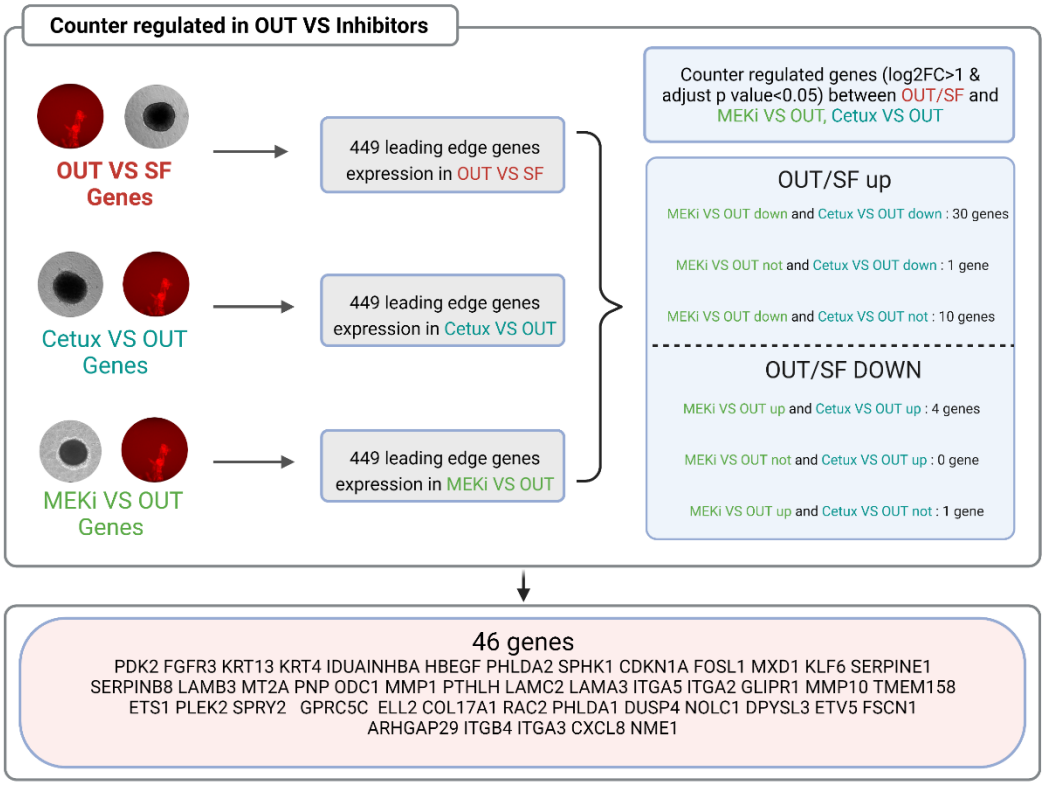

Figure 24 Counter-regulated genes in Out vs. Cetux/ MEKi groups.

The flow chart shows that by examining the gene expression levels of the OUT/SF, Cetux/OUT, and MEKi/OUT groups, 46 genes that are counter-regulated between invasion and inhibitor groups were identified from 449 leading-edge genes. OUT: Sorted invasive cells, SF: Serum free control, Cetux: Cetuximab inhibition, MEKi: MEK inhibition, UP: Up-regulated, DOWN: Down-regulated.

3.6.3 Identification of co-expression modules and biological processes/pathways correlated with EGF-mediated invasion in a 3D cellular model

To provide insight into the biological process and pathway information of those 46 genes, Zhengquan Wu applied in a cooperative work a Single Sample Geneset Enrichment Analysis (ssGSEA) to calculate the EMT (HALLMARK_EPITHELIAL_MESENCHYMAL_TRANSITION), MAPK (KEGG_MAPK_SIGNALING_PATHWAY), PI3K (HALLMARK_PI3K_AKT_MTOR_SIGNALING), and EGF_EGFR pathway (WP_EGFEGFR_SIGNALING_PATHWAY) score of patients in the single-cell RNA-seq (scRNA-seq) HNSCC dataset (GSE103322). Weighted gene co-expression network analysis (WGCNA) was used to investigate co-expression modules related to EMT, MAPK, PI3K, EGF_EGFR pathway. Genes exhibiting the most (top 25%) variation in expression levels across the scRNA-seq dataset (GSE103322) were imported to the WGCNA. The soft threshold of module analysis was calculated using scale independence and mean connectivity

analysis with various power levels. As shown in Figure 25, when the power value was set to 5, the scale independence value achieved 0.9 and lower mean connectivity. Then the soft threshold power β = 5 (scale-free R2 = 0.90) was used to construct a scale-free network. To describe the cluster amongst modules, a cluster dendrogram was created and modules containing various genes were generated and shown in multiple colors (Figure 26).

The correlation between modules and traits was used to calculate module-trait relationships. To correspond to the results of our 3D invasion experiments, modules were required to correlate with high EMT, EGFR and MAPK activity, but with low PI3K-AKT activity. From the computed modules, it was evident that the blue and greenyellow modules fit our requirements (Figure 26; Figure 27). Next, to merge these two modules and fully describe EMT, EGFR, MAPK and PI3K-AKT, the clustering of module was re-cut using mergeCutHeight with a parameter set to 0.85 (Figure 28). Blue and greenyellow modules merged into a new brown module, which was the most significant module (n = 300 genes) (Figure 29; Figure 30).

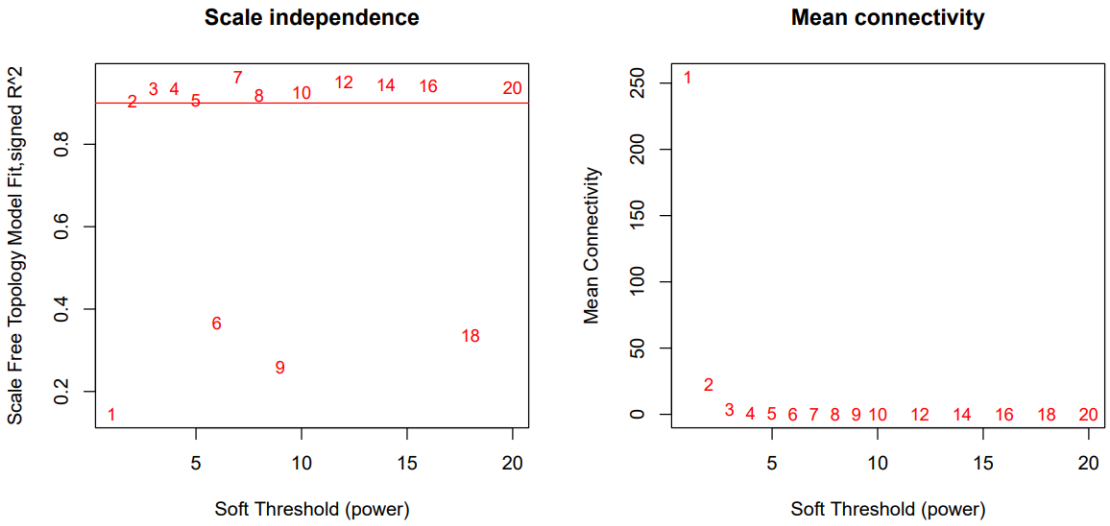

Figure 25 Scale independence and mean connectivity analysis

To establish the soft threshold of module analysis, scale independence and mean connectivity analysis of modules with various power levels were carried out (scale-free R2 = 0.90, power value was set to 5).

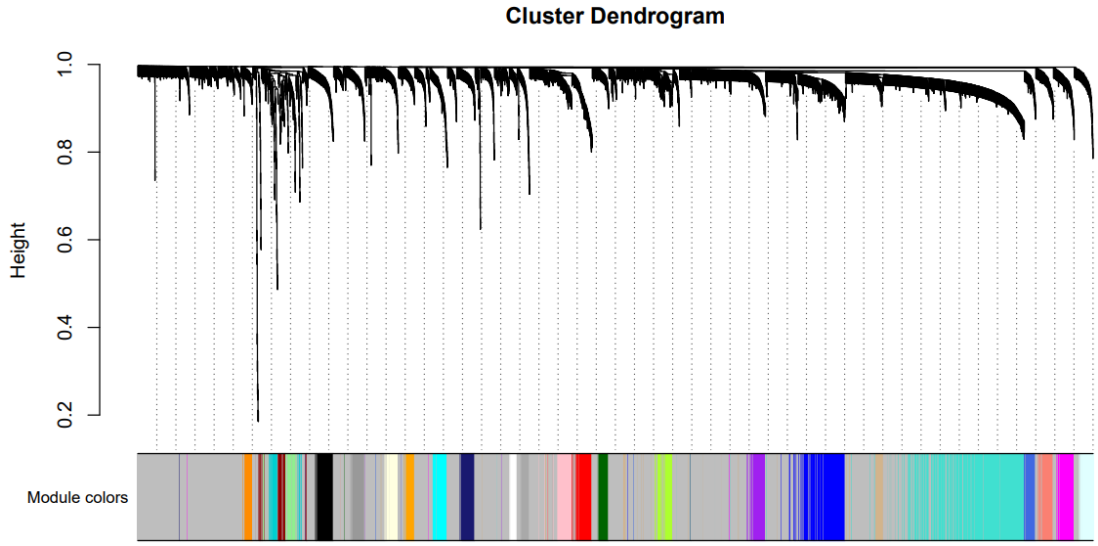

Figure 26 Cluster dendrogram among modules

A cluster dendrogram was created and modules containing various genes were generated and shown in multiple colors.

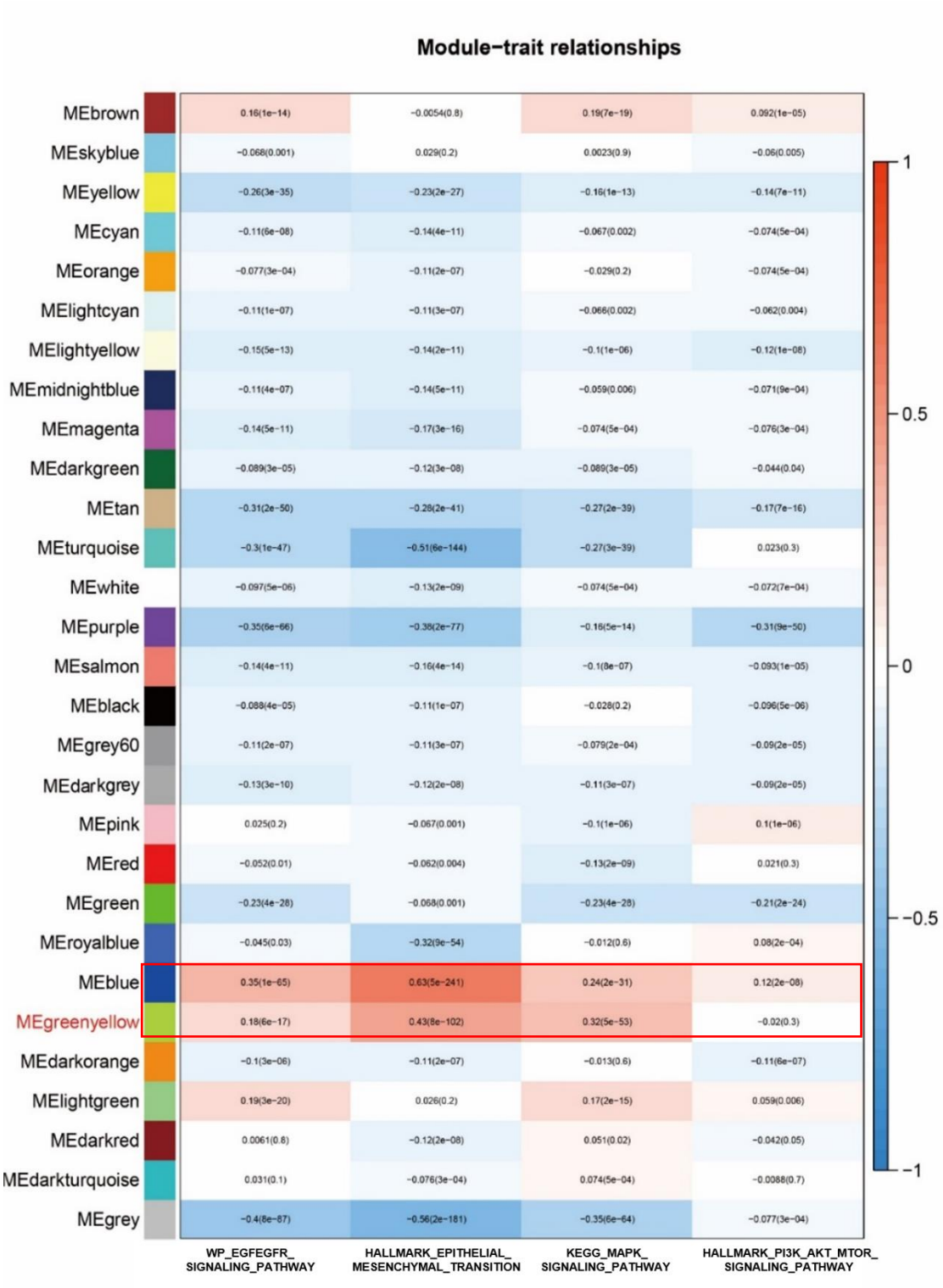

Figure 27 Module-trait relationships

The correlation between modules and traits was used to calculate module-trait relationships. (P value < 0.05, module size < 500). Includes 29 modules with d

ifferent colors and EMT(HALLMARK_EPITHELIAL_MESENCHYMAL_TRANSITION), MAPK (KEGG_MAPK_SIGNALING_PATHWAY), PI3K (HALLMARK_PI3K_AKT_MTOR_SIGNALING), and EGF_EGFR pathway (WP_EGFEGFR_SIGNALING_PATHWAY) score. The bar on the right is blue for negative correlation and red for positive correlation.

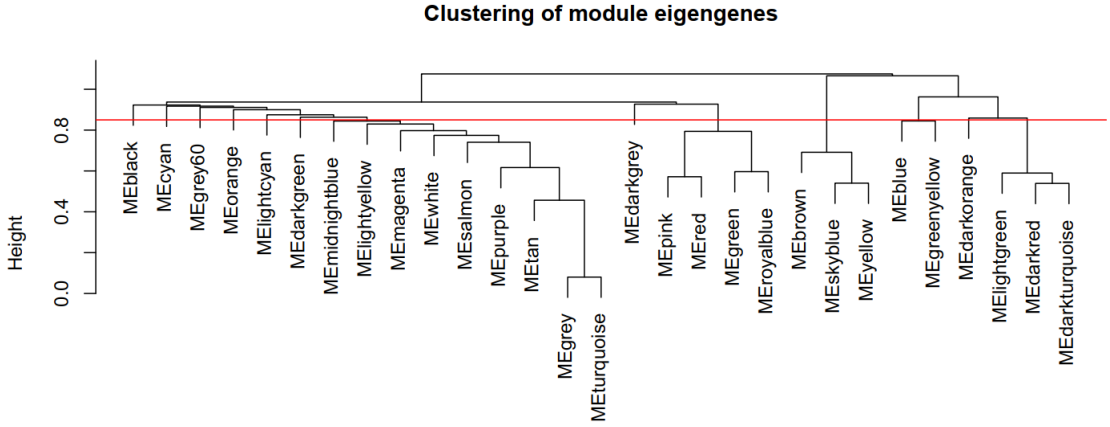

Figure 28 Re-Cut of clustering of module eigengenes

The clustering of module was re-cut using mergeCutHeight with a parameter set to 0.85. The red line is the cutting line.

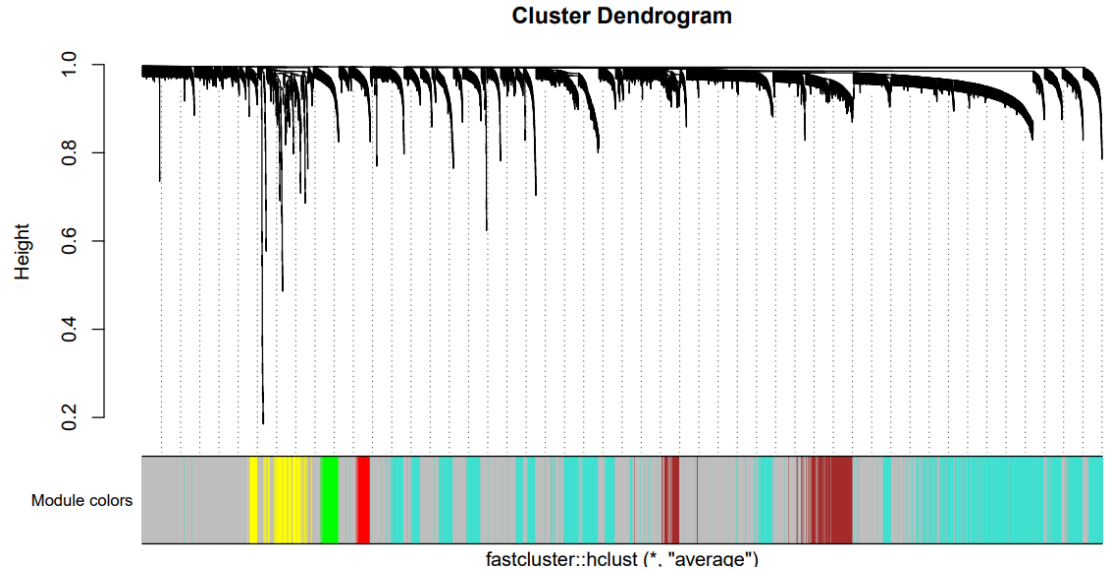

Figure 29 Merged Cluster dendrogram among modules

A Merged cluster dendrogram was created and modules containing various genes were generated and shown in multiple colors.

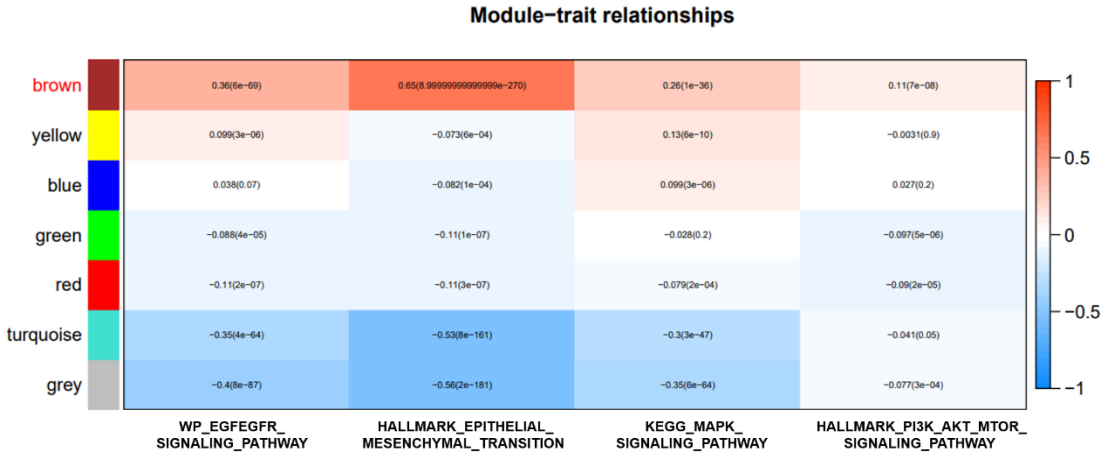

Figure 30 Merged Module-trait relationships.

The correlation between Merged modules and traits was used to calculate Merged module-trait relationships. (P value < 0.05, module size < 500). Includes 79 modules with different colors and EMT (HALLMARK_EPITHELIAL_MESENCHYMAL_TRANSITION), MAPK (KEGG_MAPK_SIGNALING_PATHWAY), PI3K (HALLMARK_PI3K_AKT_MTOR_SIGNALING), and EGF_EGFR pathway (WP_EGFEGFR_SIGNALING_PATHWAY) score. The bar on the right is blue for negative correlation and red for positive correlation.

3.6.4 Intersection of the brown module and counter-regulated genes

Next, the 300 genes of the brown module (Figure 30) were intersected with the 46 DEGs resulting from our own bulk RNA-seq analysis. From the Venn Diagram in Figure 31, after the intersection of these two lists 16 genes with the most likely contribution to EGF-mediated invasion in the 3D cellular model were extracted. They are: IL8, FOSL1, KLF6, COL17A1, INHBA, ITGA3, ITGA5, ITGB4, LAMA3, LAMB3, LAMC2, MT2A, PLEK2, PHLDA1, SERPINE1, SPHK1.

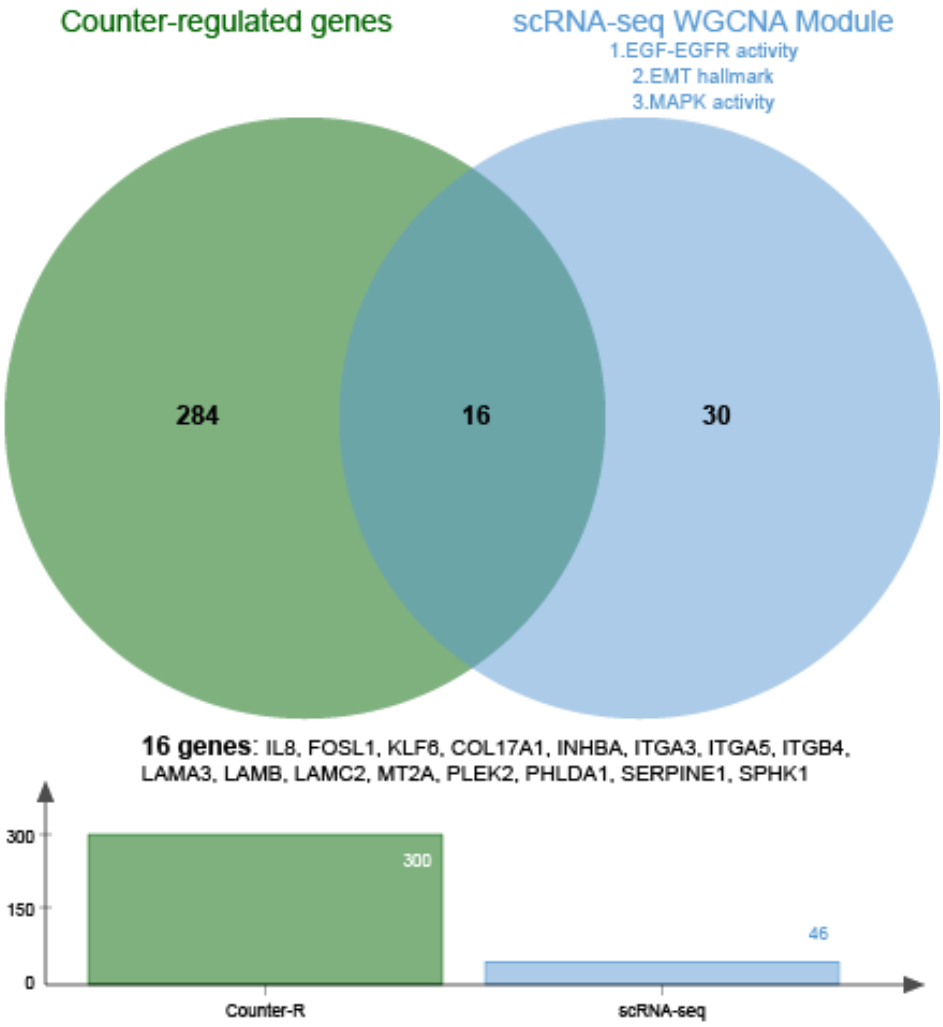

Figure 31 Venn diagram of the intersection

The intersection of counter-regulated genes (Out/SF vs. Cetux/Out and/or MEKi/Out comparisons) and the genes in the brown module (scRNA-seq WGCNA, Figure 30) was identified by the Venn diagram (Upper). The size of each list's gene number is shown in the bar below The Venn diagram was generated by http://jvenn.toulouse.inra.fr/app/example.html.

3.7 Validation of sphingosine kinase 1 as potential target

Various gene types are included in the extracted 16 genes, such as apical junction-related genes and genes encoding integrins and components of the

extracellular matrix: ITGB4, LAMA3, LAMB3, LAMC2, COL17A1, ITGA3, indicative of tissue remodeling. Additionally, among the 16 genes, EMT-related genes such as SERPINE1, INHNBA, IL8, ITGA5, LAMC2, and LAMA3 were also identified.

SPHK1 (Sphingosine Kinase 1) represented the only kinase among the 16 genes, making it a potential therapeutic target. Additionally, SPHK1 also exhibits increased expression in Cetuximab-resistant HNSCC cell lines, according to evidence from DNA microarrays of HNSCC Cetuximab-resistant and Cetuximab-sensitive cell lines (Figure 32). Hence, high expression of SPHK1 may contribute to Cetuximab treatment resistance. In order to investigate the inhibition of EGF-mediated invasion, the established 3D model was utilized to test PF-543 (a novel SPHK1 inhibitor) and Cetuximab alone or in combination with PF-543.

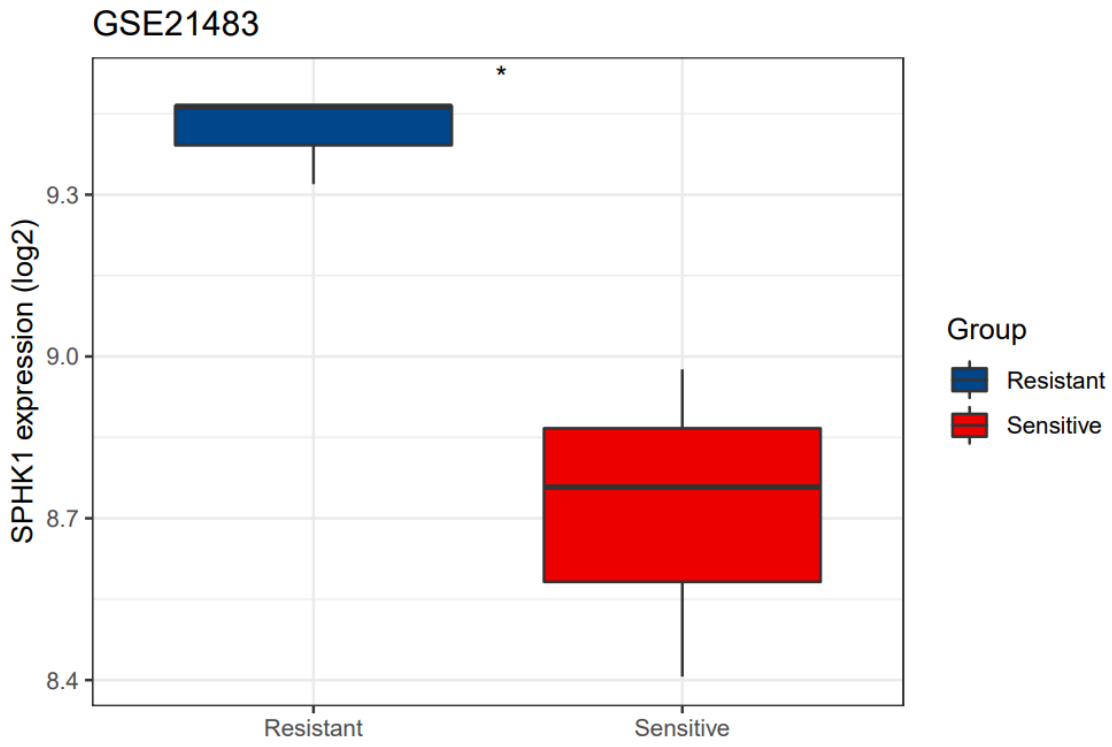

Figure 32 SPHK1 expression in Cetuximab resistance/Cetuximab-sensitive HNSCC cell lines.

*SPHK1 expression is shown in a box-plot whiskers where the expression in Ceutximab-resistant cells isdepicted in blue, and that of Cetuximab-sensitive cells is in red. T-test, p-values * 0.05.*

PF-543^{low} (5uM) and PF-543^{high} (10uM) treatment groups showed a dose-dependent significant inhibitory effect on the invasion area and invasion distance compared with the EGF^{high} group (Figure 33). Compared with the EGF^{high} group, the invasion area of low concentration Cetuximab^{low} (1 μg /mL) showed no significant difference, but a significantly inhibited invasion distance. Compared with the EGF^{high} group, the Cetuximab^{high} (10 μg/mL) had a significant inhibitory effect on the invasion area and the invasion distance. Noteworthy, compared with EGF^{high}, the combination group of

Cetuximab^{low}+PF-543^{low} showed a significant inhibitory effect on invasion area and invasion distance, and there was no significant difference with Cetuximab^{high} group.

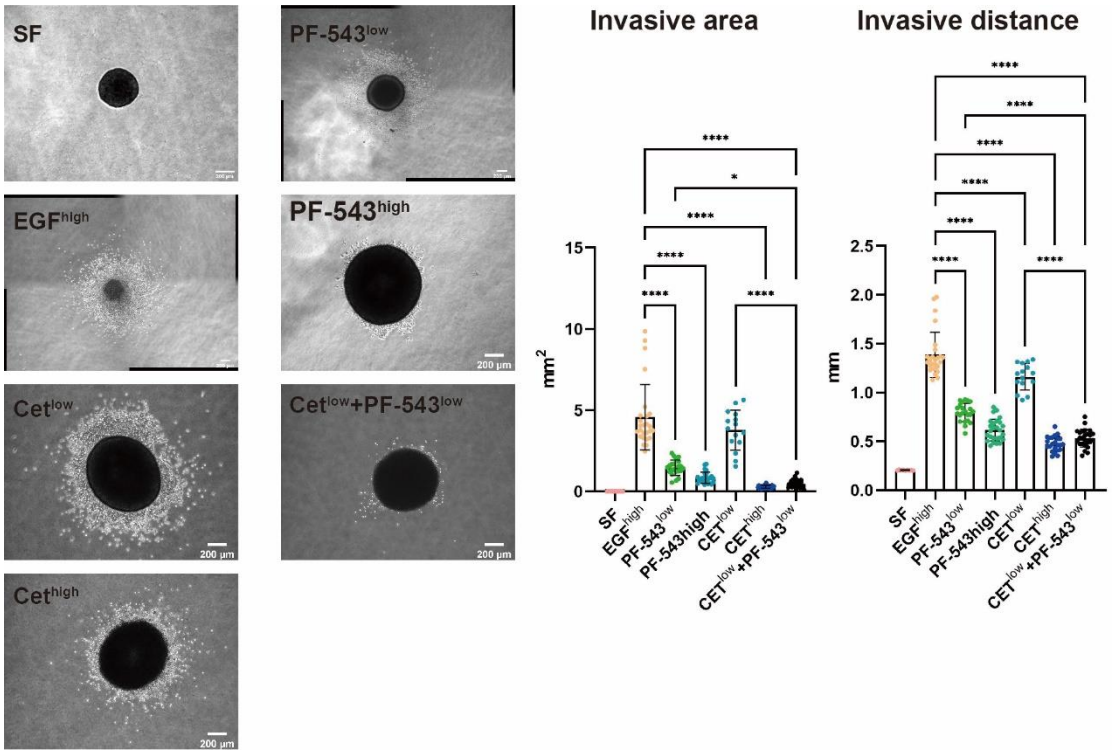

Figure 33 PF-543 and Cetuximab inhibition assay

*Representative pictures in the left shows 3D invasion in 7 different treatments group (FaDu): SF (Serum free), EGF^{high} (9 nM), EGF^{high} (9 nM)+Cet^{low} (Cetuximab^{low},1 µg/mL), EGF^{high} (9 nM)+Cet^{high} (Cetuximab^{high},10 µg/mL), EGF^{high} (9 nM)+PF-543^{low} (SPHK1 inhibitor, 5 µM), EGF^{high} (9 nM)+PF-543^{high} (10 µM) and combination of EGF^{high} (9 nM)+PF-543^{low}+Cetuximab^{low} groups. Quantification is performed as described in 2.8 Quantification of invasion. n = 3 independent experiments. One-Way ANOVA with Šídák's multiple comparisons test, Brown-Forsythe test and Bartlett's test p-values * 0.05, ** 0.01; *** 0.001, **** 0.0001. Scale bars represent 200 µm.*

In summary, the SPHK1 inhibitor PF-543 showed a strong inhibitory effect on

EGF-mediated 3D invasion in the FaDu cell line. Using PF-543^{low}+ Cetuximab^{low} in combination allowed to substantially reduce the dose of Cetuximab required for inhibition of invason. The results provide clues and a basis for further study of the tumor suppressor effects and drug-synergistic effects of SPHK1 and EGFR inhibitors in HNSCC. It also demonstrates that SPHK1, a critical regulator for the treatment of cancers, has the potential to emerge as a new target for the developing associated novel treatments.

4 DISCUSSION

Head and neck squamous cell carcinoma (HNSCC) are highly malignant and shown strong inter- and intratumor heterogeneity, bringing many obstacles to treatment for most patients (Cancer Genome Atlas, 2015; Gregoire, Langendijk, & Nuyts, 2015; J. W. Huang, Zhang, Shi, Liu, & Wei, 2016; Kriegs et al., 2016; Steinbichler et al., 2018). Researchers have recently studied HNSCC at the multi-omics level, including molecular biology, proteomic, bulk or single-cell RNA sequencing, imaging, metabolomics, etc (Eskiizmir, 2015; Faubert, Solmonson, & DeBerardinis, 2020; Mroz et al., 2013; Puram et al., 2017; Ramesh, Brabletz, & Ceppi, 2020). It was directly or indirectly proved that the degree of malignancy of HNSCC manifests at various levels, including lymph node metastasis, minimal residual disease, distant metastasis, resistance to radiotherapy and chemotherapy, and more (L. Chen et al., 2020; Jonckheere et al., 2022; Moon, Lee, & Lim, 2021; Nair, Bonner, & Bredel, 2022; Parikh et al., 2019; Winkler, Abisoye-Ogunniyan, Metcalf, & Werb, 2020; M. Zhang et al., 2021). These aspects of HNSCC progression seriously affect the survival and prognosis of HNSCC patients and make treating this disease difficult (Nair et al., 2022; Schinke et al., 2022a; Q. Zhang et al., 2021; Zhu et al., 2021).

To solve these problems, scientists have made numerous efforts to explore the biological mechanism by which HNSCC initiates local and distant dissemination

and treatment resistance. Among them, the EGFR pathway mediating EMT leading to cancer invasion is a central topic and viewpoint (Cook & Vanderhyden, 2020; Johnson et al., 2020; Jonckheere et al., 2022; Kisoda et al., 2020; C. Z. Lin et al., 2020; Nair et al., 2022). Recently, the concept of collective cancer invasion mediated by leader cells has provided a new perspective (B. J. Chen, Wu, Tang, Tang, & Liang, 2020; Kozyrska et al., 2022; Vilchez Mercedes et al., 2021) and has become a potential research direction to investigate the invasion process of HNSCC.

Therefore, to explore the biological mechanism of HNSCC invasion, in this thesis, I try to explore the mechanism of EGF-mediated invasion through the EGFR pathway. A 3D cellular model of EGF-mediated invasion was established with two tumor cell lines of the upper aerodigestive tract in ECM to simulate the environment of cancer invasion. As part of this system, photoconvertible Dendra2 protein stably expressed in tumor cells allowed to specifically locate, enrich, and RNA-sequence invasive tumor cells to explore the process of EGFR-mediated invasion in HNSCC. A major aim was to explore biological mechanisms of EGF-mediated invasion and identify potential therapeutic targets for HNSCC patients.

4.1 EGF^{high} mediated 3D invasion mainly through EGFR-MEK pathway

From previous data, Pan *et al.* revealed that high-dose EGF treatment mediates EMT in HNSCC cells, and identified pERK as a major driver of EGF-mediated EMT (Pan et al., 2018). This identification process was performed in 2D experimental conditions throughout, but whether EGF can induce EMT and invasion in HNSCC cell lines in 3D experimental conditions required additional research.

Therefore, I first assessed the effect of EGF on cell morphology in 2D confirming the induction of EMT in FaDu and Kyse30 cells (Figure 5). After 72 hours of treatment, the cells presented a highly mesenchymal state, the cell morphology became narrowly elongated, and the cell-to-cell adhesion was weakened. Scattered, unaggregated single cells were also seen. Changes in cell morphology were consistent with previous reports that high doses of EGF can indeed induce morphological changes in FaDu and Kyse30 cell lines (Pan et al., 2018).

Notably, the downstream effects of cells grown in 2D monolayers versus those exposed in a 3D tumor microenvironment *in vivo* are different. A crucial distinction to be made here is that 2D planes constrain geometry formation in contrast to the circular morphologies present in 3D systems (Almany & Seliktar, 2005). Due to the artificial geometry in 2D, epithelial cells lose their natural

polarity (Birgersdotter, Sandberg, & Ernberg, 2005), which might lead to cells with varying levels of genetic and proteomic expression (Irish et al., 2004; Roschke et al., 2003). Reviewing the genetic variations between 2D and 3D cell culture revealed upregulation in three domains: metabolism, cell cycle and turnover of macromolecules (leading to promotion of proliferation) (Birgersdotter et al., 2005). The need for 3D models is highlighted by the fact that the transition from 2D to 3D considerably enhanced the robustness of cells to toxicity in both normal and malignant situations (Almany & Seliktar, 2005; Sun, Jackson, Haycock, & MacNeil, 2006; Tevis et al., 2017).

Due to the role of collagen in the ECM and upregulation in the tumor microenvironment, it is the most commonly used embedding material. Its application in in vitro 3D models is made easier by the simplicity with which mechanical strength, pore size, and fibril fraction may be modified by adjusting concentrations and preparation techniques (Harjanto, Maffei, & Zaman, 2011). So a suitable collagen concentration was used to perform 3D experiments (Figure 6), the constructed 3D model composed of tumor cells and type I collagen was used to examine whether high-dose EGF entails functional changes in tumor cells in 3D (Figure 7). Through live imaging, I could visualize that EGF induces tumor cell invasion in type I collagen, which can be specifically blocked by Cetuximab (Figure 8). Although the blocking efficiency

was not 100%, this may be due to the different diffusion rates and concentrations of EGF and Cetuximab in collagen, resulting in a small number of cells in the spheroid that have been exposed to EGF in advance of receiving Cetuximab. As a result, few cells remained in an invasive state. Generally, EMT-inducing doses of EGF triggered local invasion of tumor cells into type I collagen, a phenotype that was reverted by co-treatment with Cetuximab.

Due to the gradients of metabolites, catabolites, and oxygenation that are present in avascular tumors or tiny micrometastases (size under 2 $mm^{3)}$, with proliferation at the edges and necrosis at the center (Friedrich, Ebner, & Kunz-Schughart, 2007). The microenvironment of the 3D tumor spheroid is different from normal tissue in terms of oxygenation, perfusion, pH, and metabolic state because of the macrostructure (Danhier, Feron, & Préat, 2010). Our 3D experiments may potentially include treatments diffusion, which would provide non-uniform or even inconsistent findings. To address the question of the diffusion range of EGF and Cetuximab and to probe the origin of EGF-induced invasive cells, two experimental approaches were designed. IHC staining of spheroids demonstrated that Cetuximab penetrated the deepest part of the spheroids at least within the first 24 hours (Figure 9). Cetuximab was evenly distributed in the spheroids, which indicated that EGF with a smaller molecular weight could also run through the entire spheroid, theoretically. The exploration

of the origin of invasive cells proved that invasive cells not only came from the periphery of the spheroid but also the inside of the spheroid, which indirectly confirmed that EGF can penetrate the entire spheroid (Figure 10).

After verifying the feasibility of studying the effects of different components including therapeutic monoclonal antibodies in the established 3D model, I used two inhibitors (AZD6244 and MK2206) of downstream effectors of EGFR to further explore central pathways crucially involved in EGF-mediated 3D invasion. From the quantitative results, it can be deduced that MEK inhibitor AZD6244 had a stronger inhibitory effect than AKT inhibitor MK2206, suggesting that the RAS-RAF-MEK-ERK signaling pathway may have a more important involvement than the PI3K-AKT-mTOR signaling pathway in EGF-mediated invasion (Figure 11). This is in line with findings by Pan et al. regarding the induction of EMT through EGFR signaling (Pan et al., 2018). However, the disadvantage is that if we want to explore this problem in a strict sense, we must also consider expression levels of ERK (MAPK/ERK) and AKT (PI3K-AKT-mTOR), and the magnitude of downstream responses. Studies in various HNSCCs have revealed that PI3K-AKT-mTOR pathways (K. Lee et al., 2020; J. Wang et al., 2020; Y. Zhang et al., 2020) or MAPK/ERK pathways (Abu-Humaidan, Ekblad, Wennerberg, & Sorensen, 2020; Cui et al., 2021; Jang et al., 2022; Pan et al., 2018) may predominate in the EGFR-mediated EMT or

tumor invasion process. Studies also suggest that both pathways are involved in this process and they may individually play a different role in a cooperative way (Kashyap et al., 2018; Peng et al., 2019; Ruicci et al., 2018; Zeng et al., 2002). Understanding this will be a more complex and challenging task and more experiments need to be done in the future for verification.

4.2 Photoconversion-based specific enrichment of locally invasive cells: a way to further understand the biological mechanism of EGF-mediated invasion.

From several reports, we know that leader cells with highly invasive traits play an indispensable role in tumor invasion (B. J. Chen et al., 2020; Kozyrska et al., 2022; Vilchez Mercedes et al., 2021; Yang et al., 2019; J. Zhang et al., 2019). However, these invasive cells have not been adequately studied in HNSCC, hence the present investigation.

Protein photolabeling was implemented using a Photoconversion-based technique to understand more about the invasive cells. The excitation and emission spectra of Dendra2 dramatically shift toward the red after photoactivation. High dynamic ranges, brightness of Dendra2, and photoconverted states make it a desirable tool for our research (Chudakov, Lukyanov, & Lukyanov, 2007). It offers a method to identify specific cells of

interest due to its green fluorescence. Moreover, Dendra2 protein can be photoconverted from green to red fluorescence under 405nm laser irradiation (Figure 15), target cells, i.e. invasive cells following high-dose EGF treatment, can be detected, specifically photoconverted, and isolated via FACs. This process must be conducted within a time frame of approximately eight hours, which corresponds to the existence of the light-converted red fluorescence protein that is rather slowly metabolized. In addition to invasive cells, four treatment groups were implemented as controls during sample collection. These included the serum-free group (Ctrl), which served as the baseline group, the EGF-mediated 3D invasion of the less invasive migrating cells within the spheroid, and two additional inhibitor groups, MEKi and Cetuximab (Figure 20). These controls were important as comparisons for transcriptomic changes associated with specific functional differences across the isolated cells. Specifically, GSEA and DEG analyses relied on these additional treatment groups to decipher genes of superior importance regarding EGF-mediated local invasion. Hence, the established pipeline enables the capture of invasive cells and the opportunity for further sequencing studies to reveal transcriptomic differences associated with specific phenotypes.

The hallmarks in the OUT/SF group that contributed most to invasion were evaluated using GSEA after sequencing samples had undergone quality control

(Figure 21;Figure 22). Of 16 common hallmarks in the FaDu and Kyse30 cell lines, 449 leading-edge genes were extracted as most likely genes to have the strongest contribution to the observed phenotype of EGF-mediated invasion (Figure 23). MEKi/OUT and Cetux/OUT comparisons were utilized to narrow the number of genes amongst the 449 leading-edge genes since previous data has shown that MEKi and Cetuximab can effectively inhibit EMT and, as shown in the present study, also hampers EGF-mediated invasion.

Hence, the inclusion criteria for the most strict selection of genes were that the expression of these 449 genes in OUT/SF should be counter-regulated in the MEKi/OUT group and/or Cetux/OUT. Additionally, each genes should be quality as a DEG with a threshold of $Log_2FC>1$ and an adjusted p-value < 0.05. within the respective comparison, finally resulting in a short-list of 46 genes (Figure 24).

To establish a connection between these 46 genes extracted from invasive cells with clinical samples, the scRNA-seq HNSCC dataset from Puram et al. was introduced (Puram et al., 2017). Modules of co-regulated genes were identified using a WGCNA and the resulting modules were analyzed for their correlation to four related parameters: EMT, MAPK pathway, PI3K pathway, and EGF_EGFR pathway (Figure 25) (Figure 29). Through this analysis a gene module comprised of 300 co-regulated genes was selected because of its

highest correlation with the selected parameters mentioned above, which reflect findings of our in vitro model. After the intersection of the 300 genes (brown module) and the 46 genes (Bulk-sequencing results), 16 genes appeared. They are: IL8, FOSL1, KLF6, COL17A1, INHBA, ITGA3, ITGA5, ITGB4, LAMA3, LAMB3, LAMC2, MT2A, PLEK2, PHLDA1, SERPINE1, SPHK1.

Those 16 genes can be used to explain the causes of EGF-mediated invasion to a certain extent. For example, high levels of EMT-related genes like Serpine Family E Member 1 (SERPINE1), Inhibin Subunit Beta A (INHBA), chemokine (C-X-C motif) ligand 8 (IL8), Integrin Subunit Alpha 5 (ITGA5), Laminin Subunit Gamma 2 (LAMC2), and Laminin Subunit Alpha 3 (LAMA3) can cause cells to change from an epithelial to a mesenchymal state, provide weaker cell-to-cell contact, lower cell adhesion, and enables cells to acquire higher mobility, increasing their capacity to invade and metastasize (C. Huang & Chen, 2021; T. Li, Wu, Liu, & Wang, 2020; X. Li et al., 2020; Okada, Takahashi, Takayama, & Goel, 2021; Pu et al., 2021; Y. Yu, Wang, Lu, Chen, & Shang, 2021). Additionally, the genes encoding for integrin and laminin, including Integrin Subunit Beta 4 (ITGB4), LAMA3, LAMC2, and the apical-junctions related genes, such as Collagen Type XVII Alpha 1 Chain (COL17A1), Integrin Subunit Alpha 3 (ITGA3) can assist tumor cells in adapting to the tumor microenvironment by degrading and secreting corresponding proteins (Bierie

et al., 2017; Feng et al., 2020; G. S. Li et al., 2022; Thangavelu, Krenács, Dray, & Duijf, 2016; Theocharis et al., 2016). Gene like Sphingosine Kinase 1 (SPHK1), is closely related to the ECM. *Ko et al.* showed that one of the important regulators of the equilibrium between cancer cell invasion and adhesion during metastasis is the temporal control of S1P (through SPHK1) secretion by the various mechanical circumstances (Ko et al., 2016). In the cellular microenvironment, the role of the ECM stiffness in regulating SPHK1 differs between aggressive metastatic cell lines and primary cell lines. While increasing ECM stiffness can decrease SPHK1 expression in primary cell lines, it can also induce it in aggressive metastatic cell lines (Ko et al., 2016). *Sheu et al.* discovered that through EGFR-MAPK-SPHK1 signaling, LRIG1 may regulate cell migration and metastasis (Sheu et al., 2014). In 2019, SPHK1 was identified by *Tsang et al*. as an oncogene associated with the super-enhancer (SE) in hepatocellular cancer (Tsang et al., 2019). Additionally, FOS Like 1 (FOSL1), an AP-1 Transcription Factor Subunit, was also found to be a master regulator in HNSCC by *M. Zhang et al*. Through a super-enhancer-driven transcriptional program, it primarily promotes tumorigenicity and metastasis by placing super-enhancers (SEs) at critical oncogenes, including SNAI2 (M. Zhang et al., 2021). Inhibin subunit beta A (INHBA), a possible biomarker, is highly expressed in HNSCC (Wu, Tang, Niu, & Cheng, 2019; Y. Yu et al., 2021).

IL8 secretion also increases migration, invasion, and chemotherapy resistance in oral cancer cells (Pu et al., 2021), etc.

However, numerous genes work together to cause tumor invasion, which is not the consequence of the action of one single gene. In addition to carrying out their individual tasks, individual genes products also connect or collaborate with others to establish transcription factor and protein network that promotes tumor invasion and leader cell movement (B. J. Chen et al., 2020; Khalil & de Rooij, 2019; Vilchez Mercedes et al., 2021; Vishwakarma et al., 2020; Yamada & Sixt, 2019; J. Zhang et al., 2019; Zoeller et al., 2019). Therefore, future work will require analyzing the acquired data from a different angle, taking regulatory transcription factor networks and inferring protein activities into account. Upcoming analyses from our group will implement the NetBit2 (Network-based Biased Tree Ensembles) algorithm that infers the expression of transcription factors and their downstream effectors across samples of RNA-seq data, and further allows to infer protein activities via metaVIPER.

Furthermore, the situation of tumor patients will be more complex as the process of tumor invasion is affected by the cell itself and the surrounding environment, including pH (Thews & Riemann, 2019), blood oxygen (Fearon, Canavan, Biniecka, & Veale, 2016), different subtypes of CAFs within and in the vicinity of the tumor (Mao et al., 2021), tumor cell differentiation stage

(including EMT, p-EMT, etc.) (T. Chen, You, Jiang, & Wang, 2017; M. A. Nieto, R. Y. J. Huang, R. A. Jackson, & J. P. Thiery, 2016b; Puram et al., 2018a), tumor heterogeneity (Bedard, Hansen, Ratain, & Siu, 2013; Kim & DeBerardinis, 2019; Torab et al., 2020; Zoeller et al., 2019), and the physiological state of surrounding tissues (wound healing and tissue morphogenesis) (Suhail et al., 2019; Vilchez Mercedes et al., 2021), reprogramming of the extracellular matrix (Y. L. Han et al., 2018; Nguyen-Ngoc et al., 2012; Winkler et al., 2020; Yamada & Sixt, 2019), more aggressive subpopulation within the same tumor type, etc (Ashing, Jones, Bedell, Phillips, & Erhunmwunsee, 2022; Dietze, Chavez, & Seewaldt, 2018; Gomez, 2020). All of these may become factors or promoters that affect tumor invasion.

4.3 Validation of SPHK1 as a potential target for the inhibition of EGFR-mediated invasion and for combinatorial treatment with Cetuximab.

Among the 16 genes, SPHK1 stood out as the only kinase-encoding gene, which makes it promising as a potential therapeutic target. Sphingosine kinase 1 (SPHK1) catalyzes the conversion of sphingosine (Sph) to sphingosine 1-phosphate (S1P), which plays a role in metabolic and inflammatory processes, cell proliferation and migration, and growth and death (X. Wang et al., 2020). The majority of cancers have widespread overexpression of SPHK1, which

promotes tumor growth and is linked to poor clinical outcome (Wang et al., 2019). At present, several inhibitors of SPHK1 have been developed, such as SK1-I (BML258), LCL351/146, VPC96091, PF-543, SKI-I, SKI-II (SKi), SKI-178, and SLC 4011540 (Bu, Wu, Deng, & Wang, 2021). Among those inhibitors, PF-543 is a novel sphingosine-competitive inhibitor of SPHK1 (Khan, Lai, Anwer, Azim, & Khan, 2020; X. Wang et al., 2020), and its inhibitory effect on cancers has been demonstrated in a variety of cancer studies, including breast cancer, prostate cancer, colorectal, lung and liver cancer (Ju, Gao, & Fang, 2016; Khan et al., 2020; H. M. Lin et al., 2021; X. Wang et al., 2020). However, there are few studies on the role of PF-543 in HNSCC, for example, *Hamada et al*. had found that PF-543 can induce autophagy in HNSCC cells (Hamada, Kameyama, Iwai, & Yura, 2017), but the role of PF-543 in inhibiting HNSCC invasion remains unclear.

PF-543 was used to assess its inhibitory function during EGF-mediated 3D invasion. The results showed that PF-543 had a strong and dose-dependent inhibitory effect on invasion, and when low-doses of PF-543 and Cetuximab were used in combination, the inhibitory effect was comparable to that of Cetuximab^{high}. The results showed that PF-543^{low} can effectively reduce the dosage of Cetuximab to one-tenth of the original dosage to achieve the same invasion inhibition, indicating a potential synergistic effect and the possibility of

increasing the sensitivity of tumor cells to Cetuximab. The expression level of SPHK1 in HNSCC Cetuximab-resistant cell lines was reportedly higher than that in Cetuximab-sensitive cell lines (Figure 32), which indirectly indicated that inhibition of SPHK1 might affect Cetuximab sensitivity (Figure 32). From the current results, SPHK1 inhibitor PF-543 can be considered as a candidate therapeutic target in future studies. Future work will aim at further corroborating SPHK1 as a therapeutic target for example using Cetuximab-resistant cell lines to test whether blocking SPHK1 with PF-543 restores Cetuximab sensitivity.

5 CONCLUSION

Taken together, this work attempted to build a 3D model based on type I collagen to simulate the microenvironment of HNSCC tumor invasion and study EGF-mediated 3D invasion at the molecular level. After intersecting genes most strongly contributing to cellular hallmarks that were significantly altered in invasive cells with genes that were co-regulated in single malignant cells and that correlated with EMT, EGFR and MAPK activity, a narrow set of 16 genes was identified. From these 16 genes, several genes like ITGB4, LAMA3, LAMC2, COL17A1 and ITGA3 support the potential of cells to reshape the tumor microenvironment (Bierie et al., 2017; Feng et al., 2020; G. S. Li et al., 2022; Thangavelu et al., 2016; Theocharis et al., 2016) , SERPINE1, INHBA, IL8, ITGA5, LAMC2, and LAMA3 regulate EMT (C. Huang & Chen, 2021; T. Li et al., 2020; X. Li et al., 2020; Okada et al., 2021; Pu et al., 2021; Y. Yu et al., 2021), and FOSL1, IL-8, SPHK1 and ITGB4 foster treatment resistance at the transcriptional level (Bierie et al., 2017; Bu et al., 2021; Pu et al., 2021; M. Zhang et al., 2021). In a proof-of-concept study, a novel inhibitor of SPHK1 was shown to hamper EGF-mediated invasion and to substantially lower concentrations of Cetuximab required for the inhibition of invasion.

Understanding the complicated process of tumor invasion in full depth remains highly challenging. The following factors might be considered to address this

issue: First, finding possible targets to halt the development of invasive cells or reduce their activity should be considered. Second, altering the tumor microenvironment, such that the metastatic potential of the tumor surrounded by ECM fibers is reduced. Third, changing the metabolic program of tumor cells to inhibit EMT. Therefore, further research into EGF-mediated invasion, particularly the transcriptomic basis of invasion, is expected to be promising and might lead to developing novel therapeutic approaches for HNSCC patients.

6 REFERENCES

Abell, A. N., Jordan, N. V., Huang, W., Prat, A., Midland, A. A., Johnson, N. L., . . . Johnson, G. L. (2011). MAP3K4/CBP-regulated H2B acetylation controls epithelial-mesenchymal transition in trophoblast stem cells. *Cell Stem Cell, 8*(5), 525-537. doi:10.1016/j.stem.2011.03.008

Abu-Humaidan, A. H. A., Ekblad, L., Wennerberg, J., & Sorensen, O. E. (2020). EGFR modulates complement activation in head and neck squamous cell carcinoma. *BMC Cancer, 20*(1), 121. doi:10.1186/s12885-020-6615-z

Albanell, J., Codony-Servat, J., Rojo, F., Del Campo, J. M., Sauleda, S., Anido, J., . . . Baselga, J. (2001). Activated extracellular signal-regulated kinases: Association with epidermal growth factor receptor/transforming growth factor alpha expression in head and neck squamous carcinoma and inhibition by anti-epidermal growth factor receptor treatments. *Cancer Research, 61*(17), 6500-6510. Retrieved from <Go to ISI>://WOS:000170637700032

Almany, L., & Seliktar, D. (2005). Biosynthetic hydrogel scaffolds made from fibrinogen and polyethylene glycol for 3D cell cultures. *Biomaterials, 26*(15), 2467-2477. doi:10.1016/j.biomaterials.2004.06.047

An, X., & Chen, L. (2018). Flow Cytometry (FCM) Analysis and Fluorescence-Activated Cell Sorting (FACS) of Erythroid Cells. *Methods Mol Biol, 1698*, 153-174. doi:10.1007/978-1-4939-7428-3_9

Arnoux, V., Nassour, M., L'Helgoualc'h, A., Hipskind, R. A., & Savagner, P. (2008). Erk5 controls Slug expression and keratinocyte activation during wound healing. *Mol Biol Cell, 19*(11), 4738-4749. doi:10.1091/mbc.E07-10-1078

Ashing, K. T., Jones, V., Bedell, F., Phillips, T., & Erhunmwunsee, L. (2022). Calling Attention to the Role of Race-Driven Societal Determinants of Health on Aggressive Tumor Biology: A Focus on Black Americans. *JCO Oncol Pract, 18*(1), 15-22. doi:10.1200/op.21.00297

Avraham, R., & Yarden, Y. (2011). Feedback regulation of EGFR signalling: decision making by early and delayed loops. *Nat Rev Mol Cell Biol, 12*(2), 104-117. doi:10.1038/nrm3048

Baccelli, I., Schneeweiss, A., Riethdorf, S., Stenzinger, A., Schillert, A., Vogel, V., . . . Trumpp, A. (2013). Identification of a population of blood circulating tumor cells from breast cancer patients that initiates metastasis in a xenograft assay. *Nat Biotechnol, 31*(6), 539-544. doi:10.1038/nbt.2576

Baumeister, P., Hollmann, A., Kitz, J., Afthonidou, A., Simon, F., Shakhtour, J., . . . Gires, O. (2018). High Expression of EpCAM and Sox2 is a Positive Prognosticator of Clinical Outcome for Head and Neck Carcinoma. *Scientific Reports, 8*. doi:10.1038/s41598-018-32178-8

Baumeister, P., Zhou, J., Canis, M., & Gires, O. (2021). Epithelial-to-Mesenchymal Transition-Derived Heterogeneity in Head and Neck Squamous Cell Carcinomas. *Cancers (Basel), 13*(21). doi:10.3390/cancers13215355

Bedard, P. L., Hansen, A. R., Ratain, M. J., & Siu, L. L. (2013). Tumour heterogeneity in the clinic. *Nature, 501*(7467), 355-364. doi:10.1038/nature12627

Beerling, E., Seinstra, D., de Wit, E., Kester, L., van der Velden, D., Maynard, C., . . . van Rheenen, J. (2016). Plasticity between Epithelial and Mesenchymal States Unlinks EMT from Metastasis-Enhancing Stem Cell Capacity. *Cell Reports, 14*(10), 2281-2288. doi:10.1016/j.celrep.2016.02.034

Bei, R., Budillon, A., Masuelli, L., Cereda, V., Vitolo, D., Di Gennaro, E., . . . Muraro, R. (2004). Frequent overexpression of multiple ErbB receptors by head and neck squamous cell carcinoma contrasts with rare antibody immunity in patients. *Journal of Pathology, 204*(3), 317-325. doi:10.1002/path.1642

Bergers, G., & Hanahan, D. (2008). Modes of resistance to anti-angiogenic therapy. *Nat Rev Cancer, 8*(8), 592-603. doi:10.1038/nrc2442

Beug, H. (2009). Breast Cancer Stem Cells: Eradication by Differentiation Therapy? *Cell, 138*(4), 623-625. doi:10.1016/j.cell.2009.08.007

Bierie, B., Pierce, S. E., Kroeger, C., Stover, D. G., Pattabiraman, D. R., Thiru, P., . . . Weinberg, R. A. (2017). Integrin-beta4 identifies cancer stem cell-enriched populations of partially mesenchymal carcinoma cells. *Proc Natl Acad Sci U S A, 114*(12), E2337-E2346. doi:10.1073/pnas.1618298114

Birgersdotter, A., Sandberg, R., & Ernberg, I. (2005). Gene expression perturbation in vitro--a growing case for three-dimensional (3D) culture systems. *Semin Cancer Biol, 15*(5), 405-412. doi:10.1016/j.semcancer.2005.06.009

Blobel, C. P. (2005). ADAMs: key components in EGFR signalling and development. *Nat Rev Mol Cell Biol, 6*(1), 32-43. doi:10.1038/nrm1548

Bossi, P., Resteghini, C., Paielli, N., Licitra, L., Pilotti, S., & Perrone, F. (2016). Prognostic and predictive value of EGFR in head and neck squamous cell carcinoma. *Oncotarget, 7*(45), 74362-74379. doi:10.18632/oncotarget.11413

Brabletz, T. (2012). EMT and MET in Metastasis: Where Are the Cancer Stem Cells? *Cancer Cell, 22*(6), 699-701. doi:10.1016/j.ccr.2012.11.009

Brabletz, T., Kalluri, R., Nieto, M. A., & Weinberg, R. A. (2018). EMT in cancer. *Nat Rev Cancer, 18*(2), 128-134. doi:10.1038/nrc.2017.118

Bray, F., Ferlay, J., Soerjomataram, I., Siegel, R. L., Torre, L. A., & Jemal, A. (2018). Global cancer statistics 2018: GLOBOCAN estimates of incidence and mortality worldwide for 36 cancers

in 185 countries. *Ca-a Cancer Journal for Clinicians, 68*(6), 394-424. doi:10.3322/caac.21492

Bu, Y., Wu, H., Deng, R., & Wang, Y. (2021). Therapeutic Potential of SphK1 Inhibitors Based on Abnormal Expression of SphK1 in Inflammatory Immune Related-Diseases. *Front Pharmacol, 12*, 733387. doi:10.3389/fphar.2021.733387

Burrell, R. A., McGranahan, N., Bartek, J., & Swanton, C. (2013). The causes and consequences of genetic heterogeneity in cancer evolution. *Nature, 501*(7467), 338-345. doi:10.1038/nature12625

Cancer Genome Atlas, N. (2015). Comprehensive genomic characterization of head and neck squamous cell carcinomas. *Nature, 517*(7536), 576-582. doi:10.1038/nature14129

Cano, A., Perez-Moreno, M. A., Rodrigo, I., Locascio, A., Blanco, M. J., del Barrio, M. G., . . . Nieto, M. A. (2000). The transcription factor Snail controls epithelial-mesenchymal transitions by repressing E-cadherin expression. *Nature Cell Biology, 2*(2), 76-83. doi:10.1038/35000025

Carmody, L. C., Germain, A. R., VerPlank, L., Nag, P. P., Munoz, B., Perez, J. R., & Palmer, M. A. J. (2012). Phenotypic High-Throughput Screening Elucidates Target Pathway in Breast Cancer Stem Cell-Like Cells. *Journal of Biomolecular Screening, 17*(9), 1204-1210. doi:10.1177/1087057112458317

Casanova-Acebes, M., Dalla, E., Leader, A. M., LeBerichel, J., Nikolic, J., Morales, B. M., . . . Merad, M. (2021). Tissue-resident macrophages provide a pro-tumorigenic niche to early NSCLC cells. *Nature, 595*(7868), 578-584. doi:10.1038/s41586-021-03651-8

Cassell, A., & Grandis, J. R. (2010). Investigational EGFR-targeted therapy in head and neck squamous cell carcinoma. *Expert Opinion on Investigational Drugs, 19*(6), 709-722. doi:10.1517/13543781003769844

Castilho, R. M., Squarize, C. H., & Almeida, L. O. (2017). Epigenetic Modifications and Head and Neck Cancer: Implications for Tumor Progression and Resistance to Therapy. *International Journal of Molecular Sciences, 18*(7). doi:10.3390/ijms18071506

Chen, B. J., Wu, J. S., Tang, Y. J., Tang, Y. L., & Liang, X. H. (2020). What makes leader cells arise: Intrinsic properties and support from neighboring cells. *Journal of Cellular Physiology, 235*(12), 8983-8995. doi:10.1002/jcp.29828

Chen, L., Sun, D. Z., Fu, Y. G., Yang, P. Z., Lv, H. Q., Gao, Y. L., & Zhang, X. Y. (2020). Upregulation of microRNA-141 suppresses epithelial-mesenchymal transition and lymph node metastasis in laryngeal cancer through HOXC6-dependent TGF-beta signaling pathway. *Cellular Signalling, 66*. doi:10.1016/j.cellsig.2019.109444

Chen, T., You, Y., Jiang, H., & Wang, Z. Z. (2017). Epithelial-mesenchymal transition (EMT): A biological process in the development, stem cell differentiation, and tumorigenesis. *J Cell*

Physiol, 232(12), 3261-3272. doi:10.1002/jcp.25797

Chua, K. N., Poon, K. L., Lim, J., Sim, W. J., Huang, R. Y. J., & Thiery, J. P. (2011). Target cell movement in tumor and cardiovascular diseases based on the epithelial-mesenchymal transition concept. *Advanced Drug Delivery Reviews, 63*(8), 558-567. doi:10.1016/j.addr.2011.02.003

Chudakov, D. M., Lukyanov, S., & Lukyanov, K. A. (2007). Tracking intracellular protein movements using photoswitchable fluorescent proteins PS-CFP2 and Dendra2. *Nat Protoc, 2*(8), 2024-2032. doi:10.1038/nprot.2007.291

Chung, C. H., Parker, J. S., Karaca, G., Wu, J. Y., Funkhouser, W. K., Moore, D., . . . Perou, C. M. (2004). Molecular classification of head and neck squamous cell carcinomas using patterns of gene expression. *Cancer Cell, 5*(5), 489-500. doi:10.1016/s1535-6108(04)00112-6

Ciardiello, F., & Tortora, G. (2008). EGFR antagonists in cancer treatment. *N Engl J Med, 358*(11), 1160-1174. doi:10.1056/NEJMra0707704

Cohen, S. (1962). Isolation of a mouse submaxillary gland protein accelerating incisor eruption and eyelid opening in the new-born animal. *J Biol Chem, 237*, 1555-1562.

Cohen, S., Carpenter, G., & King, L., Jr. (1980). Epidermal growth factor-receptor-protein kinase interactions. Co-purification of receptor and epidermal growth factor-enhanced phosphorylation activity. *J Biol Chem, 255*(10), 4834-4842.

Cohen, S., Ushiro, H., Stoscheck, C., & Chinkers, M. (1982). A native 170,000 epidermal growth factor receptor-kinase complex from shed plasma membrane vesicles. *J Biol Chem, 257*(3), 1523-1531.

Cook, D. P., & Vanderhyden, B. C. (2020). Context specificity of the EMT transcriptional response. *Nature Communications, 11*(1). doi:10.1038/s41467-020-16066-2

Cramer, J. D., Burtness, B., Le, Q. T., & Ferris, R. L. (2019). The changing therapeutic landscape of head and neck cancer. *Nat Rev Clin Oncol, 16*(11), 669-683. doi:10.1038/s41571-019-0227-z

Cui, B., Chen, J., Luo, M., Liu, Y., Chen, H., Lü, D., . . . Zhang, P. (2021). PKD3 promotes metastasis and growth of oral squamous cell carcinoma through positive feedback regulation with PD-L1 and activation of ERK-STAT1/3-EMT signalling. *Int J Oral Sci, 13*(1), 8. doi:10.1038/s41368-021-00112-w

Danhier, F., Feron, O., & Préat, V. (2010). To exploit the tumor microenvironment: Passive and active tumor targeting of nanocarriers for anti-cancer drug delivery. *J Control Release, 148*(2), 135-146. doi:10.1016/j.jconrel.2010.08.027

Dietze, E. C., Chavez, T. A., & Seewaldt, V. L. (2018). Obesity and Triple-Negative Breast Cancer: Disparities, Controversies, and Biology. *Am J Pathol, 188*(2), 280-290.

doi:10.1016/j.ajpath.2017.09.018

Eskiizmir, G. (2015). Tumor Microenvironment in Head and Neck Squamous Cell Carcinomas. *Turk Arch Otorhinolaryngol, 53*(3), 120-127. doi:10.5152/tao.2015.1065

Fasano, M., Della Corte, C. M., Califano, R., Capuano, A., Troiani, T., Martinelli, E., . . . Morgillo, F. (2014). Type III or allosteric kinase inhibitors for the treatment of non-small cell lung cancer. *Expert Opinion on Investigational Drugs, 23*(6), 809-821. doi:10.1517/13543784.2014.902934

Fasano, M., Della Corte, C. M., Viscardi, G., Di Liello, R., Paragliola, F., Sparano, F., . . . Ciardiello, F. (2021). Head and neck cancer: the role of anti-EGFR agents in the era of immunotherapy. *Ther Adv Med Oncol, 13*, 1758835920949418. doi:10.1177/1758835920949418

Faubert, B., Solmonson, A., & DeBerardinis, R. J. (2020). Metabolic reprogramming and cancer progression. *Science, 368*(6487). doi:10.1126/science.aaw5473

Fearon, U., Canavan, M., Biniecka, M., & Veale, D. J. (2016). Hypoxia, mitochondrial dysfunction and synovial invasiveness in rheumatoid arthritis. *Nat Rev Rheumatol, 12*(7), 385-397. doi:10.1038/nrrheum.2016.69

Feng, C., Jin, X., Han, Y., Guo, R., Zou, J., Li, Y., & Wang, Y. (2020). Expression and Prognostic Analyses of ITGA3, ITGA5, and ITGA6 in Head and Neck Squamous Cell Carcinoma. *Med Sci Monit, 26*, e926800. doi:10.12659/MSM.926800

Ferlay, J., Colombet, M., Soerjomataram, I., Mathers, C., Parkin, D. M., Pineros, M., . . . Bray, F. (2019). Estimating the global cancer incidence and mortality in 2018: GLOBOCAN sources and methods. *International Journal of Cancer, 144*(8), 1941-1953. doi:10.1002/ijc.31937

Fischer, K. R., Durrans, A., Lee, S., Sheng, J. T., Li, F. H., Wong, S. T. C., . . . Gao, D. C. (2015). Epithelial-to-mesenchymal transition is not required for lung metastasis but contributes to chemoresistance. *Nature, 527*(7579), 472-+. doi:10.1038/nature15748

Fischer, T., Hayn, A., & Mierke, C. T. (2019). Fast and reliable advanced two-step pore-size analysis of biomimetic 3D extracellular matrix scaffolds. *Sci Rep, 9*(1), 8352. doi:10.1038/s41598-019-44764-5

Fleming, D. S., & Miller, L. C. (2016). Leading edge analysis of transcriptomic changes during pseudorabies virus infection. *Genom Data, 10*, 104-106. doi:10.1016/j.gdata.2016.09.014

Freed, D. M., Bessman, N. J., Kiyatkin, A., Salazar-Cavazos, E., Byrne, P. O., Moore, J. O., . . . Lemmon, M. A. (2017). EGFR Ligands Differentially Stabilize Receptor Dimers to Specify Signaling Kinetics. *Cell, 171*(3), 683-695 e618. doi:10.1016/j.cell.2017.09.017

Friedl, P., Locker, J., Sahai, E., & Segall, J. E. (2012). Classifying collective cancer cell invasion. *Nature Cell Biology, 14*(8), 777-783. doi:10.1038/ncb2548

Friedrich, J., Ebner, R., & Kunz-Schughart, L. A. (2007). Experimental anti-tumor therapy in 3-D: spheroids--old hat or new challenge? *Int J Radiat Biol, 83*(11-12), 849-871. doi:10.1080/09553000701727531

Giannelli, G., Villa, E., & Lahn, M. (2014). Transforming Growth Factor-beta as a Therapeutic Target in Hepatocellular Carcinoma. *Cancer Research, 74*(7), 1890-1894. doi:10.1158/0008-5472.Can-14-0243

Gomez, H. (2020). How heterogeneity drives tumour growth: a computational study. *Philos Trans A Math Phys Eng Sci, 378*(2171), 20190244. doi:10.1098/rsta.2019.0244

Grandis, J. R., & Tweardy, D. J. (1993). ELEVATED LEVELS OF TRANSFORMING GROWTH-FACTOR-ALPHA AND EPIDERMAL GROWTH-FACTOR RECEPTOR MESSENGER-RNA ARE EARLY MARKERS OF CARCINOGENESIS IN HEAD AND NECK-CANCER. *Cancer Research, 53*(15), 3579-3584. Retrieved from <Go to ISI>://WOS:A1993LP64100025

Gregoire, V., Langendijk, J. A., & Nuyts, S. (2015). Advances in Radiotherapy for Head and Neck Cancer. *Journal of Clinical Oncology, 33*(29), 3277-+. doi:10.1200/jco.2015.61.2994

Grigore, A. D., Jolly, M. K., Jia, D., Farach-Carson, M. C., & Levine, H. (2016). Tumor Budding: The Name is EMT. Partial EMT. *J Clin Med, 5*(5). doi:10.3390/jcm5050051

Guo, Y., Ahn, M. J., Chan, A., Wang, C. H., Kang, J. H., Kim, S. B., . . . Tang, P. Z. (2019). Afatinib versus methotrexate as second-line treatment in Asian patients with recurrent or metastatic squamous cell carcinoma of the head and neck progressing on or after platinum-based therapy (LUX-Head & Neck 3): an open-label, randomised phase III trial. *Annals of Oncology, 30*(11), 1831-1839. doi:10.1093/annonc/mdz388

Gupta, P. B., Chaffer, C. L., & Weinberg, R. A. (2009). Cancer stem cells: mirage or reality? *Nature Medicine, 15*(9), 1010-1012. doi:10.1038/nm0909-1010

Gupta, P. B., Onder, T. T., Jiang, G. Z., Tao, K., Kuperwasser, C., Weinberg, R. A., & Lander, E. S. (2009). Identification of Selective Inhibitors of Cancer Stem Cells by High-Throughput Screening. *Cell, 138*(4), 645-659. doi:10.1016/j.cell.2009.06.034

Hamada, M., Kameyama, H., Iwai, S., & Yura, Y. (2017). Induction of autophagy by sphingosine kinase 1 inhibitor PF-543 in head and neck squamous cell carcinoma cells. *Cell Death Discov, 3*, 17047. doi:10.1038/cddiscovery.2017.47

Han, W., & Lo, H. W. (2012). Landscape of EGFR signaling network in human cancers: biology and therapeutic response in relation to receptor subcellular locations. *Cancer Lett, 318*(2), 124-134. doi:10.1016/j.canlet.2012.01.011

Han, Y. L., Ronceray, P., Xu, G. Q., Malandrino, A., Kamm, R. D., Lenz, M., . . . Guo, M. (2018). Cell contraction induces long-ranged stress stiffening in the extracellular matrix. *Proceedings of the National Academy of Sciences of the United States of America, 115*(16), 4075-4080.

doi:10.1073/pnas.1722619115

Hänzelmann, S., Castelo, R., & Guinney, J. (2013). GSVA: gene set variation analysis for microarray and RNA-Seq data. *Bmc Bioinformatics, 14*(1), 7. doi:10.1186/1471-2105-14-7

Harjanto, D., Maffei, J. S., & Zaman, M. H. (2011). Quantitative analysis of the effect of cancer invasiveness and collagen concentration on 3D matrix remodeling. *PLoS One, 6*(9), e24891. doi:10.1371/journal.pone.0024891

Harris, R. C., Chung, E., & Coffey, R. J. (2003). EGF receptor ligands. *Exp Cell Res, 284*(1), 2-13. doi:10.1016/s0014-4827(02)00105-2

Hay, E. D. (1995). An overview of epithelio-mesenchymal transformation. *Acta Anat (Basel), 154*(1), 8-20. doi:10.1159/000147748

Herbst, R. S. (2004). Review of epidermal growth factor receptor biology. *Int J Radiat Oncol Biol Phys, 59*(2 Suppl), 21-26. doi:10.1016/j.ijrobp.2003.11.041

Hirschhaeuser, F., Menne, H., Dittfeld, C., West, J., Mueller-Klieser, W., & Kunz-Schughart, L. A. (2010). Multicellular tumor spheroids: an underestimated tool is catching up again. *J Biotechnol, 148*(1), 3-15. doi:10.1016/j.jbiotec.2010.01.012

Huang, C., & Chen, J. (2021). Laminin-332 mediates proliferation, apoptosis, invasion, migration and epithelial-to-mesenchymal transition in pancreatic ductal adenocarcinoma. *Mol Med Rep, 23*(1). doi:10.3892/mmr.2020.11649

Huang, C., Chen, L., Savage, S. R., Eguez, R. V., Dou, Y., Li, Y., . . . Zhang, B. (2021). Proteogenomic insights into the biology and treatment of HPV-negative head and neck squamous cell carcinoma. *Cancer Cell, 39*(3), 361-379.e316. doi:10.1016/j.ccell.2020.12.007

Huang, J. W., Zhang, J., Shi, C. L., Liu, L., & Wei, Y. Q. (2016). Survival, recurrence and toxicity of HNSCC in comparison of a radiotherapy combination with cisplatin versus cetuximab: a meta-analysis. *BMC Cancer, 16*. doi:10.1186/s12885-016-2706-2

Huang, R. Y., Guilford, P., & Thiery, J. P. (2012). Early events in cell adhesion and polarity during epithelial-mesenchymal transition. *J Cell Sci, 125*(Pt 19), 4417-4422. doi:10.1242/jcs.099697

Huang, R. Y., Wong, M. K., Tan, T. Z., Kuay, K. T., Ng, A. H., Chung, V. Y., . . . Thiery, J. P. (2013). An EMT spectrum defines an anoikis-resistant and spheroidogenic intermediate mesenchymal state that is sensitive to e-cadherin restoration by a src-kinase inhibitor, saracatinib (AZD0530). *Cell Death Dis, 4*, e915. doi:10.1038/cddis.2013.442

Hynes, N. E., & Lane, H. A. (2005). ERBB receptors and cancer: The complexity of targeted inhibitors. *Nature Reviews Cancer, 5*(5), 341-354. doi:10.1038/nrc1609

Irish, J. M., Hovland, R., Krutzik, P. O., Perez, O. D., Bruserud, Ø., Gjertsen, B. T., & Nolan, G. P.

(2004). Single cell profiling of potentiated phospho-protein networks in cancer cells. *Cell, 118*(2), 217-228. doi:10.1016/j.cell.2004.06.028

Jang, T. H., Huang, W. C., Tung, S. L., Lin, S. C., Chen, P. M., Cho, C. Y., . . . Wang, L. H. (2022). MicroRNA-485-5p targets keratin 17 to regulate oral cancer stemness and chemoresistance via the integrin/FAK/Src/ERK/β-catenin pathway. *J Biomed Sci, 29*(1), 42. doi:10.1186/s12929-022-00824-z

Johnson, D. E., Burtness, B., Leemans, C. R., Lui, V. W. Y., Bauman, J. E., & Grandis, J. R. (2020). Head and neck squamous cell carcinoma. *Nat Rev Dis Primers, 6*(1), 92. doi:10.1038/s41572-020-00224-3

Jonckheere, S., Adams, J., De Groote, D., Campbell, K., Berx, G., & Goossens, S. (2022). Epithelial-Mesenchymal Transition (EMT) as a Therapeutic Target. *Cells Tissues Organs, 211*(2), 157-182. doi:10.1159/000512218

Jordan, N. V., Johnson, G. L., & Abell, A. N. (2011a). Tracking the intermediate stages of epithelial-mesenchymal transition in epithelial stem cells and cancer. *Cell Cycle, 10*(17), 2865-2873. doi:10.4161/cc.10.17.17188

Jordan, N. V., Johnson, G. L., & Abell, A. N. (2011b). Tracking the intermediate stages of epithelial-mesenchymal transition in epithelial stem cells and cancer. *Cell Cycle, 10*(17), 2865-2873. doi:10.4161/cc.10.17.17188

Ju, T., Gao, D., & Fang, Z. Y. (2016). Targeting colorectal cancer cells by a novel sphingosine kinase 1 inhibitor PF-543. *Biochem Biophys Res Commun, 470*(3), 728-734. doi:10.1016/j.bbrc.2016.01.053

Kalluri, R., & Weinberg, R. A. (2009). The basics of epithelial-mesenchymal transition. *J Clin Invest, 119*(6), 1420-1428. doi:10.1172/JCI39104

Kalyankrishna, S., & Grandis, J. R. (2006). Epidermal growth factor receptor biology in head and neck cancer. *Journal of Clinical Oncology, 24*(17), 2666-2672. doi:10.1200/jco.2005.04.8306

Kashyap, T., Pramanik, K. K., Nath, N., Mishra, P., Singh, A. K., Nagini, S., . . . Mishra, R. (2018). Crosstalk between Raf-MEK-ERK and PI3K-Akt-GSK3β signaling networks promotes chemoresistance, invasion/migration and stemness via expression of CD44 variants (v4 and v6) in oral cancer. *Oral Oncol, 86*, 234-243. doi:10.1016/j.oraloncology.2018.09.028

Khalil, A. A., & de Rooij, J. (2019). Cadherin mechanotransduction in leader-follower cell specification during collective migration. *Experimental Cell Research, 376*(1), 86-91. doi:10.1016/j.yexcr.2019.01.006

Khan, F. I., Lai, D., Anwer, R., Azim, I., & Khan, M. K. A. (2020). Identifying novel sphingosine kinase 1 inhibitors as therapeutics against breast cancer. *J Enzyme Inhib Med Chem, 35*(1), 172-

186. doi:10.1080/14756366.2019.1692828

Khoo, B. L., Lee, S. C., Kumar, P., Tan, T. Z., Warkiani, M. E., Ow, S. G. W., . . . Thiery, J. P. (2015). Short-term expansion of breast circulating cancer cells predicts response to anti-cancer therapy. *Oncotarget, 6*(17), 15578-15593. Retrieved from <Go to ISI>://WOS:000359010700069

Kim, J., & DeBerardinis, R. J. (2019). Mechanisms and Implications of Metabolic Heterogeneity in Cancer. *Cell Metab, 30*(3), 434-446. doi:10.1016/j.cmet.2019.08.013

Kisoda, S., Shao, W. H., Fujiwara, N., Mouri, Y., Tsunematsu, T., Jin, S., . . . Kudo, Y. (2020). Prognostic value of partial EMT-related genes in head and neck squamous cell carcinoma by a bioinformatic analysis. *Oral Diseases, 26*(6), 1149-1156. doi:10.1111/odi.13351

Ko, P., Kim, D., You, E., Jung, J., Oh, S., Kim, J., . . . Rhee, S. (2016). Extracellular Matrix Rigidity-dependent Sphingosine-1-phosphate Secretion Regulates Metastatic Cancer Cell Invasion and Adhesion. *Sci Rep, 6*, 21564. doi:10.1038/srep21564

Kozyrska, K., Pilia, G., Vishwakarma, M., Wagstaff, L., Goschorska, M., Cirillo, S., . . . Piddini, E. (2022). p53 directs leader cell behavior, migration, and clearance during epithelial repair. *Science, 375*(6581), eabl8876. doi:10.1126/science.abl8876

Kriegs, M., Kasten-Pisula, U., Riepen, B., Hoffer, K., Struve, N., Myllynen, L., . . . Rothkamm, K. (2016). Radiosensitization of HNSCC cells by EGFR inhibition depends on the induction of cell cycle arrests. *Oncotarget, 7*(29), 45122-45133. doi:10.18632/oncotarget.9161

Lambert, A. W., Pattabiraman, D. R., & Weinberg, R. A. (2017). Emerging Biological Principles of Metastasis. *Cell, 168*(4), 670-691. doi:10.1016/j.cell.2016.11.037

Lamouille, S., Xu, J., & Derynck, R. (2014). Molecular mechanisms of epithelial-mesenchymal transition. *Nat Rev Mol Cell Biol, 15*(3), 178-196. doi:10.1038/nrm3758

Lee, J. M., Dedhar, S., Kalluri, R., & Thompson, E. W. (2006). The epithelial-mesenchymal transition: new insights in signaling, development, and disease. *J Cell Biol, 172*(7), 973-981. doi:10.1083/jcb.200601018

Lee, K., Chang, J. W., Oh, C., Liu, L., Jung, S. N., Won, H. R., . . . Koo, B. S. (2020). HOXB5 acts as an oncogenic driver in head and neck squamous cell carcinoma via EGFR/Akt/Wnt/β-catenin signaling axis. *Eur J Surg Oncol, 46*(6), 1066-1073. doi:10.1016/j.ejso.2019.12.009

Leemans, C. R., Braakhuis, B. J., & Brakenhoff, R. H. (2011). The molecular biology of head and neck cancer. *Nat Rev Cancer, 11*(1), 9-22. doi:10.1038/nrc2982

Leemans, C. R., Snijders, P. J. F., & Brakenhoff, R. H. (2018). The molecular landscape of head and neck cancer. *Nat Rev Cancer, 18*(5), 269-282. doi:10.1038/nrc.2018.11

Lemmon, M. A., Schlessinger, J., & Ferguson, K. M. (2014). The EGFR family: not so prototypical

receptor tyrosine kinases. *Cold Spring Harb Perspect Biol, 6*(4), a020768. doi:10.1101/cshperspect.a020768

Li, G. S., Hou, W., Chen, G., Yao, Y. X., Chen, X. Y., Zhang, X. G., . . . Wei, H. Y. (2022). Clinical Significance of Integrin Subunit Beta 4 in Head and Neck Squamous Cell Carcinoma. *Cancer Biother Radiopharm, 37*(4), 256-275. doi:10.1089/cbr.2020.3943

Li, T., Wu, Q., Liu, D., & Wang, X. (2020). miR-27b Suppresses Tongue Squamous Cell Carcinoma Epithelial-Mesenchymal Transition by Targeting ITGA5. *Onco Targets Ther, 13*, 11855-11867. doi:10.2147/ott.S281211

Li, W. Y., & Kang, Y. B. (2016). Probing the Fifty Shades of EMT in Metastasis. *Trends in Cancer, 2*(2), 65-67. doi:10.1016/j.trecan.2016.01.001

Li, X., Wu, P., Tang, Y., Fan, Y., Liu, Y., Fang, X., . . . Zhao, S. (2020). Down-Regulation of MiR-181c-5p Promotes Epithelial-to-Mesenchymal Transition in Laryngeal Squamous Cell Carcinoma via Targeting SERPINE1. *Front Oncol, 10*, 544476. doi:10.3389/fonc.2020.544476

Lin, C. Z., Ren, Z. H., Yang, X., Yang, R., Chen, Y. M., Liu, Z. Q., . . . Ji, T. (2020). Nerve growth factor (NGF)-TrkA axis in head and neck squamous cell carcinoma triggers EMT and confers resistance to the EGFR inhibitor erlotinib. *Cancer Letters, 472*, 81-96. doi:10.1016/j.canlet.2019.12.015

Lin, H. M., Mak, B., Yeung, N., Huynh, K., Meikle, T. G., Mellett, N. A., . . . Horvath, L. G. (2021). Overcoming enzalutamide resistance in metastatic prostate cancer by targeting sphingosine kinase. *Ebiomedicine, 72*, 103625. doi:10.1016/j.ebiom.2021.103625

Liu, X., Li, J., Cadilha, B. L., Markota, A., Voigt, C., Huang, Z., . . . Wang, H. (2019). Epithelial-type systemic breast carcinoma cells with a restricted mesenchymal transition are a major source of metastasis. *Sci Adv, 5*(6), eaav4275. doi:10.1126/sciadv.aav4275

Lurje, G., & Lenz, H. J. (2009). EGFR Signaling and Drug Discovery. *Oncology, 77*(6), 400-410. doi:10.1159/000279388

Macha, M. A., Rachagani, S., Qazi, A. K., Jahan, R., Gupta, S., Patel, A., . . . Jain, M. (2017). Afatinib radiosensitizes head and neck squamous cell carcinoma cells by targeting cancer stem cells. *Oncotarget, 8*(13), 20961-20973. doi:10.18632/oncotarget.15468

Machiels, J. P. H., Haddad, R. I., Fayette, J., Licitra, L. F., Tahara, M., Vermorken, J. B., . . . Investigators, L.-H. N. (2015). Afatinib versus methotrexate as second-line treatment in patients with recurrent or metastatic squamous-cell carcinoma of the head and neck progressing on or after platinum-based therapy (LUX-Head & Neck 1): an open-label, randomised phase 3 trial. *Lancet Oncology, 16*(5), 583-594. doi:10.1016/s1470-2045(15)70124-5

Machtay, M., Moughan, J., Trotti, A., Garden, A. S., Weber, R. S., Cooper, J. S., . . . Ang, K. K. (2008).

Factors associated with severe late toxicity after concurrent chemoradiation for locally advanced head and neck cancer: An RTOG analysis. *Journal of Clinical Oncology, 26*(21), 3582-3589. doi:10.1200/jco.2007.14.8841

Maheswaran, S., & Haber, D. A. (2015). CELL FATE Transition loses its invasive edge. *Nature, 527*(7579), 452-453. doi:10.1038/nature16313

Mao, X., Xu, J., Wang, W., Liang, C., Hua, J., Liu, J., . . . Shi, S. (2021). Crosstalk between cancer-associated fibroblasts and immune cells in the tumor microenvironment: new findings and future perspectives. *Mol Cancer, 20*(1), 131. doi:10.1186/s12943-021-01428-1

Markovic, A., & Chung, C. H. (2012). Current role of EGF receptor monoclonal antibodies and tyrosine kinase inhibitors in the management of head and neck squamous cell carcinoma. *Expert Review of Anticancer Therapy, 12*(9), 1149-1159. doi:10.1586/era.12.91

Moon, J. H., Lee, S. H., & Lim, Y. C. (2021). Wnt/beta-catenin/Slug pathway contributes to tumor invasion and lymph node metastasis in head and neck squamous cell carcinoma. *Clinical & Experimental Metastasis, 38*(2), 163-174. doi:10.1007/s10585-021-10081-3

Mroz, E. A., Tward, A. D., Hammon, R. J., Ren, Y., & Rocco, J. W. (2015). Intra-tumor genetic heterogeneity and mortality in head and neck cancer: analysis of data from the Cancer Genome Atlas. *PLoS Med, 12*(2), e1001786. doi:10.1371/journal.pmed.1001786

Mroz, E. A., Tward, A. D., Pickering, C. R., Myers, J. N., Ferris, R. L., & Rocco, J. W. (2013). High intratumor genetic heterogeneity is related to worse outcome in patients with head and neck squamous cell carcinoma. *Cancer, 119*(16), 3034-3042. doi:10.1002/cncr.28150

Nair, S., Bonner, J. A., & Bredel, M. (2022). EGFR Mutations in Head and Neck Squamous Cell Carcinoma. *Int J Mol Sci, 23*(7). doi:10.3390/ijms23073818

Nguyen-Ngoc, K. V., Cheung, K. J., Brenot, A., Shamir, E. R., Gray, R. S., Hines, W. C., . . . Ewald, A. J. (2012). ECM microenvironment regulates collective migration and local dissemination in normal and malignant mammary epithelium. *Proceedings of the National Academy of Sciences of the United States of America, 109*(39), E2595-E2604. doi:10.1073/pnas.1212834109

Nguyen-Tan, P. F., Zhang, Q., Ang, K. K., Weber, R. S., Rosenthal, D. I., Soulieres, D., . . . Le, Q. T. (2014). Randomized Phase III Trial to Test Accelerated Versus Standard Fractionation in Combination With Concurrent Cisplatin for Head and Neck Carcinomas in the Radiation Therapy Oncology Group 0129 Trial: Long-Term Report of Efficacy and Toxicity. *Journal of Clinical Oncology, 32*(34), 3858-U3311. doi:10.1200/jco.2014.55.3925

Nieto, M. A. (2013). Epithelial Plasticity: A Common Theme in Embryonic and Cancer Cells. *Science, 342*(6159), 708-+. doi:10.1126/science.1234850

Nieto, M. A., Huang, R. Y., Jackson, R. A., & Thiery, J. P. (2016a). Emt: 2016. *Cell, 166*(1), 21-45.

doi:10.1016/j.cell.2016.06.028

Nieto, M. A., Huang, R. Y. J., Jackson, R. A., & Thiery, J. P. (2016b). EMT: 2016. *Cell, 166*(1), 21-45. doi:10.1016/j.cell.2016.06.028

Nyati, M. K., Morgan, M. A., Feng, F. Y., & Lawrence, T. S. (2006). Integration of EGFR inhibitors with radiochemotherapy. *Nature Reviews Cancer, 6*(11), 876-885. doi:10.1038/nrc1953

Ocana, O. H., Corcoles, R., Fabra, A., Moreno-Bueno, G., Acloque, H., Vega, S., . . . Nieto, M. A. (2012). Metastatic Colonization Requires the Repression of the Epithelial-Mesenchymal Transition Inducer Prrx1. *Cancer Cell, 22*(6), 709-724. doi:10.1016/j.ccr.2012.10.012

Okada, Y., Takahashi, N., Takayama, T., & Goel, A. (2021). LAMC2 promotes cancer progression and gemcitabine resistance through modulation of EMT and ATP-binding cassette transporters in pancreatic ductal adenocarcinoma. *Carcinogenesis, 42*(4), 546-556. doi:10.1093/carcin/bgab011

Ongkeko, W. M., Altuna, X., Weisman, R. A., & Wang-Rodriguez, J. (2005). Expression of protein tyrosine kinases in head and neck squamous cell carcinomas. *American Journal of Clinical Pathology, 124*(1), 71-76. doi:10.1309/btln5wtmj3pcnrrc

Pan, M., Schinke, H., Luxenburger, E., Kranz, G., Shakhtour, J., Libl, D., . . . Gires, O. (2018). EpCAM ectodomain EpEX is a ligand of EGFR that counteracts EGF-mediated epithelial-mesenchymal transition through modulation of phospho-ERK1/2 in head and neck cancers. *PLoS Biol, 16*(9), e2006624. doi:10.1371/journal.pbio.2006624

Pao, W., Miller, V., Zakowski, M., Doherty, J., Politi, K., Sarkaria, I., . . . Varmus, H. (2004). EGF receptor gene mutations are common in lung cancers from "never smokers" and are associated with sensitivity of tumors to gefitinib and erlotinib. *Proceedings of the National Academy of Sciences of the United States of America, 101*(36), 13306-13311. doi:10.1073/pnas.0405220101

Parikh, A. S., Puram, S. V., Faquin, W. C., Richmon, J. D., Emerick, K. S., Deschler, D. G., . . . Lin, D. T. (2019). Immunohistochemical quantification of partial-EMT in oral cavity squamous cell carcinoma primary tumors is associated with nodal metastasis. *Oral Oncology, 99*. doi:10.1016/j.oraloncology.2019.104458

Peirsman, A., Blondeel, E., Ahmed, T., Anckaert, J., Audenaert, D., Boterberg, T., . . . De Wever, O. (2021). MISpheroID: a knowledgebase and transparency tool for minimum information in spheroid identity. *Nat Methods, 18*(11), 1294-1303. doi:10.1038/s41592-021-01291-4

Peng, X., Liu, Y., Zhu, S., Peng, X., Li, H., Jiao, W., . . . Kong, D. (2019). Co-targeting PI3K/Akt and MAPK/ERK pathways leads to an enhanced antitumor effect on human hypopharyngeal squamous cell carcinoma. *J Cancer Res Clin Oncol, 145*(12), 2921-2936. doi:10.1007/s00432-019-03047-2

Prat, A., Parker, J. S., Karginova, O., Fan, C., Livasy, C., Herschkowitz, J. I., . . . Perou, C. M. (2010). Phenotypic and molecular characterization of the claudin-low intrinsic subtype of breast cancer. *Breast Cancer Research, 12*(5). doi:10.1186/bcr2635

Psyrri, A., Yu, Z. W., Weinberger, P. M., Sasaki, C., Haffty, B., Camp, R., . . . Burtness, B. A. (2005). Quantitative determination of nuclear and cytoplasmic epidermal growth factor receptor expression in oropharyngeal squamous cell cancer by using automated quantitative analysis. *Clinical Cancer Research, 11*(16), 5856-5862. doi:10.1158/1078-0432.Ccr-05-0420

Pu, Y., Li, Q., Wang, Y., Xu, L., Qiao, Q., Guo, Y., & Guo, C. (2021). pERK-mediated IL8 secretion can enhance the migration, invasion, and cisplatin resistance of CD10-positive oral cancer cells. *BMC Cancer, 21*(1), 1283. doi:10.1186/s12885-021-09025-7

Puram, S. V., Parikh, A. S., & Tirosh, I. (2018a). Single cell RNA-seq highlights a role for a partial EMT in head and neck cancer. *Mol Cell Oncol, 5*(3), e1448244. doi:10.1080/23723556.2018.1448244

Puram, S. V., Parikh, A. S., & Tirosh, I. (2018b). Single cell RNA-seq highlights a role for a partial EMT in head and neck cancer. *Molecular & Cellular Oncology, 5*(3). doi:10.1080/23723556.2018.1448244

Puram, S. V., Tirosh, I., Parikh, A. S., Patel, A. P., Yizhak, K., Gillespie, S., . . . Bernstein, B. E. (2017). Single-Cell Transcriptomic Analysis of Primary and Metastatic Tumor Ecosystems in Head and Neck Cancer. *Cell, 171*(7), 1611-1624 e1624. doi:10.1016/j.cell.2017.10.044

Ramesh, V., Brabletz, T., & Ceppi, P. (2020). Targeting EMT in Cancer with Repurposed Metabolic Inhibitors. *Trends Cancer, 6*(11), 942-950. doi:10.1016/j.trecan.2020.06.005

Rebbeck, T. R. (2008). Cancer Epidemiology Biomarkers & Prevention. A note from the new Editor-in-Chief. *Cancer Epidemiol Biomarkers Prev, 17*(9), 2203-2204. doi:10.1158/1055-9965.EPI-08-0740

Rodon, J., Carducci, M. A., Sepulveda-Sanchez, J. M., Azaro, A., Calvo, E., Seoane, J., . . . Baselga, J. (2015). First-in-Human Dose Study of the Novel Transforming Growth Factor-beta Receptor I Kinase Inhibitor LY2157299 Monohydrate in Patients with Advanced Cancer and Glioma. *Clinical Cancer Research, 21*(3), 553-560. doi:10.1158/1078-0432.Ccr-14-1380

Roepstorff, K., Grandal, M. V., Henriksen, L., Knudsen, S. L. J., Lerdrup, M., Grovdal, L., . . . van Deurs, B. (2009). Differential Effects of EGFR Ligands on Endocytic Sorting of the Receptor. *Traffic, 10*(8), 1115-1127. doi:10.1111/j.1600-0854.2009.00943.x

Ronan, T., Macdonald-Obermann, J. L., Huelsmann, L., Bessman, N. J., Naegle, K. M., & Pike, L. J. (2016). Different Epidermal Growth Factor Receptor (EGFR) Agonists Produce Unique Signatures for the Recruitment of Downstream Signaling Proteins. *J Biol Chem, 291*(11),

5528-5540. doi:10.1074/jbc.M115.710087

Roschke, A. V., Tonon, G., Gehlhaus, K. S., McTyre, N., Bussey, K. J., Lababidi, S., . . . Kirsch, I. R. (2003). Karyotypic complexity of the NCI-60 drug-screening panel. *Cancer Res, 63*(24), 8634-8647.

Ruicci, K. M., Pinto, N., Khan, M. I., Yoo, J., Fung, K., MacNeil, D., . . . Nichols, A. C. (2018). ERK-TSC2 signalling in constitutively-active HRAS mutant HNSCC cells promotes resistance to PI3K inhibition. *Oral Oncol, 84*, 95-103. doi:10.1016/j.oraloncology.2018.07.010

Saenz-de-Santa-Maria, I., Celada, L., & Chiara, M. D. (2020). The Leader Position of Mesenchymal Cells Expressing N-Cadherin in the Collective Migration of Epithelial Cancer. *Cells, 9*(3). doi:10.3390/cells9030731

Schinke, H., Pan, M., Akyol, M., Zhou, J., Shi, E., Kranz, G., . . . Gires, O. (2022a). SLUG-related partial epithelial-to-mesenchymal transition is a transcriptomic prognosticator of head and neck cancer survival. *Mol Oncol, 16*(2), 347-367. doi:10.1002/1878-0261.13075

Schinke, H., Pan, M., Akyol, M., Zhou, J. F., Shi, E. X., Kranz, G., . . . Gires, O. (2022b). SLUG-related partial epithelial-to-mesenchymal transition is a transcriptomic prognosticator of head and neck cancer survival. *Molecular Oncology, 16*(2), 347-367. doi:10.1002/1878-0261.13075

Schmidt, J. M., Panzilius, E., Bartsch, H. S., Irmler, M., Beckers, J., Kari, V., . . . Scheel, C. H. (2015). Stem-cell-like properties and epithelial plasticity arise as stable traits after transient Twist1 activation. *Cell Rep, 10*(2), 131-139. doi:10.1016/j.celrep.2014.12.032

Sexén, L. (1970). Epithelial - mesenchymal interactions: 18th Hahnemann Symposium. R. Fleischmajer and R. E. Billingham eds. Williams and Wilkins Co., Baltimore. 326 pp. 1968. *Teratology, 3*, 100-101.

Shamir, E. R., Pappalardo, E., Jorgens, D. M., Coutinho, K., Tsai, W. T., Aziz, K., . . . Ewald, A. J. (2014). Twist1-induced dissemination preserves epithelial identity and requires E-cadherin. *J Cell Biol, 204*(5), 839-856. doi:10.1083/jcb.201306088

Sheu, J. J., Lee, C. C., Hua, C. H., Li, C. I., Lai, M. T., Lee, S. C., . . . Lee, C. H. (2014). LRIG1 modulates aggressiveness of head and neck cancers by regulating EGFR-MAPK-SPHK1 signaling and extracellular matrix remodeling. *Oncogene, 33*(11), 1375-1384. doi:10.1038/onc.2013.98

Shin, D. M., Ro, J. Y., Hong, W. K., & Hittelman, W. N. (1994). DYSREGULATION OF EPIDERMAL GROWTH-FACTOR RECEPTOR EXPRESSION IN PREMALIGNANT LESIONS DURING HEAD AND NECK TUMORIGENESIS. *Cancer Research, 54*(12), 3153-3159. Retrieved from <Go to ISI>://WOS:A1994NQ72400017

Solca, F., Dahl, G., Zoephel, A., Bader, G., Sanderson, M., Klein, C., . . . Adolf, G. R. (2012). Target Binding Properties and Cellular Activity of Afatinib (BIBW 2992), an Irreversible ErbB Family

Blocker. *Journal of Pharmacology and Experimental Therapeutics, 343*(2), 342-350. doi:10.1124/jpet.112.197756

Stamos, J., Sliwkowski, M. X., & Eigenbrot, C. (2002). Structure of the epidermal growth factor receptor kinase domain alone and in complex with a 4-anilinoquinazoline inhibitor. *Journal of Biological Chemistry, 277*(48), 46265-46272. doi:10.1074/jbc.M207135200

Steinbichler, T. B., Alshaimaa, A., Maria, M. V., Daniel, D., Herbert, R., Jozsef, D., & Ira-Ida, S. (2018). Epithelial-mesenchymal crosstalk induces radioresistance in HNSCC cells. *Oncotarget, 9*(3), 3641-3652. doi:10.18632/oncotarget.23248

Stransky, N., Egloff, A. M., Tward, A. D., Kostic, A. D., Cibulskis, K., Sivachenko, A., . . . Grandis, J. R. (2011). The Mutational Landscape of Head and Neck Squamous Cell Carcinoma. *Science, 333*(6046), 1157-1160. doi:10.1126/science.1208130

Suhail, Y., Cain, M. P., Vanaja, K., Kurywchak, P. A., Levchenko, A., Kalluri, R., & Kshitiz. (2019). Systems Biology of Cancer Metastasis. *Cell Syst, 9*(2), 109-127. doi:10.1016/j.cels.2019.07.003

Sun, T., Jackson, S., Haycock, J. W., & MacNeil, S. (2006). Culture of skin cells in 3D rather than 2D improves their ability to survive exposure to cytotoxic agents. *J Biotechnol, 122*(3), 372-381. doi:10.1016/j.jbiotec.2005.12.021

Takes, R. P., de Jong, R. J. B., Schuuring, E., Litvinov, S. V., Hermans, J., & Van Krieken, J. (1998). Differences in expression of oncogenes and tumor suppressor genes in different sites of head and neck squamous cell. *Anticancer Research, 18*(6B), 4793-4800. Retrieved from <Go to ISI>://WOS:000078056100041

Tam, W. L., & Weinberg, R. A. (2013). The epigenetics of epithelial-mesenchymal plasticity in cancer. *Nature Medicine, 19*(11), 1438-1449. doi:10.1038/nm.3336

Tang, Q., Zhong, H. Z., Xie, F. Y., Xie, J. Y., Chen, H. M., & Yao, G. (2014). Expression of miR-106b-25 induced by salvianolic acid B inhibits epithelial-to-mesenchymal transition in HK-2 cells. *European Journal of Pharmacology, 741*, 97-103. doi:10.1016/j.ejphar.2014.07.051

Tevis, K. M., Colson, Y. L., & Grinstaff, M. W. (2017). Embedded Spheroids as Models of the Cancer Microenvironment. *Adv Biosyst, 1*(10). doi:10.1002/adbi.201700083

Thangavelu, P. U., Krenács, T., Dray, E., & Duijf, P. H. (2016). In epithelial cancers, aberrant COL17A1 promoter methylation predicts its misexpression and increased invasion. *Clin Epigenetics, 8*, 120. doi:10.1186/s13148-016-0290-6

Theocharis, A. D., Skandalis, S. S., Gialeli, C., & Karamanos, N. K. (2016). Extracellular matrix structure. *Adv Drug Deliv Rev, 97*, 4-27. doi:10.1016/j.addr.2015.11.001

Thews, O., & Riemann, A. (2019). Tumor pH and metastasis: a malignant process beyond hypoxia. *Cancer Metastasis Rev, 38*(1-2), 113-129. doi:10.1007/s10555-018-09777-y

Thiery, J. P. (2002). Epithelial-mesenchymal transitions in tumour progression. *Nat Rev Cancer, 2*(6), 442-454. doi:10.1038/nrc822

Thiery, J. P., Acloque, H., Huang, R. Y. J., & Nieto, M. A. (2009). Epithelial-Mesenchymal Transitions in Development and Disease. *Cell, 139*(5), 871-890. doi:10.1016/j.cell.2009.11.007

Thiery, J. P., & Sleeman, J. P. (2006). Complex networks orchestrate epithelial-mesenchymal transitions. *Nature Reviews Molecular Cell Biology, 7*(2), 131-142. doi:10.1038/nrm1835

Ting, D. T., Wittner, B. S., Ligorio, M., Vincent Jordan, N., Shah, A. M., Miyamoto, D. T., . . . Haber, D. A. (2014). Single-cell RNA sequencing identifies extracellular matrix gene expression by pancreatic circulating tumor cells. *Cell Rep, 8*(6), 1905-1918. doi:10.1016/j.celrep.2014.08.029

Torab, P., Yan, Y., Yamashita, H., Warrick, J. I., Raman, J. D., DeGraff, D. J., & Wong, P. K. (2020). Three-Dimensional Microtumors for Probing Heterogeneity of Invasive Bladder Cancer. *Analytical Chemistry, 92*(13), 8768-8775. doi:10.1021/acs.analchem.0c00057

Trimboli, A. J., Fukino, K., de Bruin, A., Wei, G., Shen, L., Tanner, S. M., . . . Leone, G. (2008). Direct evidence for epithelial-mesenchymal transitions in breast cancer. *Cancer Research, 68*(3), 937-945. doi:10.1158/0008-5472.Can-07-2148

Troiani, T., Napolitano, S., Della Corte, C. M., Martini, G., Martinelli, E., Morgillo, F., & Ciardiello, F. (2016). Therapeutic value of EGFR inhibition in CRC and NSCLC: 15 years of clinical evidence. *Esmo Open, 1*(5). doi:10.1136/esmoopen-2016-000088

Tsai, J. H., Donaher, J. L., Murphy, D. A., Chau, S., & Yang, J. (2012). Spatiotemporal Regulation of Epithelial-Mesenchymal Transition Is Essential for Squamous Cell Carcinoma Metastasis. *Cancer Cell, 22*(6), 725-736. doi:10.1016/j.ccr.2012.09.022

Tsang, F. H., Law, C. T., Tang, T. C., Cheng, C. L., Chin, D. W., Tam, W. V., . . . Wong, C. M. (2019). Aberrant Super-Enhancer Landscape in Human Hepatocellular Carcinoma. *Hepatology, 69*(6), 2502-2517. doi:10.1002/hep.30544

Tsuji, T., Ibaragi, S., & Hu, G. F. (2009). Epithelial-Mesenchymal Transition and Cell Cooperativity in Metastasis. *Cancer Research, 69*(18), 7135-7139. doi:10.1158/0008-5472.Can-09-1618

Vermorken, J. B., Trigo, J., Hitt, R., Koralewski, P., Diaz-Rubio, E., Rolland, F., . . . Baselga, J. (2007). Open-label, uncontrolled, multicenter phase II study to evaluate the efficacy and toxicity of cetuximab as a single agent in patients with recurrent and/or metastatic squamous cell carcinoma of the head and neck who failed to respond to platinum-based therapy. *Journal of Clinical Oncology, 25*(16), 2171-2177. doi:10.1200/jco.2006.06.7447

Vilchez Mercedes, S. A., Bocci, F., Levine, H., Onuchic, J. N., Jolly, M. K., & Wong, P. K. (2021). Decoding leader cells in collective cancer invasion. *Nat Rev Cancer, 21*(9), 592-604. doi:10.1038/s41568-021-00376-8

Vishwakarma, M., Spatz, J. P., & Das, T. (2020). Mechanobiology of leader-follower dynamics in epithelial cell migration. *Current Opinion in Cell Biology, 66*, 97-103. doi:10.1016/j.ceb.2020.05.007

Wang, J., Jiang, C., Li, N., Wang, F., Xu, Y., Shen, Z., . . . He, C. (2020). The circEPSTI1/mir-942-5p/LTBP2 axis regulates the progression of OSCC in the background of OSF via EMT and the PI3K/Akt/mTOR pathway. *Cell Death Dis, 11*(8), 682. doi:10.1038/s41419-020-02851-w

Wang, P., Yuan, Y., Lin, W., Zhong, H., Xu, K., & Qi, X. (2019). Roles of sphingosine-1-phosphate signaling in cancer. *Cancer Cell Int, 19*, 295. doi:10.1186/s12935-019-1014-8

Wang, X., Sun, Y., Peng, X., Naqvi, S., Yang, Y., Zhang, J., . . . Lu, Y. (2020). The Tumorigenic Effect of Sphingosine Kinase 1 and Its Potential Therapeutic Target. *Cancer Control, 27*(1), 1073274820976664. doi:10.1177/1073274820976664

Weinstein, G. S., Quon, H., O'Malley, B. W., Kim, G. G., & Cohen, M. A. (2010). Selective Neck Dissection and Deintensified Postoperative Radiation and Chemotherapy for Oropharyngeal Cancer: A Subset Analysis of the University of Pennsylvania Transoral Robotic Surgery Trial. *Laryngoscope, 120*(9), 1749-1755. doi:10.1002/lary.21021

Wilson, K. J., Mill, C., Lambert, S., Buchman, J., Wilson, T. R., Hernandez-Gordillo, V., . . . Riese, D. J. (2012). EGFR ligands exhibit functional differences in models of paracrine and autocrine signaling. *Growth Factors, 30*(2), 107-116. doi:10.3109/08977194.2011.649918

Winkler, J., Abisoye-Ogunniyan, A., Metcalf, K. J., & Werb, Z. (2020). Concepts of extracellular matrix remodelling in tumour progression and metastasis. *Nature Communications, 11*(1). doi:10.1038/s41467-020-18794-x

Wu, Z. H., Tang, Y., Niu, X., & Cheng, Q. (2019). Expression and gene regulation network of INHBA in Head and neck squamous cell carcinoma based on data mining. *Sci Rep, 9*(1), 14341. doi:10.1038/s41598-019-50865-y

Yamada, K. M., & Sixt, M. (2019). Mechanisms of 3D cell migration. *Nat Rev Mol Cell Biol, 20*(12), 738-752. doi:10.1038/s41580-019-0172-9

Yang, C. X., Cao, M. L., Liu, Y. W., He, Y. Q., Du, Y., Zhang, G. L., & Gao, F. (2019). Inducible formation of leader cells driven by CD44 switching gives rise to collective invasion and metastases in luminal breast carcinomas. *Oncogene, 38*(46), 7113-7132. doi:10.1038/s41388-019-0899-y

Ye, X., Tam, W. L., Shibue, T., Kaygusuz, Y., Reinhardt, F., Eaton, E. N., & Weinberg, R. A. (2015). Distinct EMT programs control normal mammary stem cells and tumour-initiating cells. *Nature, 525*(7568), 256-+. doi:10.1038/nature14897

Yeung, K. T., & Yang, J. (2017). Epithelial-mesenchymal transition in tumor metastasis. *Mol Oncol,*

11(1), 28-39. doi:10.1002/1878-0261.12017

Yu, M., Bardia, A., Wittner, B., Stott, S. L., Smas, M. E., Ting, D. T., . . . Maheswaran, S. (2013). Circulating Breast Tumor Cells Exhibit Dynamic Changes in Epithelial and Mesenchymal Composition. *Science, 339*(6119), 580-584. doi:10.1126/science.1228522

Yu, Y., Wang, W., Lu, W., Chen, W., & Shang, A. (2021). Inhibin β-A (INHBA) induces epithelial-mesenchymal transition and accelerates the motility of breast cancer cells by activating the TGF-β signaling pathway. *Bioengineered, 12*(1), 4681-4696. doi:10.1080/21655979.2021.1957754

Zadran, S., Arumugam, R., Herschman, H., Phelps, M. E., & Levine, R. D. (2014). Surprisal analysis characterizes the free energy time course of cancer cells undergoing epithelial-to-mesenchymal transition. *Proc Natl Acad Sci U S A, 111*(36), 13235-13240. doi:10.1073/pnas.1414714111

Zeng, Q., Chen, S., You, Z., Yang, F., Carey, T. E., Saims, D., & Wang, C. Y. (2002). Hepatocyte growth factor inhibits anoikis in head and neck squamous cell carcinoma cells by activation of ERK and Akt signaling independent of NFkappa B. *J Biol Chem, 277*(28), 25203-25208. doi:10.1074/jbc.M201598200

Zhang, J., Goliwas, K. F., Wang, W. J., Taufalele, P. V., Bordeleau, F., & Reinhart-King, C. A. (2019). Energetic regulation of coordinated leader-follower dynamics during collective invasion of breast cancer cells. *Proceedings of the National Academy of Sciences of the United States of America, 116*(16), 7867-7872. doi:10.1073/pnas.1809964116

Zhang, M., Hoyle, R. G., Ma, Z., Sun, B., Cai, W., Cai, H., . . . Li, J. (2021). FOSL1 promotes metastasis of head and neck squamous cell carcinoma through super-enhancer-driven transcription program. *Mol Ther, 29*(8), 2583-2600. doi:10.1016/j.ymthe.2021.03.024

Zhang, Q., Wang, Y., Xia, C., Ding, L., Pu, Y., Hu, X., . . . Hu, Q. (2021). Integrated analysis of single-cell RNA-seq and bulk RNA-seq reveals distinct cancer-associated fibroblasts in head and neck squamous cell carcinoma. *Ann Transl Med, 9*(12), 1017. doi:10.21037/atm-21-2767

Zhang, Y., Cai, H., Liao, Y., Zhu, Y., Wang, F., & Hou, J. (2020). Activation of PGK1 under hypoxic conditions promotes glycolysis and increases stem cell-like properties and the epithelial-mesenchymal transition in oral squamous cell carcinoma cells via the AKT signalling pathway. *Int J Oncol, 57*(3), 743-755. doi:10.3892/ijo.2020.5083

Zheng, X. F., Carstens, J. L., Kim, J., Scheible, M., Kaye, J., Sugimoto, H., . . . Kalluri, R. (2015). Epithelial-to-mesenchymal transition is dispensable for metastasis but induces chemoresistance in pancreatic cancer. *Nature, 527*(7579), 525-+. doi:10.1038/nature16064

Zhu, G., Cao, B., Liang, X., Li, L., Hao, Y., Meng, W., . . . Li, L. (2021). Small extracellular vesicles containing miR-192/215 mediate hypoxia-induced cancer-associated fibroblast

development in head and neck squamous cell carcinoma. *Cancer Lett, 506*, 11-22. doi:10.1016/j.canlet.2021.01.006

Zoeller, E. L., Pedro, B., Konen, J., Dwivedi, B., Rupji, M., Sundararaman, N., . . . Vertino, P. M. (2019). Genetic heterogeneity within collective invasion packs drives leader and follower cell phenotypes. *Journal of Cell Science, 132*(19). doi:10.1242/jcs.231514

7 CONTRIBUTION STATEMENT

Immunohistochemistry staining was performed by **Gisela Kranz** (Department of Otorhinolaryngology, Head and Neck Surgery, Grosshadern Medical Center, Ludwig-Maximilians-University, Munich, Germany). RNAseq-related analysis was performed by **Zhengquan Wu** (Grosshadern Medical Center, Ludwig-Maximilians-University, Munich, Germany) and **Zhongyang Lin** (Department of Otorhinolaryngology, Head and Neck Surgery, Grosshadern Medical Center, Ludwig Maximilians-University, Munich, Germany), and in collaboration with **Kristian Unger** (Clinical Cooperation Group “Personalized Radiotherapy in Head and Neck Cancer “, Helmholtz Zentrum München). Acquisition of bulk-sequencing samples by **Pardis khosravani** (The instruments and services of the CFFlowCyt at BMC, Ludwig-Maximilians-Universität München, Biomedical Center, Planegg-Martinsried, Germany). Samples preparation for bulk-sequencing was performed in collaboration with **Steffen Heuer** and **Julia Heß** (Helmholtz Zentrum München Research Center for Environmental Health (GmbH), Research Unit Radiation Cytogenetics, Neuherberg, Germany)

8 AFFIDAVIT

Hiermit versichere ich an Eides statt, dass ich die vorliegende Dissertation „ Molecular characterization of EGF-mediated invasion in a 3D cellular model“ selbstständig angefertigt habe, mich außer der angegebenen keiner weiteren Hilfsmittel bedient und alle Erkenntnisse, die aus dem Schrifttum ganz oder annähernd übernommen sind, als solche kenntlich gemacht und nach ihrer Herkunft unter Bezeichnung der Fundstelle einzeln nachgewiesen habe.

I hereby confirm that the dissertation “Molecular characterization of EGF-mediated invasion in a 3D cellular model” is the result of my own work and that I have only used sources or materials listed and specified in the dissertation.

Munich, 21.07.2022	Jiefu Zhou
Place, date	Name

9 LIST OF PUBLICATIONS

Manuscripts published / in preparation

- Isolation and Characterization of Head and Neck Cancer-derived Peritumoral and Cancer-associated Fibroblasts
  Jiefu Zhou, Sabina Schwenk-Zieger, Gisela Kranz, Christoph Walz, Frederik Klauschen, Sharduli Sharduli, Martin Canis, Frank Haubner, Philipp Baumeister, Olivier Gires, Vera Kohlbauer*(**published, Frontiers in Oncology**)
- Molecular characterization of EGF-mediated invasion in a 3D cellular model
  Jiefu Zhou, Zhongyang Lin, Zhengquan Wu, Gisela Kranz, Kristian Unger, Pardis khosravani, Steffen Heuer, Julia Hess, Olivier Gires etc. **(In preparation)**

Other contributions

- A Transcriptomic Map of EGFR-induced Epithelial-to-Mesenchymal Transition Identifies Prognostic and Therapeutic Targets for Head and Neck Cancer.
  Henrik Schinke*, Enxian Shi*, Zhongyang Lin*, Tanja Quadt, Gisela Kranz, **Jiefu Zhou**, Hongxia Wang, Julia Hess, Steffen Heuer, Claus Belka, Horst Zitzelsberger, Udo Schumacher, Sandra Genduso, Kristoffer Riecken, Yujing Gao, Zhengquan Wu, Christoph A Reichel, Christoph Walz, Martin Canis, Kristian Unger, Philipp Baumeister, Min Pan, and Olivier Gires (**Revised & resubmitted, Molecular Cancer**)
- Epithelial-to-Mesenchymal Transition-Derived Heterogeneity in Head and Neck Squamous Cell Carcinomas.
  Baumeister P, **Zhou J**, Canis M, Gires O.Cancers (Basel). 2021 Oct 26;13(21):5355. doi: 10.3390/cancer
- Human Adipose-Derived Stem/Stromal Cells Promote Proliferation and Migration in Head and Neck Cancer Cells.
  Sharaf K, Eggersmann TK, Haider SP, Schwenk-Zieger S, **Zhou J**, Gires O, Lechner A, Canis M, Haubner F.Cancers (Basel) .2021 Jun 1;13(11):2751. doi: 10.3390/cancers13112751.
- SLUG-related partial epithelial-to-mesenchymal transition is a transcriptomic prognosticator of head and neck cancer survival.
  Schinke H, Pan M, Akyol M, **Zhou J**, Shi E, Kranz G, Libl D, Quadt T, Simon F, Canis M, Baumeister P, Gires O.Mol Oncol . 2022 Jan;16(2):347-367. doi: 10.1002/1878-0261.13075. Epub 2021 Aug 21.
- Comparison of bone surface and trough fixation on bone-tendon healing in a rabbit patella-patellar tendon injury model.
  Li M, Tang Y, Chen C, **Zhou J,** Zheng C, Chen H, Lu H, Qu J.J Orthop Translat. 2020 Jan 18;21:49-56. doi: 10.1016/j.jot.2019.12.007. eCollection 2020 Mar.

10 ACKNOWLEDGEMENT

First of all, I would like to express my sincere gratitude to Prof. Olivier Gires, who over the last three years has taught me to view life dialectically and has given me unparalleled guidance in scientific research. Without his support and understanding, I couldn't be a better version of myself (Spezi).

I worked with a group of incredible coworkers for three of my most memorable years. Excellent advice on experimental methods and incredibly imaginative scientific thinking were given by Alexandra Blancke Soares, who is intelligent and patient. I was warmly greeted by Vera, Henrik, Gisela, Sabina, Darko, Yuanchi, and Min when I came to Germany. In addition, I want to acknowledge Zhongyang, Zhengquan, Kristian, Pardis, Steffen, Gisela, Sabina, Darko, and Julia Heß for their extraordinary contributions to the data analysis, staining, and sample collection. Professors Frank Haubner and Philipp Baumeister provided clinical guidance and insightful theoretical and practical advice that significantly improved my comprehension of the project. I also acknowledge younger generations like Enxian, Ningyue, Sharduli, and Tanja for their encouragement and support. My doctoral journey was made feasible and colorful by all of you.

Finally, my family's unwavering support helped me get to where I am now. Especially my beloved Nanxi came to Germany without hesitation to support me; her love gave me the confidence and bravery to face all the challenges.